

ATMOSPHERIC TRANSPORT OF HYDROGEN SULFIDE
FROM PROPOSED GEOTHERMAL POWER PLANT (UNIT 19)

Predictions by Physical Modeling
in a Wind Tunnel

by

R. L. Petersen* and J. E. Cermak**

Prepared for

Pacific Gas and Electric Company
San Francisco, California

Engineering Sciences

FEB 1 '79

Branch Library

Fluid Dynamics and Diffusion Laboratory
Fluid Mechanics and Wind Engineering Program
Colorado State University
Fort Collins, Colorado 80523

*Research Assistant Professor, Department of Civil Engineering
**Director, Fluid Dynamics and Diffusion Laboratory

September 1978

CER78-79RLP-JEC10



U18401 0075015

ABSTRACT

Tests were conducted in the Colorado State University wind tunnel facility of the transport and dispersion of H_2S plumes emanating from cooling towers positioned at three locations in the Geysers Geothermal Area.

The wind tunnel tests were conducted with the cooling towers and terrain modeled to a scale of 1:1920. The first phase of the testing was conducted in the Environmental Wind Tunnel under neutral stratification. Ground level concentrations were measured in the vicinity of Anderson Springs and Whispering Pines for two wind directions and four wind speeds. The second phase of the testing was conducted outside the wind tunnel in a specially enclosed area. Nighttime drainage flow conditions were simulated by cooling the terrain. Concentration measurements in the vicinity of Anderson Springs were obtained as well as the velocity and temperature distributions of the resulting flow. A complete description of the test methodology, concentration measurements and flow visualization is included in the report.

ACKNOWLEDGMENTS

Mr. James A. Garrison supervised construction of the terrain model and photographic recording of the flow visualizations. Mr. Jim Maxton collected and processed the velocity, temperature and concentration data and Mr. Evan Twombly assisted in the data reduction and report preparation. The manuscript was typed by Kathy Meikel and the figures were drafted by Kenneth Streeb.

TABLE OF CONTENTS

<u>Chapter</u>	<u>Page</u>
ABSTRACT	ii
ACKNOWLEDGEMENTS	iii
LIST OF TABLES	v
LIST OF FIGURES.	vi
LIST OF SYMBOLS.	x
1.0 INTRODUCTION	1
2.0 SIMULATION OF ATMOSPHERIC MOTION	3
2.1 Neutral Stratification.	3
2.2 Drainage Flow--Stable Stratification.	4
3.0 EXPERIMENTAL METHOD.	6
3.1 Model	6
3.2 Wind Tunnels and Scale Models	7
3.3 Flow Visualization Techniques	7
3.4 Gas Tracer Technique.	8
3.5 Wind Profile Measurements	8
3.6 Drainage Flow--Special Considerations	10
4.0 TEST PROGRAM RESULTS--VISUALIZATION.	11
4.1 Neutral Atmosphere.	11
4.2 Drainage Flow	11
5.0 TEST PROGRAM RESULTS--CONCENTRATION MEASUREMENTS	13
5.1 Neutral Atmosphere.	13
5.2 Drainage Flow	14
6.0 DRAINAGE FLOW--VELOCITY, TEMPERATURE AND CO ₂ DISTRIBUTIONS	16
REFERENCES	17
APPENDIX A	18
TABLES	21
FIGURES.	36

LIST OF TABLES

<u>Table</u>		<u>Page</u>
2.1	Model and prototype dimensional parameters, Unit 19, Sites R, Q, H	22
2.2	Model and prototype dimensionless parameters, Unit 19, Sites R, Q, H	23
3.1	Tracer gas sampling location key for the 198° wind direction	24
3.2	Tracer gas sampling location key for the 325° wind direction	25
4.1	Summary of photographs taken for the neutral flow tests	26
5.1	Nondimensional concentration coefficient, K, (x 10 ⁵) for Site R and a 198° wind direction	27
5.2	Nondimensional concentration coefficient, K, (x 10 ⁵) for Site Q and a 198° wind direction	28
5.3	Nondimensional concentration coefficient, K, (x 10 ⁵) for Site H and a 198° wind direction	29
5.4	Nondimensional concentration coefficient, K, (x 10 ⁵) for Site R and a 325° wind direction	30
5.5	Nondimensional concentration coefficient, K, (x 10 ⁵) for Site Q and a 325° wind direction	31
5.6	Nondimensional concentration coefficient, K, (x 10 ⁵) for Site H and a 325° wind direction	32
5.7	Nondimensional concentration coefficient, K, (x 10 ⁶) for the drainage flow test	33
6.1	Velocity, CO ₂ and temperature profiles at Site R - drainage flow	34
6.2	Velocity, CO ₂ and temperature profile at sampling Site 16 - drainage flow	35

LIST OF FIGURES

<u>Figure</u>		<u>Page</u>
A-1	Concentration, χ (ppb) versus nondimensional concentration coefficient K for an input steam concentration equivalent to 100 ppb H ₂ S	22
1.1-1	Map showing location of cooling tower sites for Unit 19	37
1.1-2	Wind rose from meteorological station (SRI-2), near Units 13 and 14 on Anderson Ridge	38
2.1-1	Reynolds number at which flow becomes independent of Reynolds number for prescribed relative roughness	39
3.1-1	Photograph of cooling tower model (Scale 1:1920)	40
3.1-2	Photograph of terrain model in the Environmental Wind Tunnel	40
3.1-3	Sampling location key for the 198° wind direction	41
3.1-4	Sampling location key for the 325° wind direction	42
3.2-1	Environmental Wind Tunnel	43
3.3-1	Schematic of plume visualization equipment	44
3.4-1	Schematic of tracer gas sampling system	45
3.4-2	Calibration curve for the CARLE gas chromatograph	46
3.5-1	Calibration curve for Datametric (DM) Model 800 Linear Flow Meter	47
3.5-2	Calibration curve for TSI hot-film sensor - a) 325° wind tunnel tests; b) 198° wind tunnel tests	48
3.5-3	Wind tunnel calibration for a) 325° wind direction and b) 198° wind direction	49
3.6-1	Picture of drainage flow test set up	50
4.1-1	Plume visualization for Unit 19, Site R for wind speeds of a) 3.0, b) 4.2, c) 8.1 and d) 11.1 m/s and a 198° wind direction	51

LIST OF FIGURES (continued)

<u>Figure</u>		<u>Page</u>
4.1-2	Plume visualization for Unit 19, Site Q for wind speeds of a) 3.0, b) 4.2, c) 8.1 and d) 11.1 m/s and a 198° wind direction	52
4.1-3	Plume visualization for Unit 19, Site H for wind speeds of a) 3.0, b) 4.2, c) 8.1 and d) 11.1 m/s and a 198° wind direction	53
4.1-4	Plume visualization for Unit 19, Site R for wind speeds of a) 3.0, b) 4.2, c) 8.1 and d) 11.1 m/s and a 325° wind direction	54
4.1-5	Plume visualization for Unit 19, Site Q for wind speeds of a) 3.0, b) 4.2, c) 8.1 and d) 11.1 m/s and a 325° wind direction	55
4.1-6	Plume visualization for Unit 19, Site H for wind speeds of a) 4.2, b) 8.1 and c) 11.1 m/s and a 325° wind direction	56
4.2-1	Visualization of drainage flow field and smoke from Site Q	57
5.1-1a	Isopleths ($\times 10^5$) of nondimensional concentration coefficient K for Unit 19, Site R and a wind speed of 3.0 m/s for the 198° wind direction	58
5.1-1b	Isopleths ($\times 10^5$) of nondimensional concentration coefficient K for Unit 19, Site R and a wind speed of 4.2 m/s for the 198° wind direction	59
5.1-1c	Isopleths ($\times 10^5$) of nondimensional concentration coefficient K for Unit 19, Site R and a wind speed of 8.1 m.s for the 198° wind direction	60
5.1-1d	Isopleths ($\times 10^5$) of nondimensional concentration coefficient K for Unit 19, Site R and a wind speed of 11.1 m/s for the 198° wind direction	61
5.1-2a	Isopleths ($\times 10^5$) of nondimensional concentration coefficient K for Unit 19, Site Q and a wind speed of 3.0 m/s for the 198° wind direction	62
5.1-2b	Isopleths ($\times 10^5$) of nondimensional concentration coefficient K for Unit 19, Site Q and a wind speed of 4.2 m/s for the 198° wind direction	63
5.2-2c	Isopleths ($\times 10^5$) of nondimensional concentration coefficient K for Unit 19, Site Q and a wind speed of 8.1 m/s for the 198° wind direction	64

LIST OF FIGURES (continued)

<u>Figure</u>		<u>Page</u>
5.1-2d	Isopleths ($\times 10^5$) of nondimensional concentration coefficient K for Unit 19, Site Q and a wind speed of 11.1 m/s for the 198° wind direction . . .	65
5.1-3a	Isopleths ($\times 10^5$) of nondimensional concentration coefficient K for Unit 19, Site H and a wind speed of 3.0 m/s for the 198° wind direction	66
5.1-3b	Isopleths ($\times 10^5$) of nondimensional concentration coefficient K for Unit 19, Site H and a wind speed of 4.2 m/s for the 198° wind direction	67
5.1-3c	Isopleths ($\times 10^5$) of nondimensional concentration coefficient K for Unit 19, Site H and a wind speed of 8.1 m/s for the 198° wind direction	68
5.1-3d	Isopleths ($\times 10^5$) of nondimensional concentration coefficient K for Unit 19, Site H and a wind speed of 11.1 m/s for the 198° wind direction . . .	69
5.1-4a	Isopleths ($\times 10^5$) of nondimensional concentration coefficient K for Unit 19, Site R and a wind speed of 3.0 m/s for the 325° wind direction	70
5.1-4b	Isopleths ($\times 10^5$) of nondimensional concentration coefficient K for Unit 19, Site R and a wind speed of 4.2 m/s for the 325° wind direction	71
5.1-4c	Isopleths ($\times 10^5$) of nondimensional concentration coefficient K for Unit 19, Site R and a wind speed of 8.1 m/s for the 325° wind direction	72
5.1-4d	Isopleths ($\times 10^5$) of nondimensional concentration coefficient K for Unit 19, Site R and a wind speed of 11.1 m/s for the 325° wind direction . . .	73
5.1-5a	Isopleths ($\times 10^5$) of nondimensional concentration coefficient K for Unit 19, Site Q and a wind speed of 3.0 m/s for the 325° wind direction	74
5.1-5b	Isopleths ($\times 10^5$) of nondimensional concentration coefficient K for Unit 19, Site Q and a wind speed of 4.2 m/s for the 325° wind direction	75
5.1-5c	Isopleths ($\times 10^5$) of nondimensional concentration coefficient K for Unit 19, Site Q and a wind speed of 8.1 m/s for the 325° wind direction	76

LIST OF FIGURES (continued)

<u>Figure</u>		<u>Page</u>
5.1-5d	Isopleths ($\times 10^5$) of nondimensional concentration coefficient K for Unit 19, Site Q and a wind speed of 11.1 m/s for the 325° wind direction . . .	77
5.1-6a	Isopleths ($\times 10^5$) of nondimensional concentration coefficient K for Unit 19, Site H and a wind speed of 3.0 m/s for the 325° wind direction	78
5.1-6b	Isopleths ($\times 10^5$) of nondimensional concentration coefficient K for Unit 19, Site H and a wind speed of 4.2 m/s for the 325° wind direction	79
5.1-6c	Isopleths ($\times 10^5$) of nondimensional concentration coefficient K for Unit 19, Site H and a wind speed of 8.1 m/s for the 325° wind direction	80
5.1-6d	Isopleths ($\times 10^5$) of nondimensional concentration coefficient K for Unit 19, Site H and a wind speed of 11.1 m/s for the 325° wind direction . . .	81
5.2-1a	Isopleths ($\times 10^6$) of nondimensional concentration coefficient K for Unit 19, Site H, nighttime drainage flow	82
5.2-1b	Isopleths ($\times 10^6$) of nondimensional concentration coefficient K for Unit 19, Site R, nighttime drainage flow	83
5.2-1c	Isopleths ($\times 10^6$) of nondimensional concentration coefficient K for Unit 19, Site Q, nighttime drainage flow	84
6.1-1	Velocity field plotted on a terrain cross section for the drainage flow test	85
6.1-2	CO ₂ distributions plotted on a terrain cross section for the drainage flow test	86
6.1-3	Temperature profile plotted on a terrain cross section for the drainage flow tests	87

LIST OF SYMBOLS

<u>Symbol</u>	<u>Definition</u>	<u>Dimensions</u>
(Roman)		
D	Stack diameter	(L)
E	Gas chromatograph response	(mvs)
Fr	Froude number $\left(\frac{v^2}{gD}\right)$	(-)
g	Gravitational constant	(L/T ²)
Gr	Grashof number $\left(\frac{Re^2}{Ri}\right)$	(-)
h	Cooling tower height	(L)
H	Height of terrain above cooling tower elevation or to top of boundary layer	(L)
H _m	Height of maximum velocity above ground level	(L/T)
k	von Kármán constant	(-)
K	Concentration coefficient $\left(\frac{\chi V_a D^2}{\Lambda Q_s}\right)$	(-)
L _o	Distance from beginning of wind tunnel or length scale	(L)
Q _s	Source strength	(M/T)
R	Exhaust velocity ratio (V _s /V _a)	(-)
Re	Reynolds number $\left(\frac{VL_o}{\nu}\right)$	(-)
Ri _T	Bulk Richardson number based on top of drainage flow layer	
	$\left[\left(\frac{g}{T} \frac{T_\infty - T_{max}}{V_{max}^2} (H - H_m)\right)\right]$	(-)

LIST OF SYMBOLS (continued)

<u>Symbol</u>	<u>Definition</u>	<u>Dimensions</u>
(Roman)		
Ri_D	Bulk Richardson number based on height to maximum drainage flow velocity	$\left[\frac{g}{\bar{T}} \frac{(T_{max} - T_g)(H_m)}{V_{max}^2} \right]$ (-)
Ri	Gradient Richardson number	$\left(\frac{g}{\bar{T}} \frac{\frac{\partial \theta}{\partial z}}{\left(\frac{\partial V}{\partial z} \right)^2} \right)$ (-)
T	Temperature	(θ)
U_*	Friction velocity	(L/T)
V	Ambient velocity	(L/T)
V_s	Stack exit velocity	(L/T)
x, y	General coordinates--downwind, lateral	(L)
z_o	Surface roughness parameter	(L)
(Greek Symbols)		
γ	Density ratio $\left(\frac{\rho_a - \rho_s}{\rho_a} \right)$	(-)
δ	Boundary layer thickness	(L)
Δ	Difference	(-)
θ	Potential temperature	(θ)
Λ	Volume flow rate	(L ³ /T)
μ	Dynamic viscosity	M/(TL)
ν	Kinematic viscosity	(L ² /T)
ρ	Density	(M/L ³)
σ	Standard deviation of either plume dispersion or wind angle fluctuations	(L) (-)
τ	Sampling time	(T)

LIST OF SYMBOLS (continued)

<u>Symbol</u>	<u>Definition</u>	<u>Dimensions</u>
(Greek Symbols)		
χ	Local mean concentration	(M/L ³ or ppm)
Ω	Angular velocity	(1/T)
(Subscripts)		
a	Meteorological tower	
FS	Free stream	
g	Ground level	
m	Model	
max	Maximum	
p	Prototype	
rms	Root-mean-square	
s	Stack	
∞	Reference value or top of thermal boundary layer	

CONVERSION TABLE

(English to Metric Units)

Multiply Units	by	To Obtain
inches	2.540	centimeters
square inches	6.452	square centimeters
cubic inches	16.39	cubic centimeters
feet	0.3048	meters
square feet	0.0929	square meters
cubic feet	0.02832	cubic meters
feet/second	0.3048	meters/second
miles/hour	0.4470	meters/second
cubic feet/minute	0.02832	cubic meters/minute
cubic feet/minute	0.00047	cubic meters/second

1.0 INTRODUCTION

The purpose of this study was to determine the transport characteristics of hydrogen sulfide (H_2S) released in plumes emanating from cooling towers at three possible locations for Unit 19 in the Geysers Geothermal Area. The location of these cooling towers is shown in Figure 1.1-1 in relation to Anderson Springs and Whispering Pines. Using 1:1920 scale models of the cooling towers and surrounding topography in a wind tunnel the dispersion characteristics were studied under neutral stratification for the southwest and northwest wind directions. Tests were also conducted for the northwest wind direction under simulated nighttime drainage flow conditions.

Downwind ground level H_2S concentrations were determined by sampling tracer gases (propane, ethane and methane) released from the model cooling towers. Overall plume geometry was obtained by photographing the plumes made visible by releasing smoke (titanium tetrachloride) from the sources.

The primary focus of this study was on the H_2S concentrations in the vicinity of Anderson Springs and Whispering Pines for neutral thermal stratification and only in the vicinity of Anderson Springs for drainage flow conditions. The ridgeline and free air winds were confined to the 198° and 325° azimuths. Figure 1.1-2 shows the wind rose which was obtained from the meteorological tower in the vicinity of Anderson Ridge (SRI-Station 2). Information from the meteorological station indicated that winds in the sector containing 198° occur approximately 0.5 percent of the time and winds in the sector containing 325° occur approximately 3 percent of the time. Wind speeds of 3.0,

4.2, 8.1 and 11.1 m/s at site Q were modeled to obtain representative concentrations under beneficial and adverse plume rise conditions.

Included in this report are a brief description of the similarity requirements for atmospheric motion, an explanation of test methodology and procedures, results of plume visualization and concentration measurements, and results of wind flow measurements.

This report is supplemented by a motion picture (in color) which shows plume behavior for the various wind speeds studied. Black and white photographs as well as slides of each plume visualization further illustrate the material presented.

2.0 SIMULATION OF ATMOSPHERIC MOTION

2.1 Neutral Stratification

The use of wind tunnels for model tests of gas diffusion by the atmosphere is based upon the concept that nondimensional concentration coefficients will be the same at corresponding points in the model and the prototype and will not be a function of the length scale ratio. Concentration coefficients will only be independent of scale if the wind tunnel boundary layer is made similar to the atmospheric boundary layer by satisfying certain similarity criteria. These criteria are obtained by inspectional analyses of physical statements for conservation of mass, momentum, and energy. Detailed discussions have been given by Halitsky (1963), Martin (1965), and Cermak et al. (1966). Basically, the model laws may be divided into requirements for geometric, dynamic, thermic, and kinematic similarity. In addition, similarity of upwind flow characteristics and ground boundary conditions must be achieved. A detailed discussion of the similarity requirements for this study is found in Cermak and Petersen (1977) and will not be repeated here.

To summarize, the following scaling criteria were applied for the neutral boundary layer simulation:

1. $Fr = \frac{V^2}{g\gamma D}$; $(Fr)_m = (Fr)_p$,
2. $R = \frac{V_s}{V_a}$; $R_m = R_p$,
3. $L_o/K_s > 300$ (implies Reynolds number independence),
4. $\left(\frac{z_o}{H}\right)_m = \left(\frac{z_o}{H}\right)_p$,

5. Similar geometric dimensions, and
6. Similar velocity and turbulence profiles upwind.

2.2 Drainage Flow--Stable Stratification

In this instance the wind patterns are achieved by reproducing density differences caused by heating or cooling topographic surfaces. Because surface-air temperature differences are not known with precision, a physical model can be expected to provide only a first approximation to the flow field and related dispersion of H_2S .

The similarity requirements for the drainage flow test in addition to the geometrical similarities, include equality of the following parameters:

1. $Fr = \frac{V_a^2}{g\gamma D}$; $(Fr)_m = (Fr)_p$
2. $R = V_s/V_a$; $R_m = R_p$
3. $Gr = \frac{g H^3 (T_\infty - T_g)}{v_a^2 \bar{T}}$

The Grashof number (Gr) is the ratio squared of a representative buoyancy force to a representative viscous force.

Because of the small scale, 1:1920, equality of Grashof numbers for model and prototype cannot be achieved. However, as in the case of flow dependence on Reynolds number, the flow is expected to become invariant at a Grashof number much smaller in magnitude than the full-scale Grashof number. Unfortunately, data on heat transfer coefficients for rough surfaces is not as extensive as for drag coefficients. Because of this it is not possible to determine at this time what the minimum value of the Grashof number is for flow invariance.

The Grashof number is also equal to the Reynolds number squared divided by the Richardson number, or,

$$Gr = \frac{Re^2}{Ri}$$

If the following parameters are defined:

$$Re = \frac{V_{\max} H_m}{\nu_a}$$

$$Ri_T = \frac{g}{\bar{T}_1} \frac{(T_\infty - T_{\max})(H - H_m)}{V_{\max}^2}$$

$$Ri_D = \frac{g}{\bar{T}_2} \frac{(T_{\max} - T_g)(H_m)}{V_{\max}^2}$$

where

V_{\max} = the maximum drainage flow velocity at a given location

H_m = height of the maximum velocity above ground level

H = height of thermal boundary layer

T_∞ = temperature at top of thermal boundary layer

T_{\max} = temperature at height of maximum velocity

T_g = temperature at surface

\bar{T}_1 and \bar{T}_2 = average temperature over appropriate height interval, then it is hypothesized that once the drainage flow has developed, the Richardson number can be used to categorize the flow, and provide a relation between model and prototype test conditions. This seems a logical hypothesis since it effectively says that if the Reynolds number is high enough, the flow will be similar in model and prototype. Tables 2.1 and 2.2 summarize the model and prototype parameters for both the neutral and drainage flow tests. For the drainage flow tests the prototype conditions were derived from the observed conditions over the model.

3.0 EXPERIMENTAL METHOD

3.1 Model

The cooling towers were modeled at a scale of 1:1920. The relevant building dimensions are given in Table 2.1 and a photograph of the model is shown in Figure 3.1-1.

Topography was modeled to the same scale by cutting Styrofoam sheets of 0.6 cm and 1.27 cm thicknesses to match contour lines of a topographic map enlarged to the 1:1920 scale. The scale model of the topography is shown mounted in the wind tunnel in Figure 3.1-2. The model terrain was not smoothed so as to increase the surface roughness and thereby prevent the formation of a laminar sublayer. This increased roughness also contributed toward achieving Reynolds number independence of flow over the test section.

An array of sampling tubes was inserted into the model terrain to give a minimum of 30 representative sampling locations. The sampling locations are shown in Figures 3.1-3 and 3.1-4 and enumerated in Tables 3.1 and 3.2.

Metered quantities of gas were allowed to flow from the cooling tower to simulate the exit velocity. Helium, compressed air, and propane, ethane, or methane (the tracers) were mixed to give the highest practical specific weight. Fischer-Porter flow meter settings were adjusted for pressure, temperature, and molecular weight effects as necessary. When a visible plume was required, the gas was bubbled through titanium tetrachloride before emission.

3.2 Wind Tunnels and Scale Models

The Environmental Wind Tunnel (EWT) shown in Figure 3.2-1 was used for the neutral flow study. This wind tunnel, especially designed to study atmospheric flow phenomena, incorporates special features such as adjustable ceiling, rotating turntables, transparent boundary walls, and a long test section to permit adequate reproduction of micrometeorological behavior. Mean wind speeds of 0.3 to 11.6 m/s in the EWT can be obtained. In the EWT, boundary layers 1.4m thick over the downstream 12.2 meters can be obtained with the use of vortex generators at the test section entrance. The flexible test section roof on the EWT is adjustable in height to permit the longitudinal pressure gradient to be set approximately equal to zero.

3.3 Flow Visualization Techniques

Smoke was used to define plume behavior from the three cooling towers. The smoke was produced by passing the air mixture through a container of titanium tetrachloride located outside the wind tunnel (or test area) and transported through the tunnel wall by means of a tygon tube terminating at the cooling tower inlet. A schematic of the process is shown in Figure 3.3-1.

The plume was illuminated with arc-lamp beams and a visible record was obtained by means of pictures taken with a Speed Graphic camera. Additional still pictures were obtained with a Hasselblad camera. A series of 16 mm color motion pictures was also taken with a Bolex motion picture camera.

3.4 Gas Tracer Technique

After the desired atmospheric conditions were obtained, a mixture of helium and a tracer of predetermined concentration was released from the cooling tower at the required rate to simulate prototype plume rise. Samples of gas were withdrawn from the sample points and analyzed. The flow rate of the propane, ethane or methane mixture was controlled by a pressure regulator at the supply cylinder outlet and monitored by a precision flow meter. The sampling system is shown in Figure 3.4-1.

A more complete discussion of the gas sampling and analysis techniques is given in Cermak and Petersen (1977). All concentration data presented herein are in dimensionless form. Appendix A enumerates the procedures for converting the data to prototype concentrations.

For the drainage flow tests the same gas sampling procedures as discussed above were used for the ground level tracer gas measurements. To measure the vertical distribution of CO_2 (for converting the velocity measurements) a Carle Thermal Conductivity Gas Chromatograph was used. A calibration of this instrument was performed by injecting a known concentration of CO_2 into the sensor and measuring the voltage response. Figure 3.4-2 shows the calibration curve.

3.5 Wind Profile Measurements

The following instruments were used during the course of this study to measure velocity:

1. A Model 800 LV Datametrics Linear Flow Meter with Probe-- used for the drainage flow tests.
2. Thermo System (TSI Model 1050) constant temperature hot-film anemometer--used for the neutral tests.

The Datametrics is a linear mass flow meter which is sensitive down to 0.03 m/s. Hence, this probe was used for the drainage flow

tests where very low wind speeds could be expected. A calibration curve shown in Figure 3.5-1 at low velocities was obtained using a TSI calibrator. The curve is assumed linear above the range of calibration. A velocity profile was measured at Site R and sampling location 16 (see Figure 3.1-3 for location). The Datametric readings were corrected for density variations by referring to the measured temperature and CO₂ profiles.

The TSI hot-film anemometer was used for the neutral flow test in the EWT. Calibration of the anemometer was also carried out with a TSI calibrator. The calibration measurements were correlated to King's law and put in the following form:

$$E^2 = A + BV^n$$

where

E = the output signal of the wire (mv),

V = the velocity sensed (m/s), and

n, A and B = the constants of King's law.

The coefficients A, B, and n for the velocity range from 0.25 to 2.5 m/s were found to be

A = 5.05 B = 1.442 n = 0.67 for 198° azimuth, and

A = 4.72 B = 1.78 n = 0.60 for 325° azimuth.

King's law fit to the calibration of the hot-film is shown in Figure 3.5-2.

To set the wind tunnel conditions the velocity at Site Q (1.3 cm above the modeled terrain) was correlated to the upwind freestream velocity. The velocity at Site Q was measured with the TSI hot-film anemometer for both the 198° and 325° wind directions while the freestream velocity was measured with the Datametrics. The curve

relating the two (Site Q versus freestream) is shown in Figure 3.5-3. Thus the desired speed at Site Q was obtained by varying the freestream velocity. Also shown in the figures are the Datametrics reading versus the wind speed 0.6 cm above Cobb Mountain for the 325° wind direction and 0.6 cm above the meteorological tower location for the 198° wind direction.

3.6 Drainage Flow--Special Considerations

For the drainage flow tests the model was isolated in order to minimize any unwanted drafts. The entire surface was covered with a fine rock layer (0.6 cm) in order to maintain a cold surface temperature for an extended period of time. Figure 3.6-1 shows the model and enclosure.

Dry ice blocks (frozen CO₂) were placed uniformly on the model and thereafter it was covered with a tarp and left overnight to obtain maximum cooling. Prior to testing the tarp was removed and the remaining dry ice was placed on the high ground to act as a source of cold air.

Surface temperature was monitored at Site R and 20 cm above Cobb Mountain throughout all tests. The temperature, velocity and CO₂ profiles taken at Site R and sampling location 16 to document the drainage flow conditions are given in Figures 6.1-1, -2 and -3.

4.0 TEST PROGRAM RESULTS--VISUALIZATION

4.1 Neutral Atmosphere

The visualization test results consist of photographs and movies showing the plume behavior for Unit 19, Sites R, Q, and H for the northwest and southwest wind directions and four wind speeds.

The sequence of photographs in Figures 4.1-1 to 4.1-3 shows the plume behavior from Sites H, Q, and R for the 198° wind direction and full-scale wind speeds at Site Q (prototype height = 24 m, AGL) of 3.0, 4.2, 8.1 and 11.1 m/s. Figures 4.1-4 to 4.1-6 show a similar sequence of photographs for the 325° wind direction. For the light wind speed cases (3.0 m/s) the plumes remained elevated downwind of the stack. However, as the wind speed increased, the plume altitude decreased, and for the high wind speeds, tended to follow the terrain confluences. For wind speeds of 8.1 and 11.1 m/s the plumes emanating from the cooling tower appeared to flow along the terrain at a relatively low effective plume altitude.

Complete sets of still photographs supplement this report. Color motion pictures have been arranged into titled sequences and the sets available are given by photograph number in Table 4.1.

4.2 Drainage Flow

The visualization test results for this phase of the project consist of a series of photographs and movies showing the plume behavior for Unit 19, Sites R and Q for the northwest wind direction and one wind speed. No visualization was obtained for Site H since the sampling lines became clogged during the testing. Figure 4.2-1 shows the smoke from Site Q. The smoke from Site Q appeared to penetrate the stable drainage flow layer due to its location on a small hill whereas the

plume from Site R was trapped and flowed down the slope toward Anderson Springs. For Site R, both the photographs and movies did not show the plume behavior clearly due to the CO₂ vapor masking the plume. Hence, no figure showing plume behavior is presented and the plume description is based only on visual observation.

Color motion pictures were taken from the northeast side of the valley and looking down the valley from atop Cobb Mountain.

5.0 TEST PROGRAM RESULTS--CONCENTRATION MEASUREMENTS

The diffusion of gaseous effluents from the three model cooling towers was studied for drainage flow (one wind direction) and for a neutral atmosphere (two wind directions--198° and 325° azimuth). A different tracer material was released from each model site (propane from Site R, ethane from Site Q, and methane from Site H). Concentrations of the tracer were measured at 32 locations in the vicinity of Anderson Springs and Whispering Pines. The sampling arrays are shown in Figures 3.1-3 and 3.1-4 and prototype locations for all sampling points are summarized in Tables 3.1 and 3.2. The zero coordinate is located at Site R for all figures.

All concentration data have been reported in dimensionless form as explained in Cermak and Petersen (1977). To convert from a dimensionless concentration coefficient, K , to a prototype H_2S concentration, refer to Appendix A.

5.1 Neutral Atmosphere

The concentration results are summarized for the two wind directions in Tables 5.1 through 5.6. In order to visually and quantitatively assess the effect of wind speed and site location on ground level concentration patterns for these wind directions, Figures 5.1-1 through 5.1-6 were prepared. These figures show isopleths of the dimensionless coefficient, K , for each site and wind speed studied. The maximum nondimensional concentration occurs with either an 8.1 or 11.1 m/s wind speed depending upon the site.

Based on Figures 5.1-1 through 5.1-6, the highest K values near Whispering Pines and associated wind speed for each site are approximately:

Site R	10×10^{-5} (8.1 m/s)
Site Q	20×10^{-5} (11.1 m/s)
Site H	50×10^{-5} (11.1 m/s).

Near Anderson Springs the maximum K values achieved were approximately:

Site R	10×10^{-5} (11.1 m/s)
Site Q	20×10^{-5} (8.1 m/s)
Site H	50×10^{-5} (11.1 m/s).

Hence it appears that Site R gave the least H_2S impact near Anderson Springs or Whispering Pines and Site H the greatest impact.

5.2 Drainage Flow

The concentration results for this test are summarized in Table 5.7. Sample locations are defined in Table 3.2 and Figure 3.1-4. Figure 5.2-1 shows the isopleths of the dimensionless coefficient, K, for each site studied. The figure shows that the maximum isopleth magnitudes were reduced by nearly two orders of magnitude over that observed for the neutral tests. The highest concentrations are generally observed on the high terrain to the south of Anderson Springs. All concentration levels measured in the wind tunnel were extremely small and close to the background values for methane, ethane, and propane. Hence local variations in background tracer concentration could produce errors in the data. The largest errors due to background variation are for methane (Site H) and the least error for ethane (Site Q) which has nearly a zero background.

Based on Figure 5.2-1 the highest K values near Anderson Springs for each site are approximately:

Site R	0.05×10^{-5}
Site Q	0.10×10^{-5}
Site H	0.20×10^{-5}

These values are extremely low and suggest that the stable drainage flow condition (with no superimposed upper level wind) will give negligible impact in Anderson Springs.

6.0 DRAINAGE FLOW--VELOCITY, TEMPERATURE AND CO₂ DISTRIBUTIONS

A part of the drainage flow test scenario included obtaining vertical distributions of velocity, temperature, and CO₂ to document the depth and nature of the flow field. Vertical profiles of the three parameters were obtained at Site R and sampling location 16.

Tables 6.1 and 6.2 enumerate the results.

To visually assess the character of the flow the vertical velocity, CO₂, and temperature distribution are plotted in Figures 6.1-1 through 6.1-3 on a vertical terrain cross section taken through a straight line connecting Cobb Mountain, Site R and sampling location 16. The velocity profiles in Figure 6.1-1 show a peak velocity approximately 50 m above the ground at Site R and at sampling location 16. The depth of the disturbed flow is about 200 m at Site R and grows to approximately 400 m at sampling location 16. [Note: velocities of approximately 0.03 m/s may be considered equal to zero due to the instrument threshold.] The CO₂ distribution (Figure 6.1-2) also shows a similar depth for the disturbed flow. The ground level CO₂ concentrations were on the order of 7 percent CO₂. The thermal boundary layer, as shown in Figure 6.1-3, ranged from 200 m in depth at Site R to 400 m at sampling location 16.

In general the results of this section show what would be expected of a nighttime drainage flow situation with no upper level wind (Sutton, 1953). The velocity increases with height above the ground until it reaches a maximum and then decreases to zero again at some finite height. The temperature is cold at the surface and gradually approaches a warmer free stream value.

REFERENCES

- Cermak, J. E., "Laboratory Simulation of the Atmospheric Boundary Layer," AIAA Journal, Vol. 9, No. 9, September 1971, pp. 1746-1754.
- Cermak, J. E. and R. L. Petersen, "Atmospheric Transport of Hydrogen Sulfide from Proposed Geothermal Power Plant (Unit 16) Predictions by Physical Modeling in a Wind Tunnel," Colorado State University, CER76-77JEC-RLP47, March 1977.
- Halitsky, J., "Gas Diffusion near Buildings," Geophysical Sciences Laboratory Report No. 63-3, New York University, February 1963.
- Martin, J. E., "The Correlation of Wind Tunnel and Field Measurements of Gas Diffusion Using Kr-85 as a Tracer," Ph.D. Thesis, MMPP 272, University of Michigan, June 1965.
- Sutton, O. G., Micrometeorology - McGraw-Hill Book Company, Inc., 1953.

APPENDIX A

Method for Calculating Prototype Concentrations
From Nondimensional Concentration Coefficient K

● Basic Equation:

$$K = \frac{\chi V_a D^2}{\Lambda Q_s} \text{ Prototype}$$

where

$K \equiv$ nondimensional concentration coefficient from wind tunnel study

$\chi \equiv$ H_2S concentration (ppm)

$V_a \equiv$ wind speed at the meteorological station (m/s)

$D \equiv$ cell diameter (equal to 8.5 m)

$\Lambda \equiv$ total volume flow (use $4313 \text{ m}^3/\text{s}$)

$Q_s \equiv$ equivalent H_2S concentration in the incoming stack gas [(ppm) (1²- fraction removed)]

● Now solving for $\chi_{\text{prototype}}$:

$$\begin{aligned} \chi_{\text{prototype}} &= K \frac{\Lambda Q_s}{V_a D^2} \\ &= 59.7 \frac{K Q_s}{V_a} \end{aligned}$$

● Example:

let $K = 20 \times 10^{-5}$

$Q_s = 10 \text{ ppm}$

$V_a = 9.8 \text{ m/s}$

then $\chi_{\text{prototype}} = \frac{(59.7)(20 \times 10^{-5})(10)}{9.8} = 0.012 \text{ ppm}$

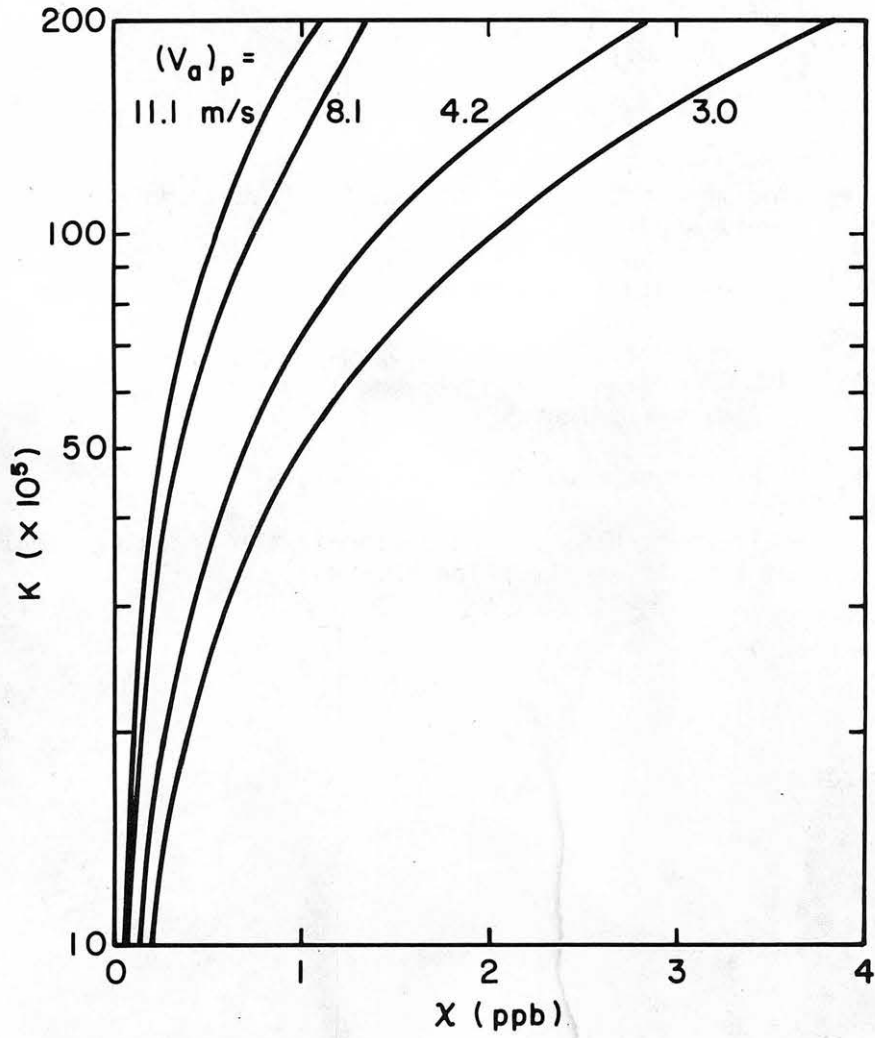


Figure A-1. Concentration, $\chi(\text{ppb})$, versus nondimensional concentration coefficient K for an input steam concentration equivalent to 100 ppb H_2S .

T A B L E S

Table 2.1. Model and prototype dimensional parameters, Unit 19, Sites R, Q, H.

Parameter	Prototype	Model
•Neutral Flow		
1. Building		
a. length (l)	98 m	5.1 cm
b. width (w)	21.5	1.1 cm
c. height (h)	20 m	1.0 cm
2. Exit Temperature (T_s)	319°K	293°K
3. Cell Diameter (D)	8.5	0.44 cm
4. Number of Cells	10	10
5. Exit Velocity (V_s)	7.6 m/s	0.49 m/s
6. Volumetric Emission Rate (Λ)	4312.6 m ³ /s	74.51 cc/s
7. Gas Density (ρ_s)	0.97 kg/m ³	0.21 kg/m ³
8. Ambient Density (ρ_a)	1.08	1.02
9. Wind Speed at Site Q (V_a)	3.0, 4.2, 8.1, 11.1 m/s	0.19, 0.27, 0.52, 0.71 m/s
10. Wind Directions	Northwest, Southwest	Northwest, Southwest
11. Surface Roughness (z_o)	0.5 m	0.02 cm
12. Ambient Pressure	900 mb	850 mb
13. Ambient Temperature	293°K	293 °K
14. Virtual Temperature Increment	2.92°C	N/A
•Drainage Flow*		
1. Free Stream Temperature (T_∞)	297.6°K	21°C
2. Surface Temperature (T_g)	291.9°K	-20°C
3. Temperature at V_{max} (T_{max})	293.0°K	-12°C
4. Average Temperature		
$\bar{T}_1 = (T_\infty + T_g)/2$	295.3°K	273.5°K
$\bar{T}_2 = (T_m + T_g)/2$	292.4°K	257°K
5. Maximum Velocity at Site R (V_{max})	5.5 m/s	0.35 m/s
6. Depth to (V_{max}) (H_m)	48.0 m	2.5 cm
7. Depth to Free Stream (H)	780.0 m	40.6 cm
8. Viscosity (ν_a)	$0.144 \times 10^{-4} \text{ m}^2/\text{s}$	$0.12 \times 10^{-4} \text{ m}^2/\text{s}$
9. Velocity at Cooling Tower Height	4.4 m/s	0.28 m/s

* The prototype parameters were estimated from the scaling laws $[(Fr)_m = (Fr)_p]$;
 $(Ri_T)_m = (Ri_T)_p$; $(Ri_D)_m = (Ri_D)_p$.

Table 2.2. Model and prototype dimensionless parameters, Unit 19, Sites R, Q, H.

Parameter	Prototype	Model
Neutral Flow		
1. $\frac{\delta}{H}$	1.84	2.15
2. $\frac{z_o}{H}$	2.0×10^{-3}	1.5×10^{-3}
3. $\frac{D}{H}$	3.5×10^{-2}	3.5×10^{-2}
4. $\frac{h}{H}$	1.6×10^{-2}	1.6×10^{-2}
5. $R = \frac{V_s}{V_a}$	2.5, 1.8, 0.9, 0.7	2.5, 1.8, 0.9, 0.7
6. $Fr = \frac{V_a^2}{g\gamma D}$	1.1, 2.1, 7.9, 14.8	1.1, 2.1, 7.9, 14.8
7. $\gamma = \frac{\rho_a - \rho_s}{\rho_a}$	0.10	0.79
Drainage Flow		
1. $Gr = \frac{g H^3 (T_\infty - T_g)}{\bar{T}_1 \nu_a^2}$	4.33×10^{17}	6.83×10^8
2. $Re = \frac{V_{\max} H_m}{\nu_a}$	1.83×10^7	7.29×10^2
3. $Ri_T = \frac{g(H-H_m)(T_\infty - T_m)}{\bar{T}_1 V_{\max}^2}$	3.68	3.68
4. $Ri_D = \frac{gH_m(T_m - T_g)}{\bar{T}_2 V_{\max}^2}$	0.06	0.06
5. $Fr = \frac{V_a^2}{g\gamma D}$	3.6	3.6
6. $R = V_s/V_a$	1.73	1.75

Table 3.1. Tracer gas sampling location key for the 198° wind direction.

SAMPLE NUMBER	COORDINATES *		
	X (KM)	Y (KM)	Z (M,MSL)
1	0.37	1.24	847.34
2	0.71	1.16	777.24
3	1.71	0.82	633.98
4	0.47	1.56	926.59
5	0.82	1.48	804.67
6	1.82	1.17	646.18
7	0.23	2.02	1118.62
8	0.57	1.91	1030.22
9	0.91	1.81	877.82
10	1.25	1.71	765.05
11	1.65	1.62	682.75
12	1.94	1.49	719.33
13	0.34	2.35	963.17
14	0.68	2.27	890.02
15	1.02	2.18	816.86
16	1.34	2.06	762.00
17	0.91	2.82	957.07
18	0.44	2.73	877.82
19	0.78	2.62	826.01
20	1.12	2.50	792.48
21	1.46	2.41	797.05
22	1.79	2.32	826.01
23	2.13	2.21	841.25
24	2.46	2.07	926.59
25	0.20	3.17	853.44
26	0.53	3.07	810.77
27	0.88	2.96	792.48
28	1.28	2.86	798.58
29	1.55	2.76	816.86
30	0.63	3.40	774.19
31	0.98	3.35	841.25
32	2.34	2.88	969.26

*(0,0) Coordinate at Site R.

Table 3.2. Tracer gas sampling location key for the 325° wind direction.

SAMPLE NUMBER	COORDINATES *		
	X (KM)	Y (KM)	Z (M,MSL)
4	3.21	-1.60	426.72
5	3.19	-1.85	451.10
6	3.20	-2.51	530.35
7	3.19	-3.07	670.56
17	2.74	-1.24	438.91
18	2.72	-1.52	414.53
19	2.72	-1.85	423.67
20	2.70	-2.51	475.49
21	2.70	-3.12	621.79
23	2.46	-0.57	512.11
24	2.45	-1.22	469.39
25	2.45	-1.48	426.72
26	2.45	-1.85	512.06
27	2.44	-3.35	445.01
28	2.47	-3.14	573.02
30	2.18	-0.49	530.35
31	2.18	-1.18	487.68
32	2.15	-1.58	426.72
33	2.13	-1.86	515.11
34	2.11	-2.52	499.87
35	2.18	-3.13	560.83
37	1.77	-0.51	560.83
38	1.77	-1.20	499.87
39	1.77	-1.53	438.91
40	1.77	-1.91	530.35
41	1.76	-2.52	621.79
43	1.44	-0.52	597.41
44	1.39	-1.24	487.68
45	1.37	-1.54	475.49
46	1.37	-1.88	512.06

*(0,0) Coordinate at Site R.

Table 4.1. Summary of photographs taken for the neutral flow tests.

Photograph #	Site	Wind Direction	Prototype Wind Speed (m/s)
1	H	325°	3.0
2			4.2
3			8.1
4			11.1
5	Q		3.0
6			4.2
7			8.1
8			11.1
9	R		3.0
10			4.2
11			8.1
12			11.1
13	H	198°	3.0
14			4.2
15			8.1
16			11.1
17	Q		3.0
18			4.2
19			8.1
20			11.1
21	R		3.0
22			4.2
23			8.1
24			11.1

Table 5.1. Nondimensional concentration coefficient, K , ($\times 10^5$) for Site R and a 198° wind direction.

Location #	Prototype Wind Speed (m/s)			
	3.0	4.2	8.1	11.1
1	1.08	1.46	29.90	25.70
2	2.77	4.20	33.30	75.50
3	--	0.09	4.20	7.08
4	1.28	0.56	33.60	24.50
5	3.56	5.91	12.70	40.90
6	--	0.11	--	--
7	1.28	0.88	13.20	8.77
8	1.56	0.63	32.20	25.20
9	1.68	3.43	3.94	6.29
10	--	--	--	--
11	--	--	--	--
12	--	--	--	--
13	1.45	0.41	19.50	9.82
14	1.56	1.58	11.90	20.10
15	1.36	3.94	0.67	0.80
16	--	--	--	--
17	0.33	0.36	9.67	3.65
18	1.66	1.97	14.10	16.20
19	1.34	5.48	2.08	6.91
20	0.18	1.33	--	--
21	--	--	--	--
22	--	--	--	--
23	--	--	--	--
24	--	--	--	--
25	0.35	0.22	11.80	6.94
26	2.59	1.75	11.90	4.89
27	1.58	4.13	0.56	0.58
28	0.06	0.39	0.47	--
29	--	--	10.90	--
30	2.06	3.59	6.99	9.51
31	0.56	1.51	1.41	0.72
32	--	--	--	--

Table 5.2. Nondimensional concentration coefficient, K , ($\times 10^5$) for Site Q and a 198° wind direction.

Location #	Prototype Wind Speed (m/s)			
	3.0	4.2	8.1	11.1
1	--	--	--	--
2	0.04	0.50	5.46	2.46
3	--	--	0.02	0.30
4	--	--	--	--
5	1.08	4.57	21.20	41.00
6	--	--	--	--
7	0.43	1.01	1.58	0.81
8	--	0.09	0.22	--
9	2.70	8.99	22.70	33.70
10	1.03	8.14	2.24	1.20
11	--	0.07	--	--
12	--	--	--	--
13	0.91	0.33	6.72	3.30
14	1.74	2.02	15.50	17.90
15	3.91	13.20	8.58	17.60
16	0.16	1.91	0.17	0.07
17	0.09	0.15	3.83	1.01
18	0.76	1.09	9.06	5.61
19	3.07	5.89	10.70	14.80
20	1.02	7.55	3.87	0.20
21	0.10	11.68	1.27	--
22	--	--	--	--
23	--	--	--	--
24	--	--	--	--
25	0.12	0.18	4.88	1.85
26	1.68	1.83	10.50	1.92
27	2.73	6.76	9.12	5.96
28	1.59	4.28	8.47	0.46
29	0.13	1.18	4.97	--
30	1.61	3.65	11.80	10.20
31	1.46	3.08	7.26	3.06
32	--	--	0.11	--

Table 5.3. Nondimensional concentration coefficient, K , ($\times 10^5$) for Site H and a 198° wind direction.

Location #	Prototype Wind Speed (m/s)			
	3.0	4.2	8.1	11.1
1	0.07	0.04	0.00	0.00
2	0.00	0.00	0.00	0.00
3	0.79	5.34	7.15	1.29
4	0.00	0.00	0.00	0.00
5	0.00	0.04	0.00	0.00
6	0.94	2.36	1.48	0.12
7	--	0.00	0.00	--
8	--	0.00	0.00	0.00
9	0.00	0.00	1.39	4.54
10	0.68	0.05	23.80	65.90
11	3.34	8.16	39.00	24.50
12	0.69	1.34	0.38	0.00
13	0.00	0.00	0.38	0.31
14	0.10	--	1.20	3.30
15	0.05	0.00	16.40	15.80
16	1.75	1.01	43.90	54.90
17	0.00	0.00	0.67	1.13
18	0.10	0.00	1.36	1.37
19	0.27	0.00	13.30	30.10
20	1.51	1.10	21.60	51.90
21	3.17	3.39	35.60	40.30
22	1.84	5.04	15.20	4.01
23	0.00	1.18	0.19	0.00
24	0.00	0.00	0.00	0.00
25	0.00	0.05	1.26	0.47
26	0.00	--	5.33	0.85
27	0.39	0.17	11.30	32.80
28	2.24	1.21	11.00	41.80
29	2.53	4.45	5.76	20.80
30	0.08	0.00	7.07	14.80
31	0.78	0.18	3.89	24.20
32	0.69	3.67	1.00	0.46

Table 5.4. Nondimensional concentration coefficient, K , ($\times 10^5$) for Site R and a 325° wind direction.

Location #	Prototype Wind Speed (m/s)			
	3.0	4.2	8.1	11.1
4	0.44	--	--	--
5	1.18	0.27	--	0.06
6	3.14	2.11	0.87	2.02
7	0.89	1.23	0.84	1.54
17	0.36	--	--	0.08
18	1.48	0.49	0.07	0.63
19	1.14	2.58	2.47	5.23
20	0.57	3.59	2.13	4.85
21	0.24	2.18	2.46	3.53
23	0.01	--	--	0.00
24	0.78	0.13	0.06	--
25	1.10	2.08	1.72	3.75
26	0.78	3.76	4.16	6.08
27	0.35	3.52	2.99	4.60
28	0.18	3.03	4.75	6.15
30	0.09	--	--	--
31	0.65	0.26	--	0.21
32	0.52	2.88	4.49	8.74
33	0.62	3.86	5.36	9.18
34	0.11	2.21	4.70	6.26
35	0.03	1.54	7.08	6.25
37	1.00	--	0.13	--
38	0.46	1.97	1.44	3.36
39	0.50	2.98	7.60	10.20
40	0.58	3.93	7.11	9.20
41	0.10	1.64	6.80	6.38
43	0.73	0.45	0.70	0.77
44	0.61	3.28	7.58	14.20
45	0.25	4.15	12.20	13.10
46	0.10	3.00	10.60	9.75

Table 5.5. Nondimensional concentration coefficient, K , ($\times 10^5$) for Site Q and a 325° wind direction.

Location #	Prototype Wind Speed (m/s)			
	3.0	4.2	8.1	11.1
4	1.31	0.58	0.61	0.73
5	0.59	1.40	2.21	2.78
6	0.78	3.44	8.52	5.67
7	0.14	1.56	3.80	3.00
17	1.32	0.54	0.60	0.68
18	0.80	1.80	8.23	7.91
19	0.08	2.37	15.30	6.44
20	--	2.96	13.70	6.78
21	--	0.79	3.08	2.64
23	0.60	0.13	--	0.01
24	0.74	0.09	0.04	4.63
25	0.07	2.63	13.00	10.10
26	--	3.22	12.00	7.45
27	--	2.94	10.60	8.34
28	--	0.35	5.45	4.02
30	0.36	0.57	0.50	0.89
31	0.28	2.51	12.20	13.40
32	--	2.37	10.70	7.85
33	--	2.18	7.82	4.34
34	--	0.18	4.18	1.91
35	--	1.87	0.76	0.11
37	0.56	2.42	7.92	10.20
38	0.03	1.09	20.50	19.70
39	--	1.02	5.92	3.73
40	--	2.44	3.94	2.35
41	--	0.02	2.40	1.57
43	0.16	0.43	35.30	37.00
44	0.00	0.08	7.41	3.95
45	--	--	1.95	0.46
46	--	0.35	1.39	0.51

Table 5.6. Nondimensional concentration coefficient, K , ($\times 10^5$) for Site H and a 325° wind direction

Location #	Prototype Wind Speed (m/s)			
	3.0	4.2	8.1	11.1
4	0.85	3.37	5.94	14.30
5	0.48	4.67	11.90	22.70
6	0.66	4.67	15.10	21.50
7	0.22	2.27	5.55	5.71
17	1.11	1.61	7.05	21.30
18	0.49	4.86	26.90	55.70
19	0.09	2.43	15.70	13.70
20	0.02	2.42	14.30	8.47
21	0.01	0.39	1.78	1.49
23	0.06	0.57	0.88	1.71
24	0.47	0.49	0.66	49.80
25	0.03	2.36	22.30	25.40
26	0.00	1.37	5.17	1.60
27	0.00	2.40	11.10	9.10
28	0.00	0.09	3.13	2.36
30	0.00	3.24	7.77	19.40
31	0.07	6.27	34.90	66.00
32	0.02	0.05	2.01	1.65
33	0.00	0.45	0.74	0.49
34	--	0.00	2.10	0.95
35	0.00	0.00	0.17	0.00
37	0.48	12.70	62.60	125.00
38	0.00	0.13	7.41	5.66
39	0.00	0.00	0.02	0.00
40	0.02	0.00	0.60	0.00
41	0.02	0.00	0.97	0.99
43	0.00	3.17	35.80	27.00
44	0.00	0.00	0.82	0.46
45	0.02	0.00	--	--
46	0.00	0.00	0.00	0.00

Table 5.7. Nondimensional concentration coefficient, K , ($\times 10^6$) for the drainage flow test.

Location	Dimensionless Concentration ($\times 10^6$)		
	R (Propane)	Site (Tracer) Q (Ethane)	H (Methane)
4	0.76	1.61	2.78
5	1.39	1.35	0.95
6	0	0	0.37
7	0.19	0.07	1.10
19	0.69	0.67	1.68
20	3.25	0.07	1.10
21	0	0	1.24
24	0.07	0	0.51
26	0.12	0	0.51
27	0	0.07	0.66
30	0.88	0	0.88
31	0.76	0.26	0.29
32	0	0	0
33	0.07	0	2.78
34	0.12	0.13	1.61
35	0	0	0.29
37	0.07	0.13	2.42
38	0	0	0.73
40	0.19	0.20	2.20
* 41	0.23	0.26	4.83
43	1.69	1.28	1.61
* 44	0.59	0.26	2.93
45	0.19	0.13	1.46
46	0.37	0.54	1.83

*Blocked sampling line (data questionable).

Table 6.1. Velocity, CO₂ and temperature profiles at Site R - drainage flow.

Z (m, AGL)	% CO ₂	V (m/s)	$\frac{V}{V_{\max}}$	Z (m,AGL)	T (°K)	$\frac{T - T_g}{T_{FS} - T_g}$
24.4	5.73	0.30	0.86	0.0	245.0	0.00
43.9	3.80	0.35	1.00	12.2	258.0	0.26
64.9	3.24	0.30	0.86	24.4	262.0	0.34
72.2	2.69	0.26	0.74	36.6	267.0	0.44
93.2	1.60	0.21	0.60	48.8	272.0	0.55
108.8	0.80	0.12	0.34	73.2	281.0	0.73
127.3	0.31	0.08	0.23	97.6	284.6	0.80
148.3	0.09	0.00	0.00	146.3	287.0	0.85
172.2	0.00	0.03	0.09	195.1	288.8	0.87
207.3	0.20	0.00	0.00	292.7	291.0	0.93
251.2	0.31	0.00	0.00	390.2	292.0	0.95
				585.4	293.0	0.97
				780.5	293.7	0.98
				975.6	294.5	1.00

Table 6.2. Velocity, CO₂ and temperature profile at sampling location 16 - drainage flow.

Z (m,AGL)	% CO ₂	V (m/s)	$\frac{V}{V_{\max}}$	Z (m,AGL)	T (°K)	$\frac{T - T_g}{T_{FS} - T_g}$
24.4	7.43	0.25	0.89	12.2	251.0	0.12
43.9	7.29	0.28	1.00	31.7	257.5	0.25
71.2	6.86	0.22	0.79	59.0	263.0	0.36
85.4	5.71	0.22	0.79	73.2	265.0	0.40
96.1	5.14	0.18	0.64	83.9	267.0	0.45
114.2	3.43	0.13	0.46	102.0	271.0	0.53
152.2	2.57	0.11	0.39	140.0	274.0	0.59
175.1	2.00	0.12	0.43	162.9	276.5	0.64
201.5	1.86	0.12	0.43	189.3	279.4	0.70
255.6	2.00	0.11	0.39	243.4	284.0	0.79
289.8	1.14	0.10	0.36	277.6	286.3	0.84
342.9	0.14	0.06	0.21	330.7	288.9	0.89
395.1	0.14	0.04	0.14	382.9	290.8	0.93
503.4	0.00	0.05	0.18	491.2	292.6	0.96
817.6	0.00	0.02	0.07	805.4	294.4	1.00

FIGURES



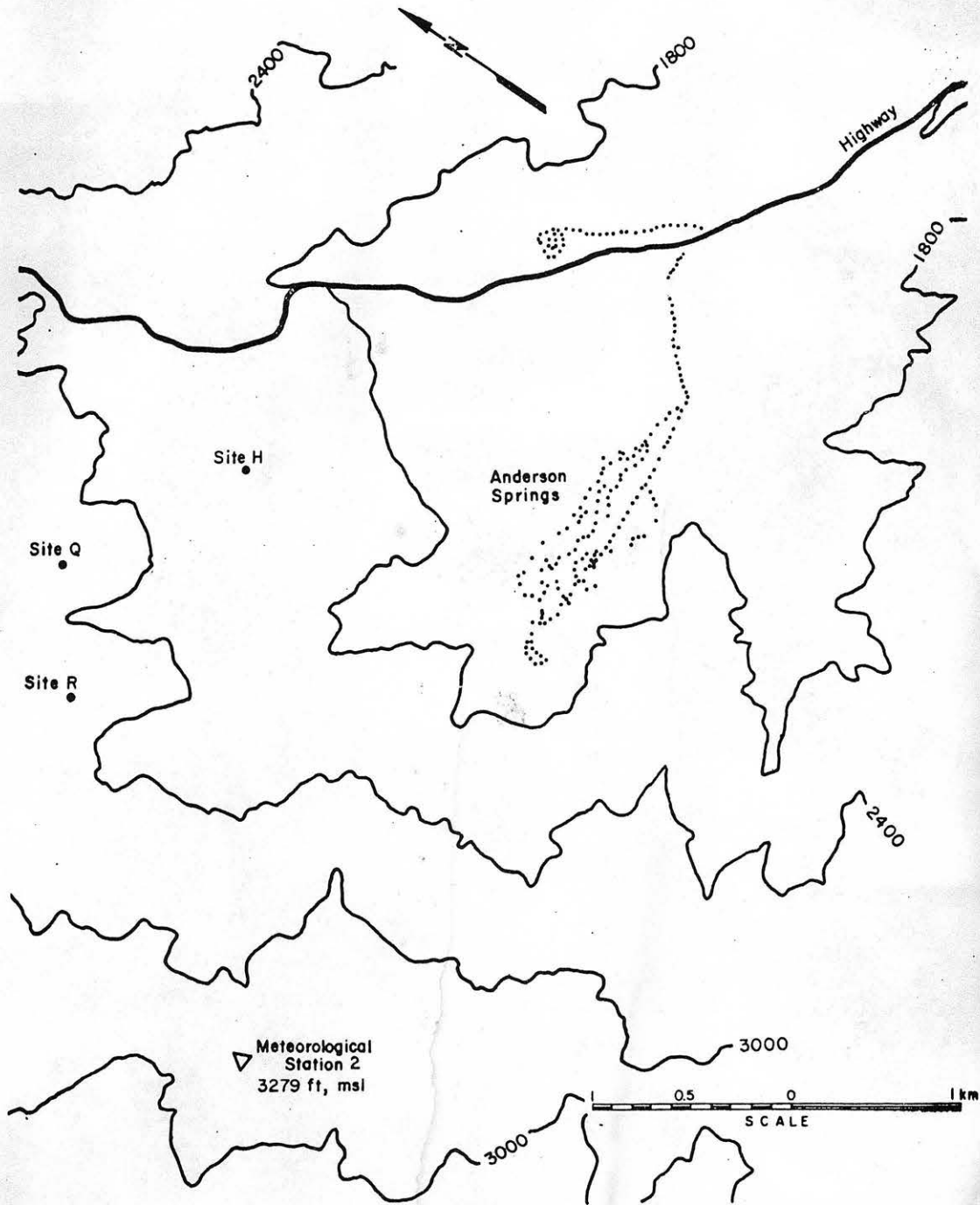


Figure 1.1-1. Map showing location of cooling tower sites for Unit 19.

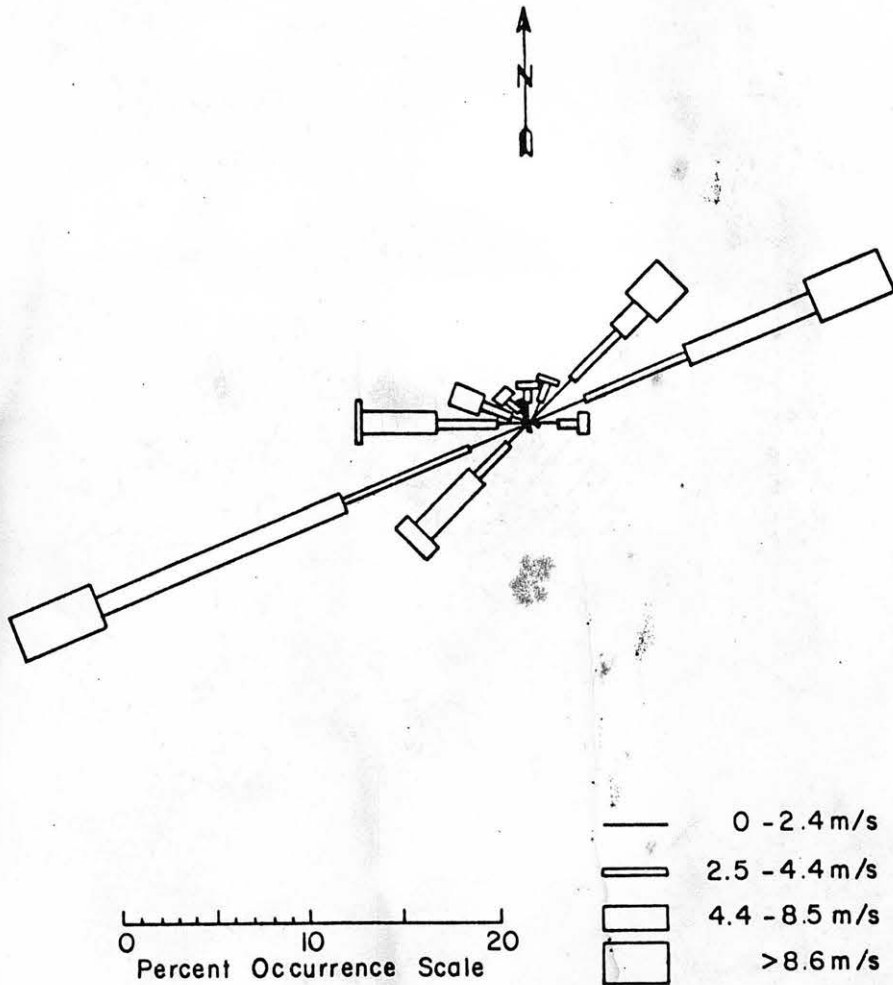


Figure 1.1-2. Wind rose from meteorological Station 2 (SRI-2) near Units 13 and 14 on Anderson Ridge.

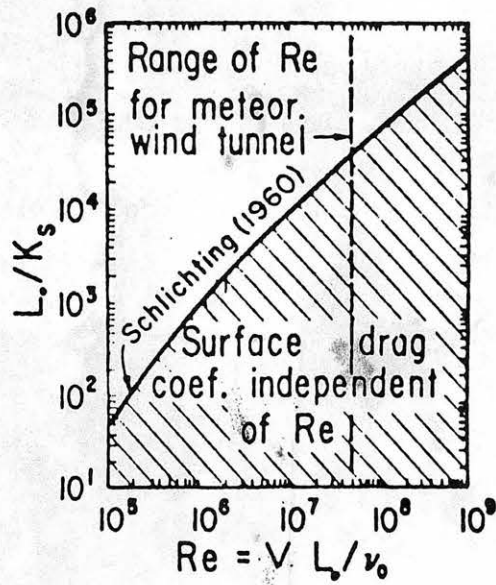


Figure 2.1-1. Reynolds number at which flow becomes independent of Reynolds number for prescribed relative roughness.

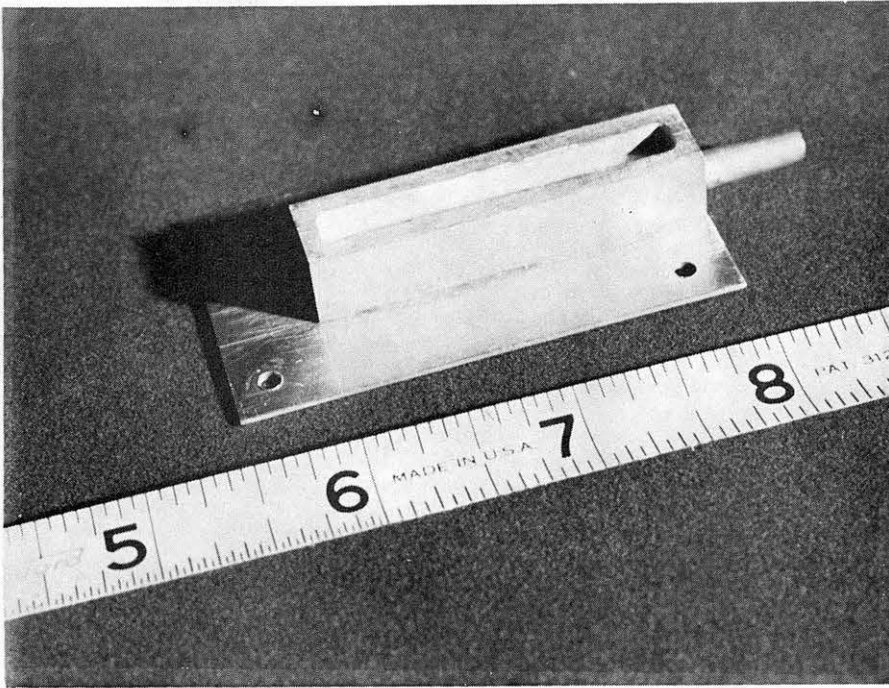


Figure 3.1-1. Photograph of cooling tower model (Scale 1:1920).



Figure 3.1-2. Photograph of terrain model in the Environmental Wind Tunnel.

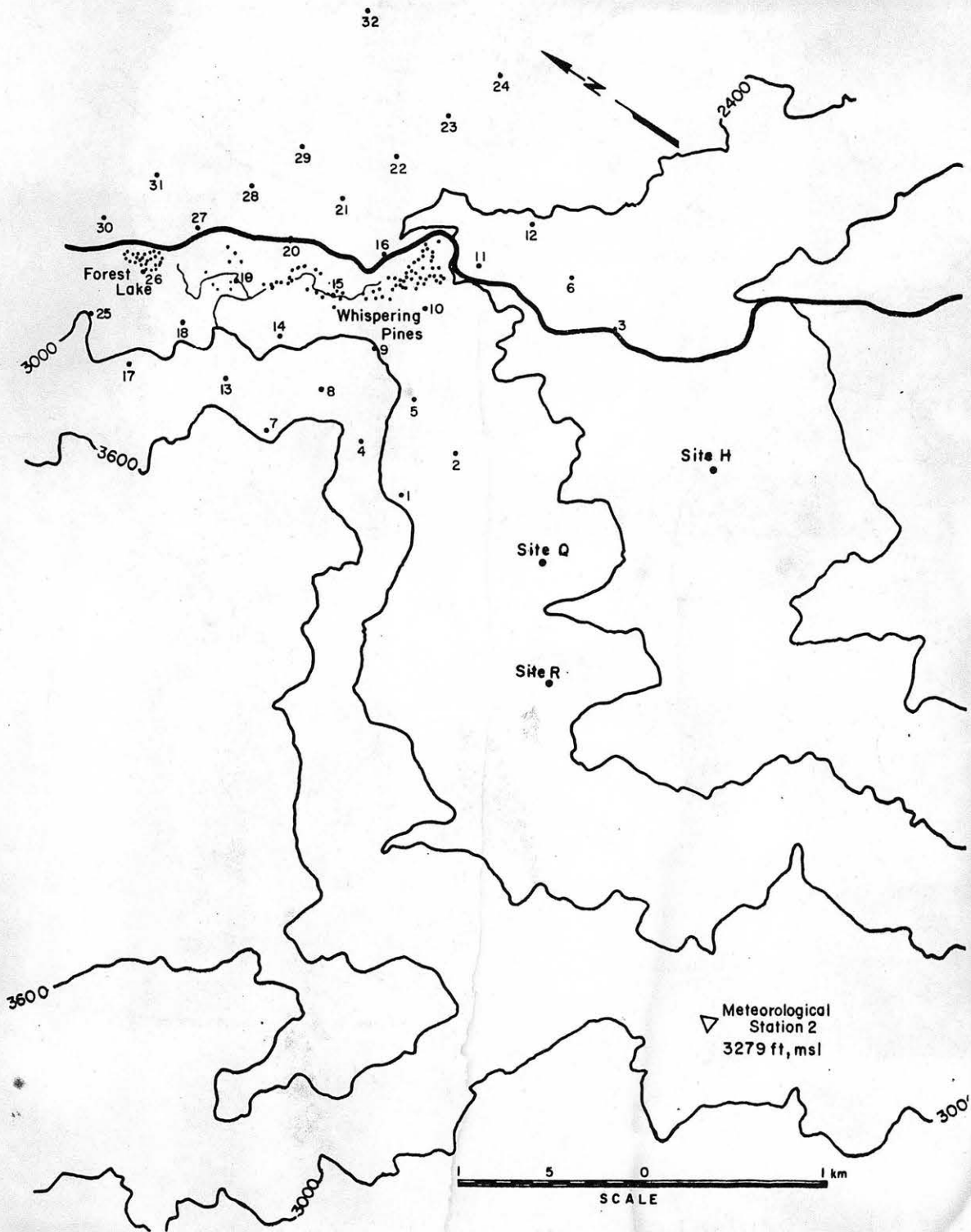


Figure 3.1-3. Sampling location key for the 198° wind direction.

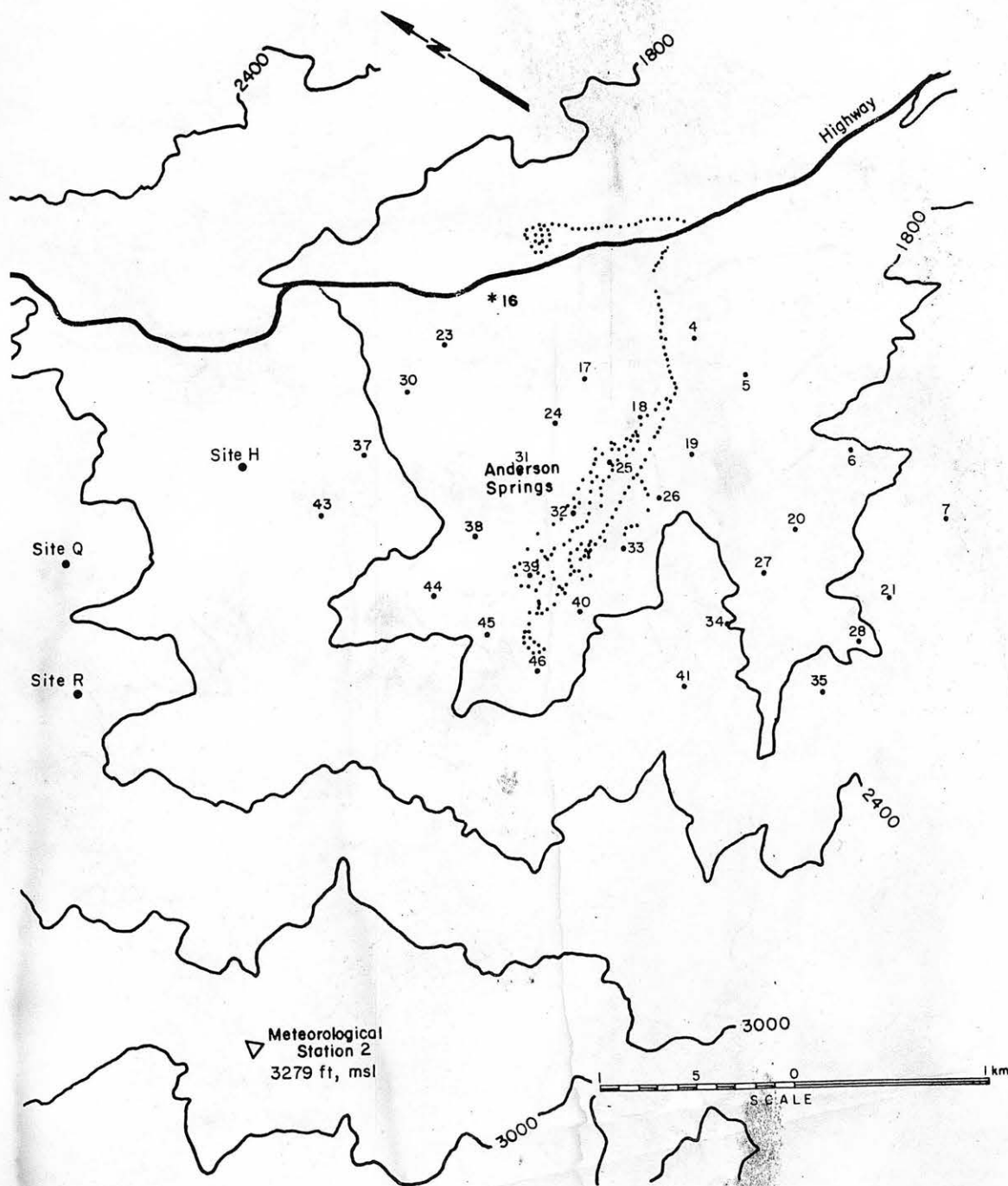
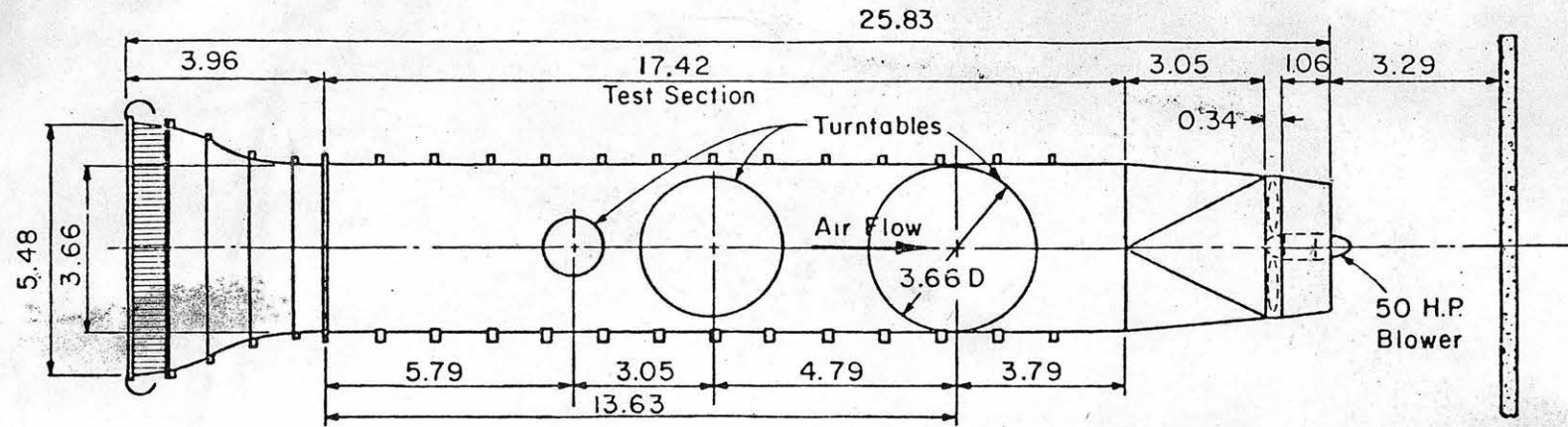
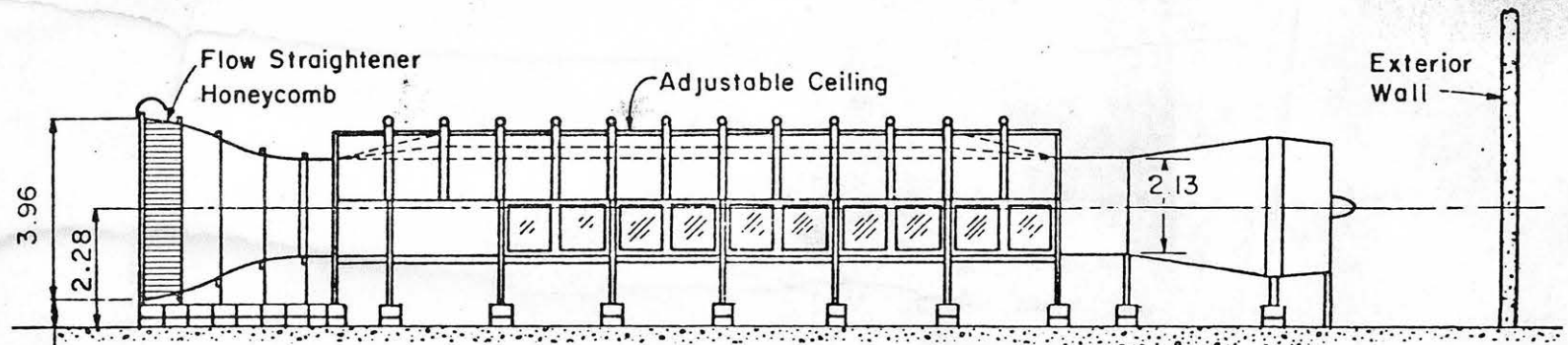


Figure 3.1-4 Sampling location key for the 325° wind direction (sampling location 16 was used only as a reference point for concentration, velocity and temperature profiles).



PLAN

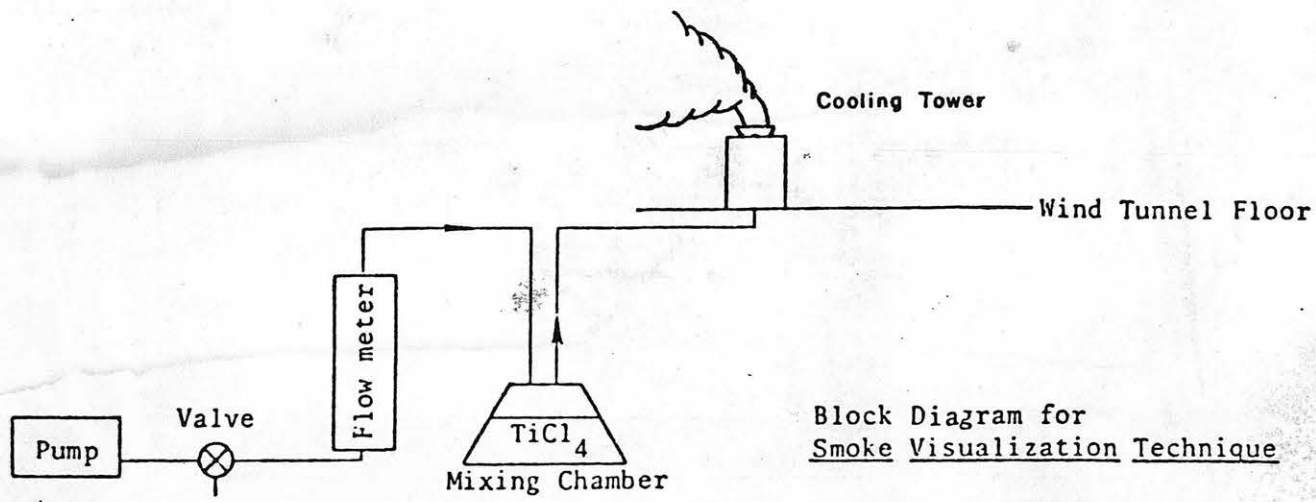


All Dimensions in m

ELEVATION

FLUID DYNAMICS & DIFFUSION LABORATORY
 COLORADO STATE UNIVERSITY

Figure 3.2-1. Environmental Wind Tunnel.



Block Diagram for
Smoke Visualization Technique

Figure 3.3-1. Schematic of plume visualization equipment.

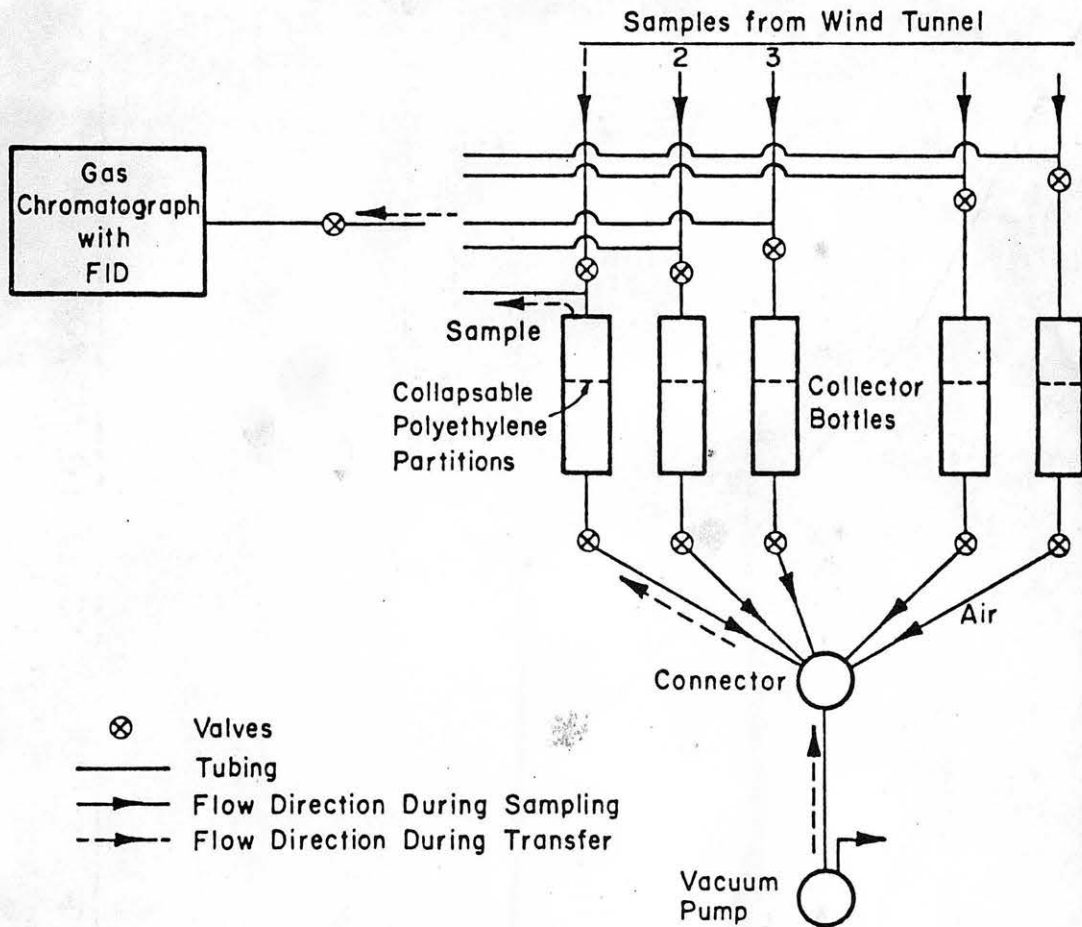


Figure 3.4-1. Schematic of tracer gas sampling system.

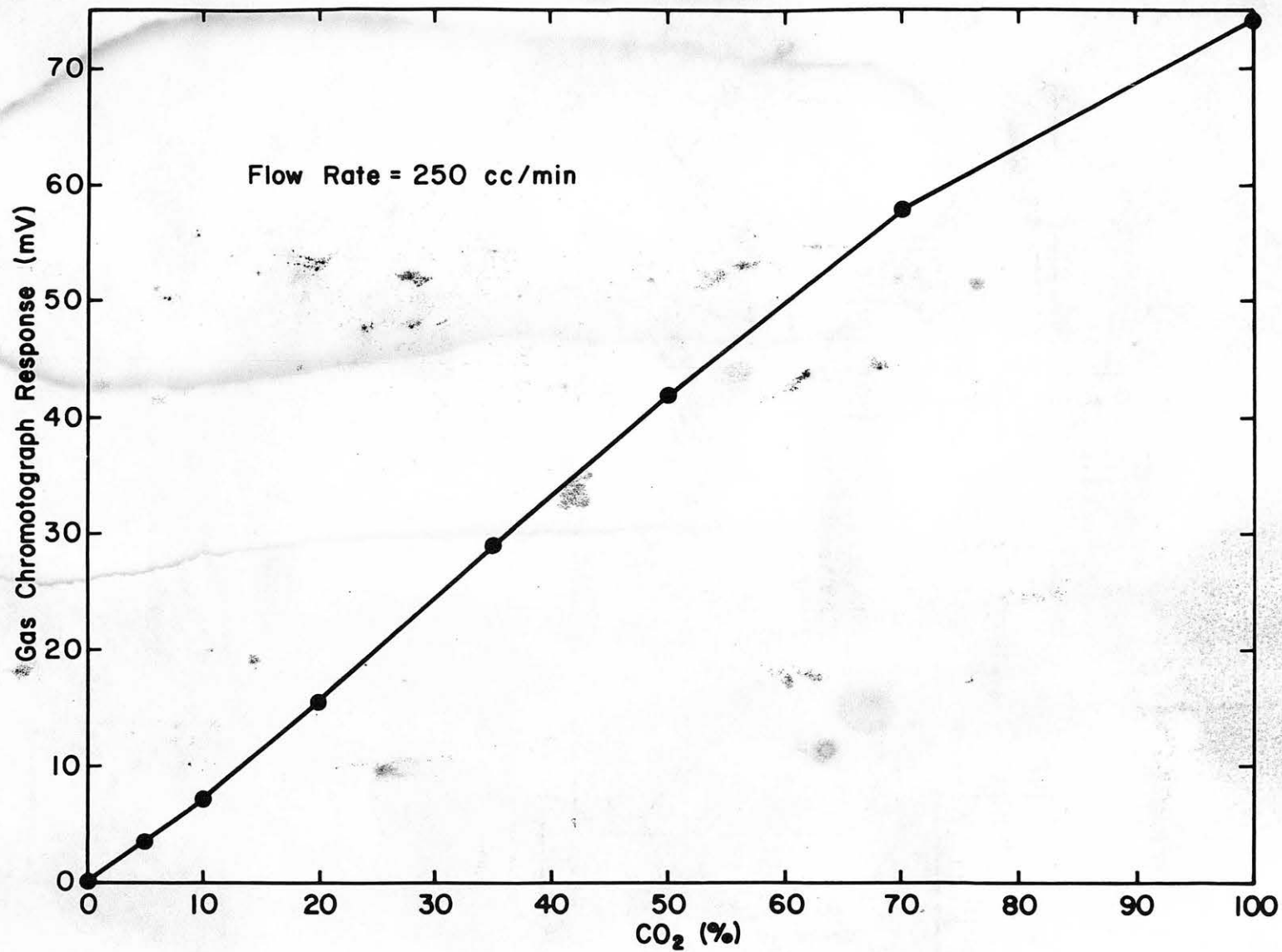


Figure 3.4-2. Calibration curve for the CARLE gas chromatograph.

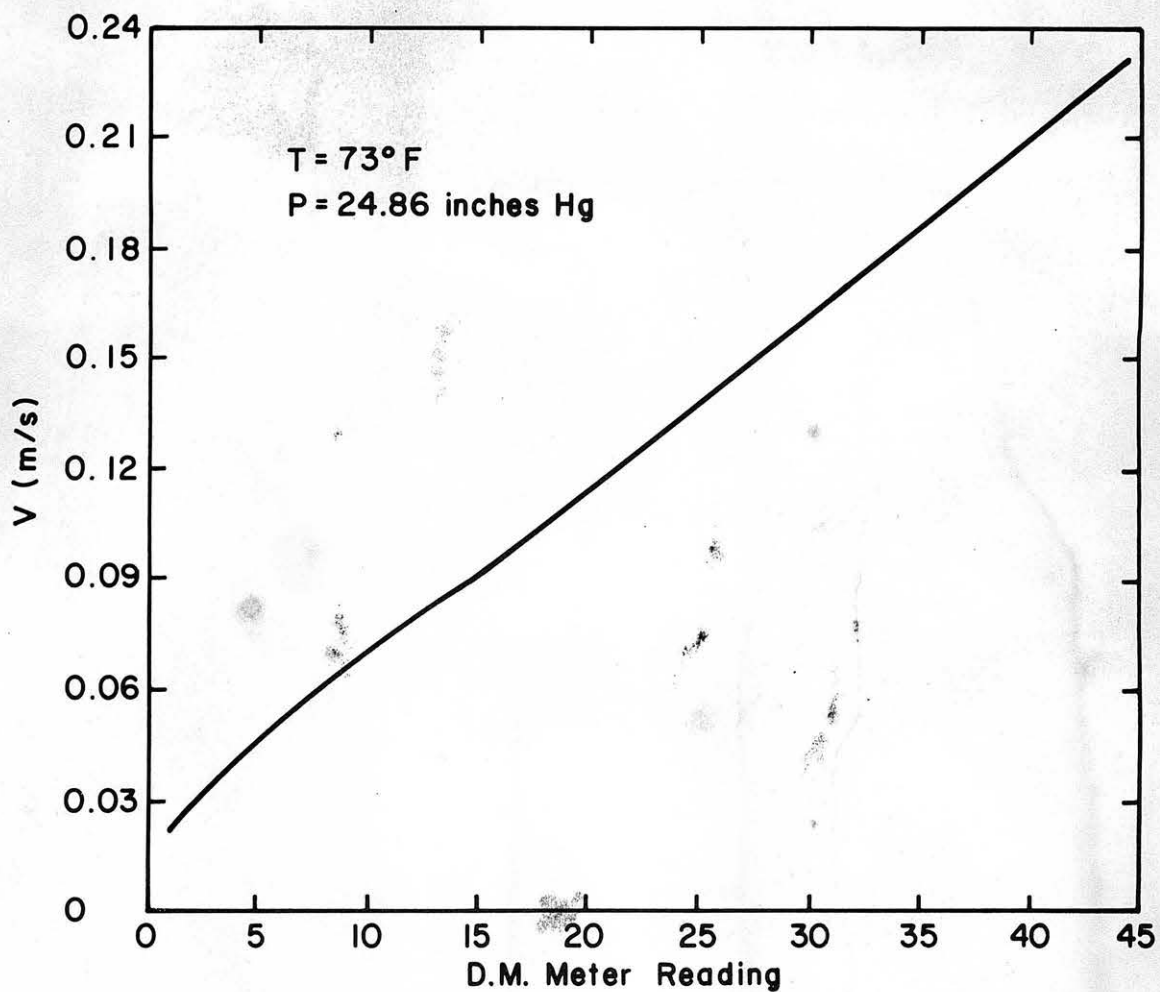


Figure 3.5-1. Calibration curve for Datametric (DM) Model 800 Linear Flow Meter.

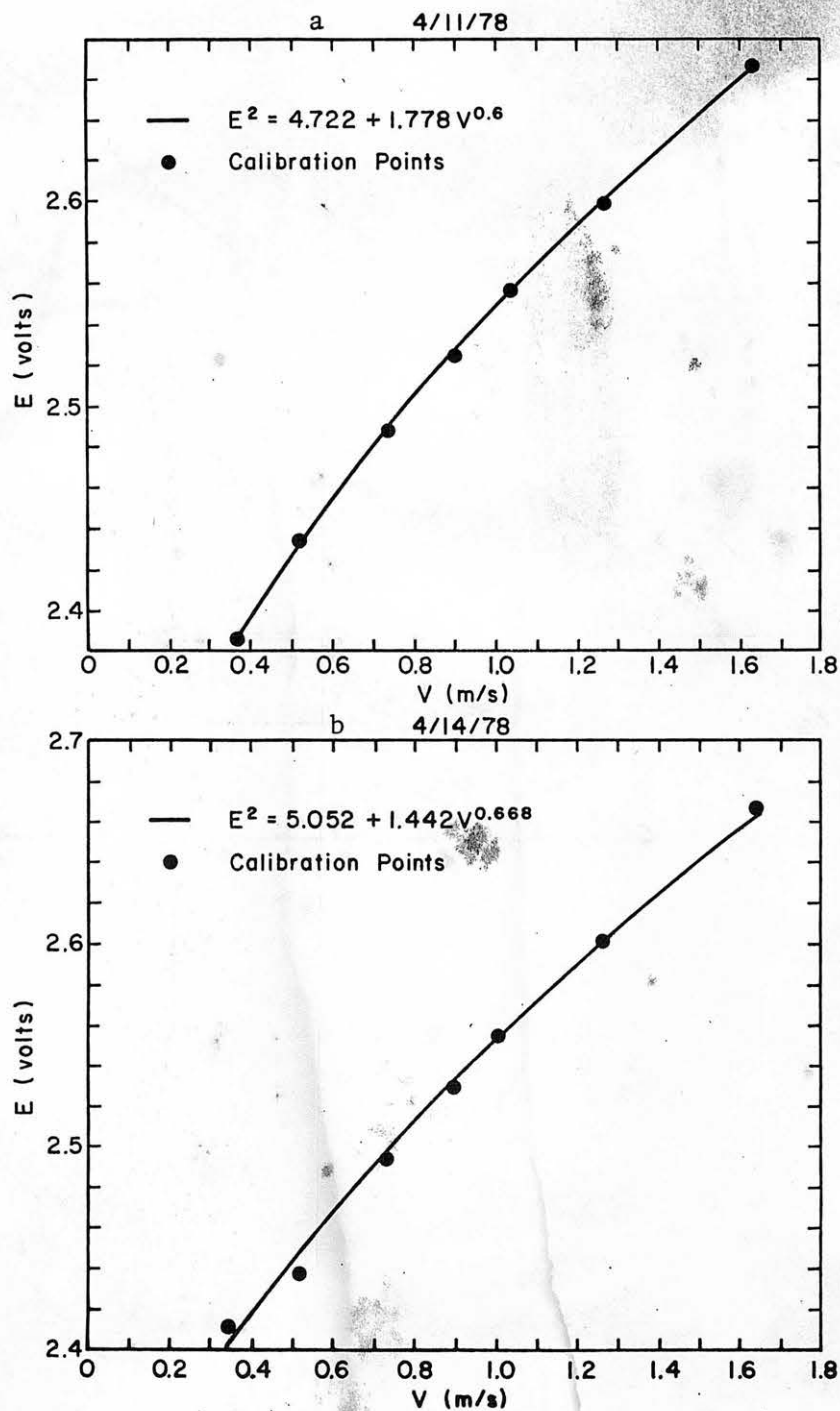


Figure 3.5-2. Calibration curve for TSI hot-film sensor - a) 325° wind tunnel tests; b) 198° wind tunnel tests.

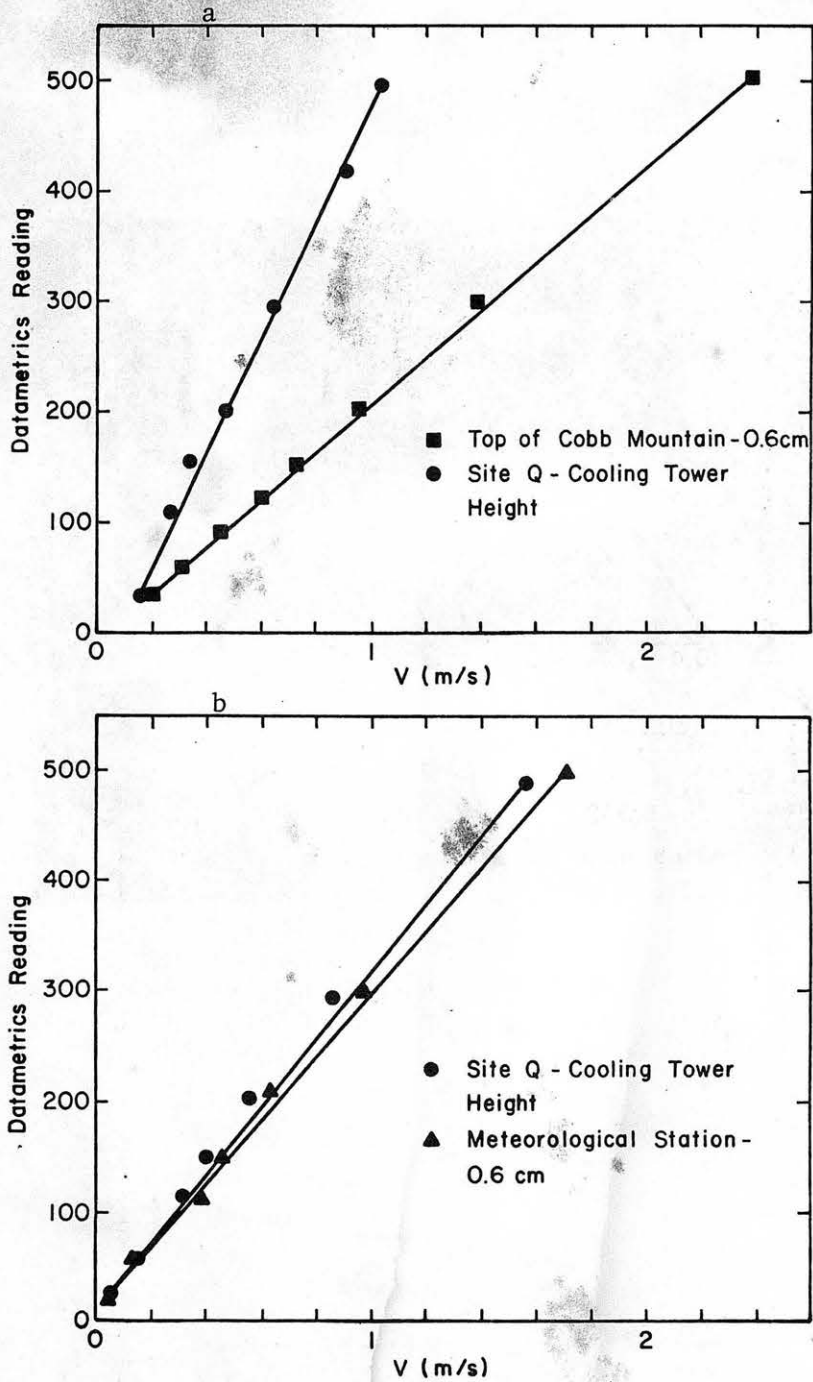
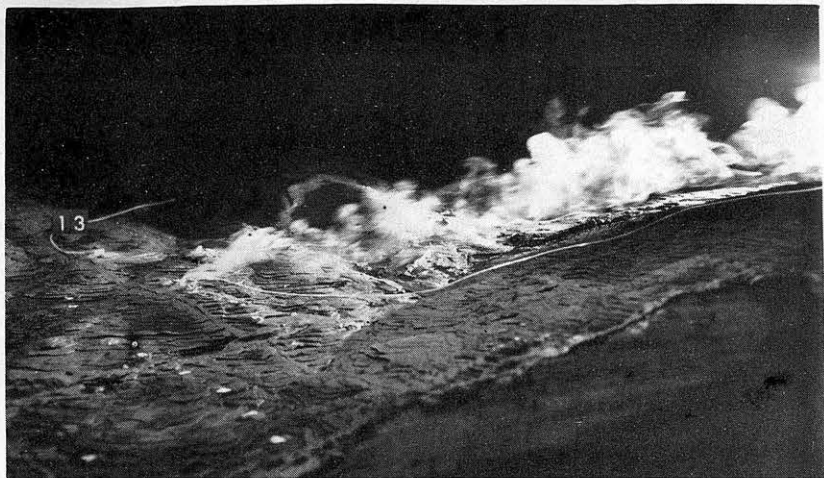


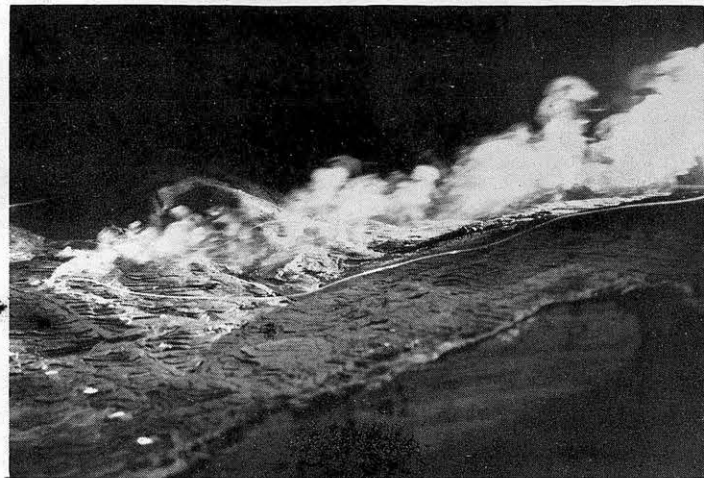
Figure 3.5-3. Wind tunnel calibration for a) 325° wind direction and b) 198° wind direction [Datametrics reading versus velocity at indicated location].



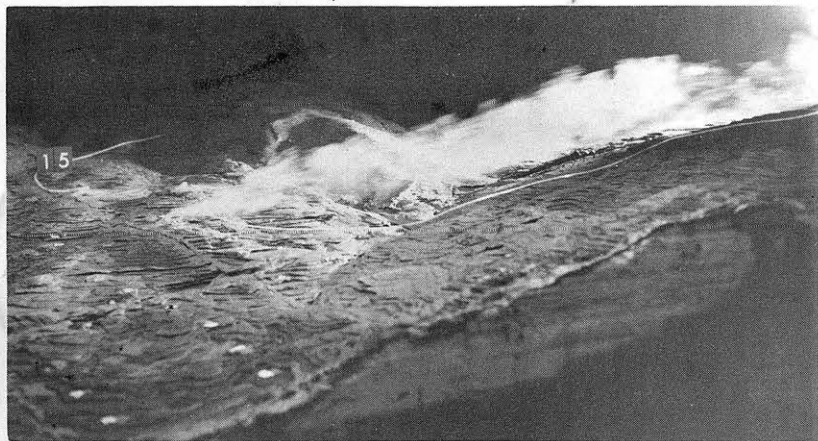
Figure 3.6-1. Picture of drainage flow test set up.



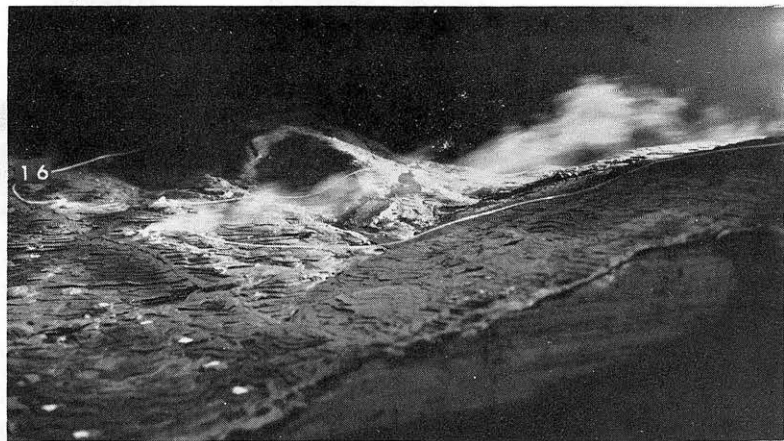
(a)



(b)

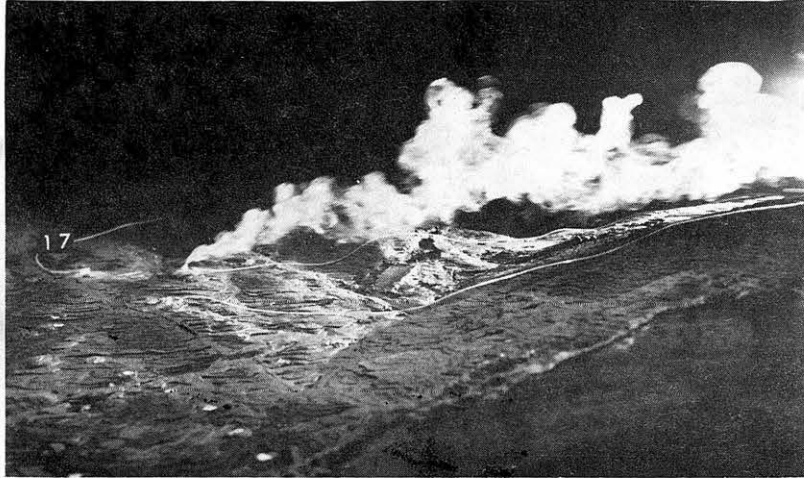


(c)



(d)

Figure 4.1-1. Plume visualization for Unit 19, Site H for wind speeds of a) 3.0, b) 4.2, c) 8.1 and d) 11.1 m/s and a 198° wind direction.



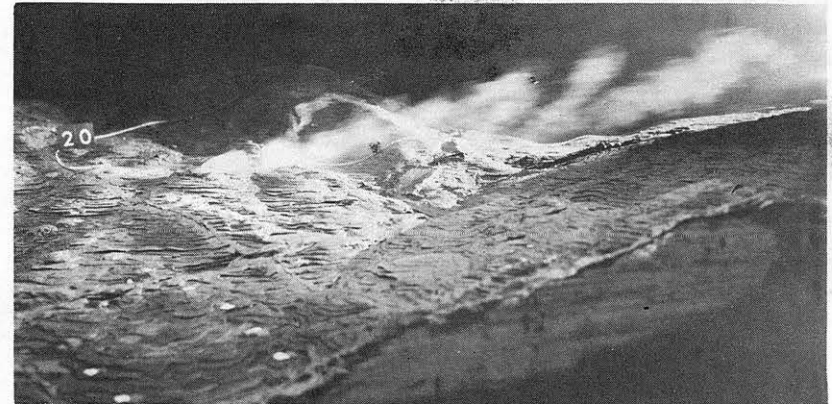
(a)



(b)

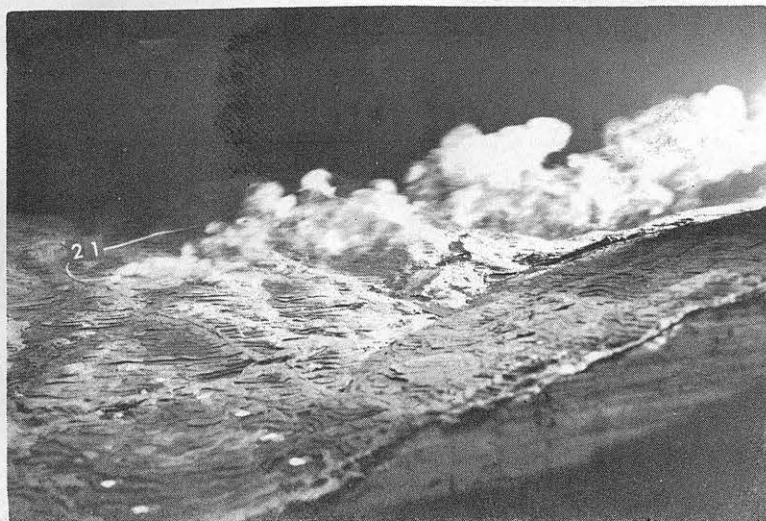


(c)

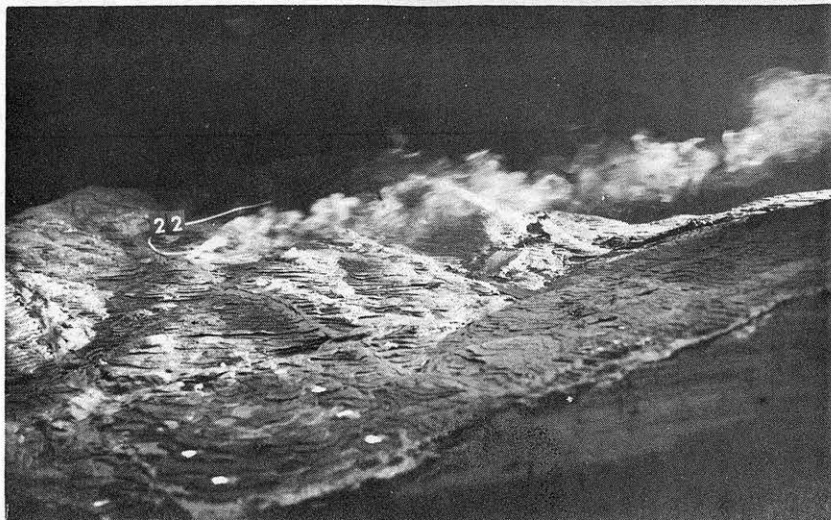


(d)

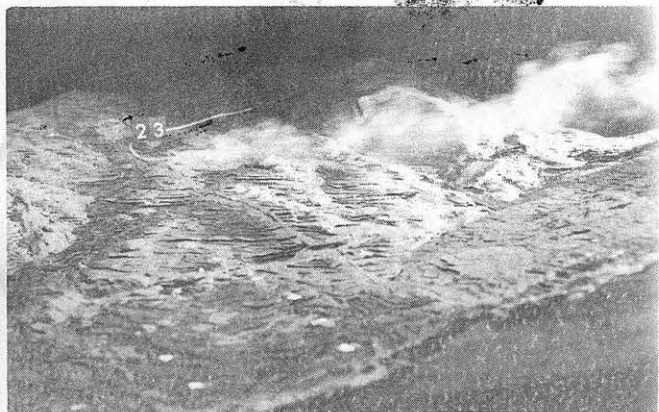
Figure 4.1-2. Plume visualization for Unit 19, Site Q for wind speeds of a) 3.0, b) 4.2 c) 8.1 and d) 11.1 m/s and a 198° wind direction.



(a)



(b)

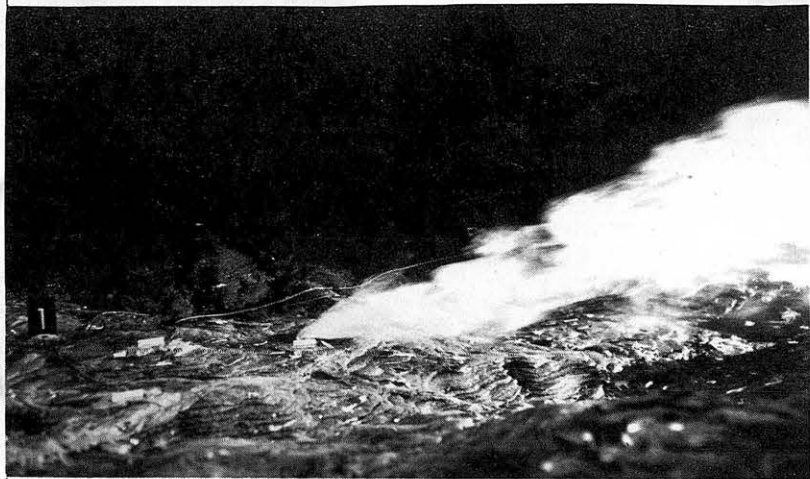


(c)



(d)

Figure 4.1-3. Plume visualization for Unit 19, Site R for wind speeds of a) 3.0, b) 4.2, c) 8.1 and d) 11.1 m/s and a 198° wind direction.



(a)



(b)



(c)



(d)

Figure 4.1-4. Plume visualization for Unit 19, Site H for wind speeds of a) 3.0, b) 4.2, c) 8.1 and d) 11.1 m/s and a 325° wind direction.



(a)



(b)



(c)



(d)

Figure 4.1-5. Plume visualization for Unit 19, Site Q for wind speeds of a) 3.0, b) 4.2, c) 8.1 and d) 11.1 m/s and a 325° wind direction.

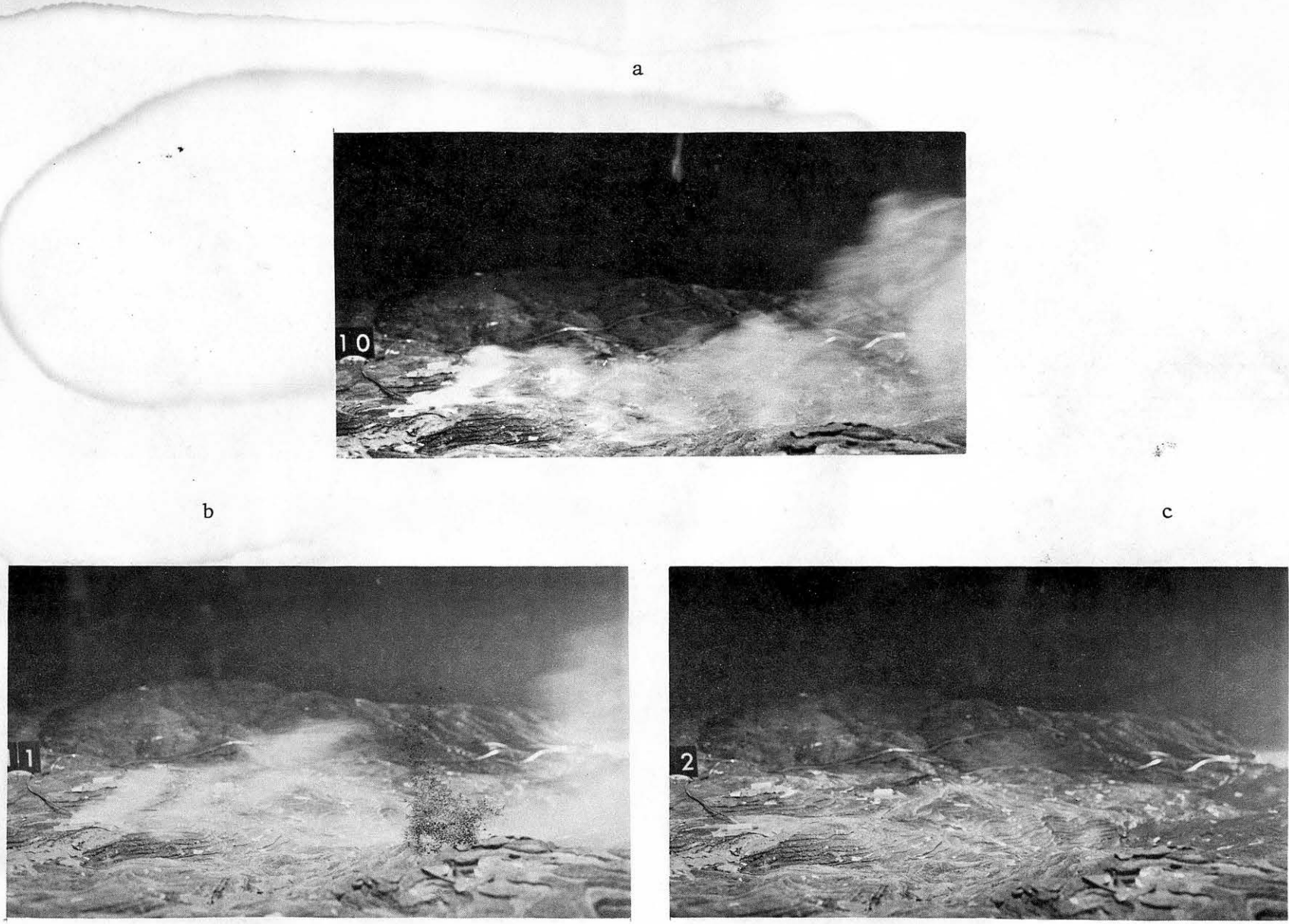


Figure 4.1-6. Plume visualization for Unit 19, Site R for wind speeds of a) 4.2, b) 8.1 and c) 11.1 m/s and a 325° wind direction.



Figure 4.2-1. Visualization of drainage flow field and smoke from Site Q.

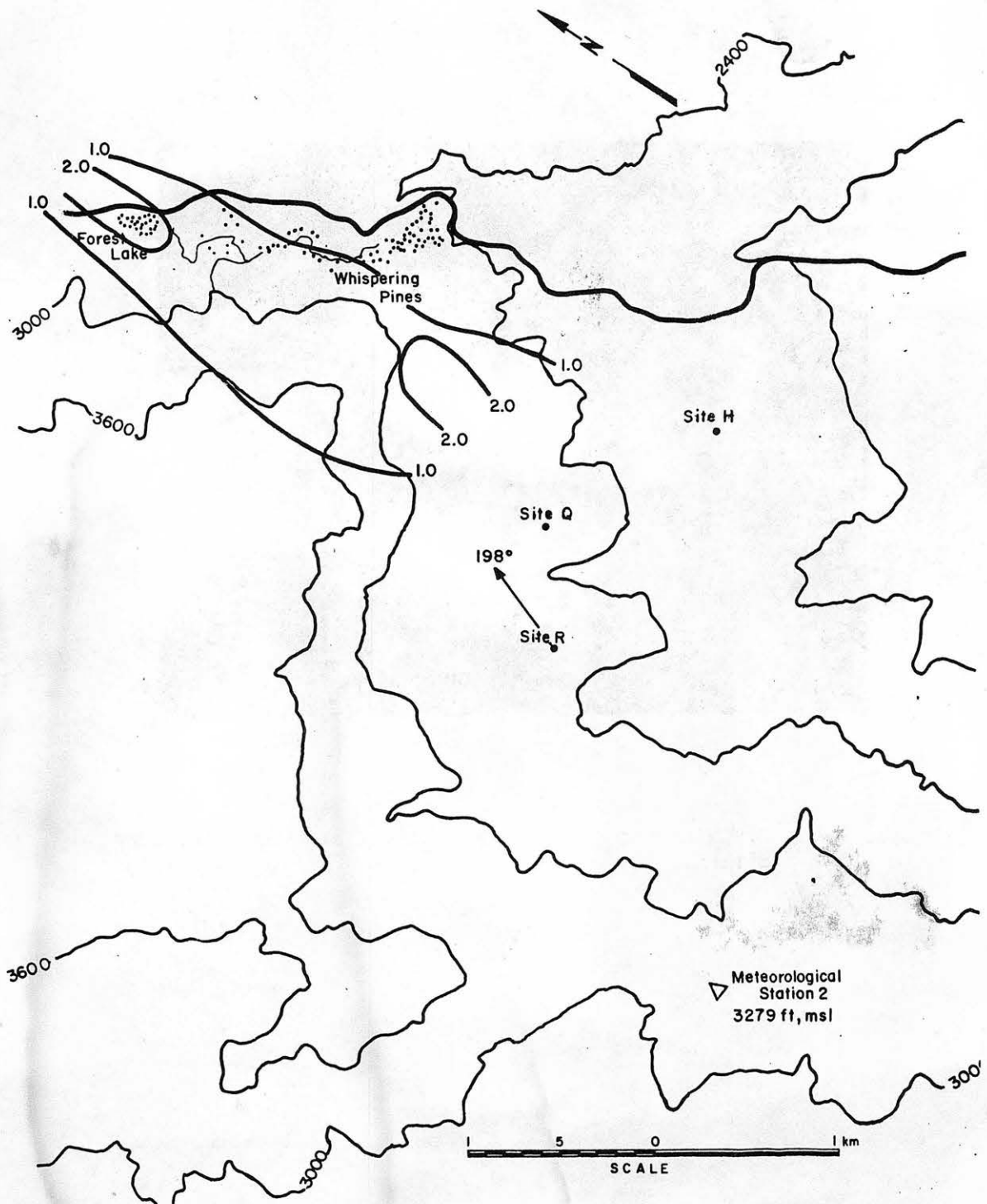


Figure 5.1-1a. Isopleths ($\times 10^5$) of nondimensional concentration coefficient K for Unit 19, Site R and a wind speed of 3.0 m/s for the 198° wind direction.

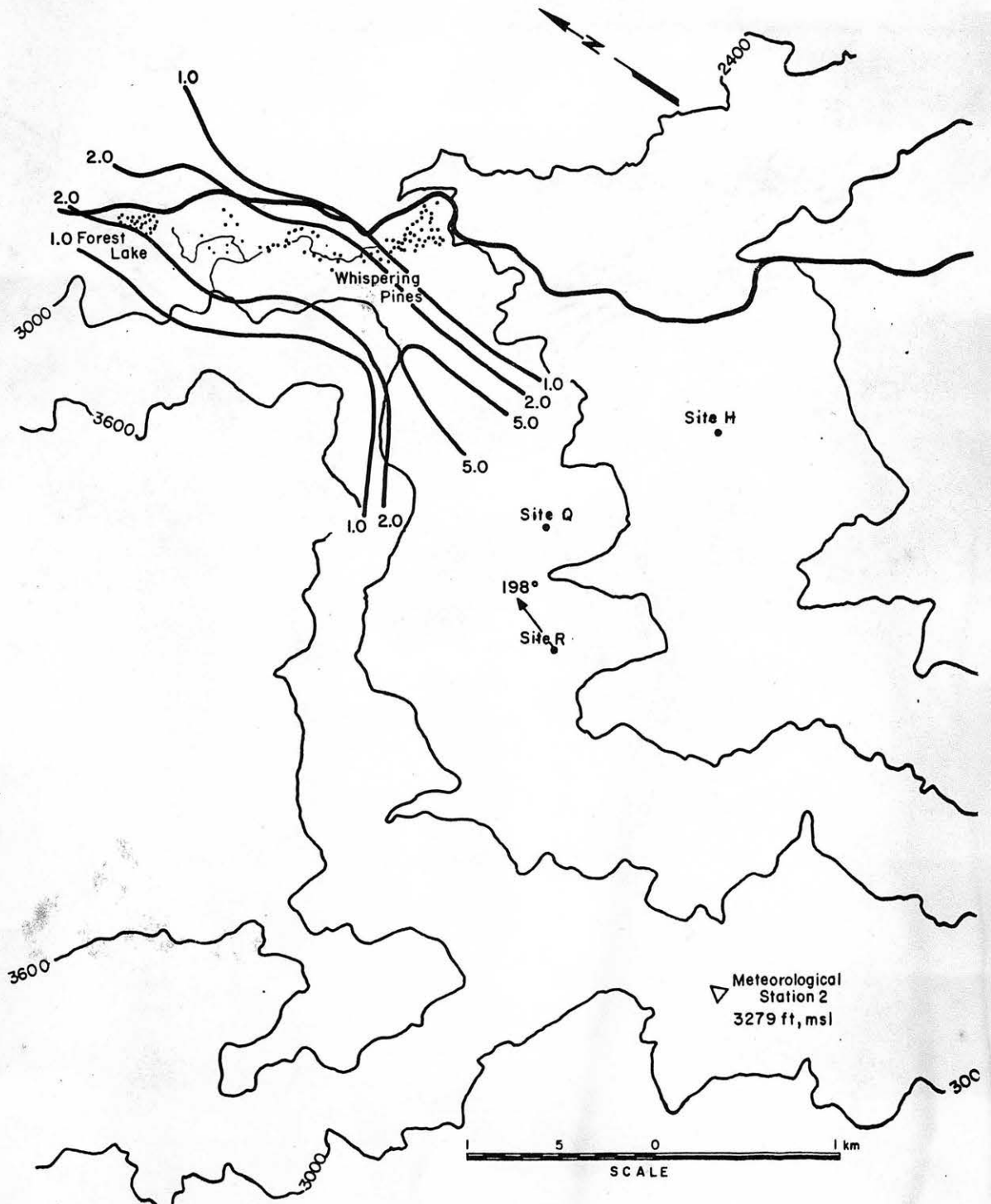


Figure 5.1-1b. Isopleths ($\times 10^5$) of nondimensional concentration coefficient K for Unit 19, Site R and a wind speed of 4.2 m/s for the 198° wind direction.

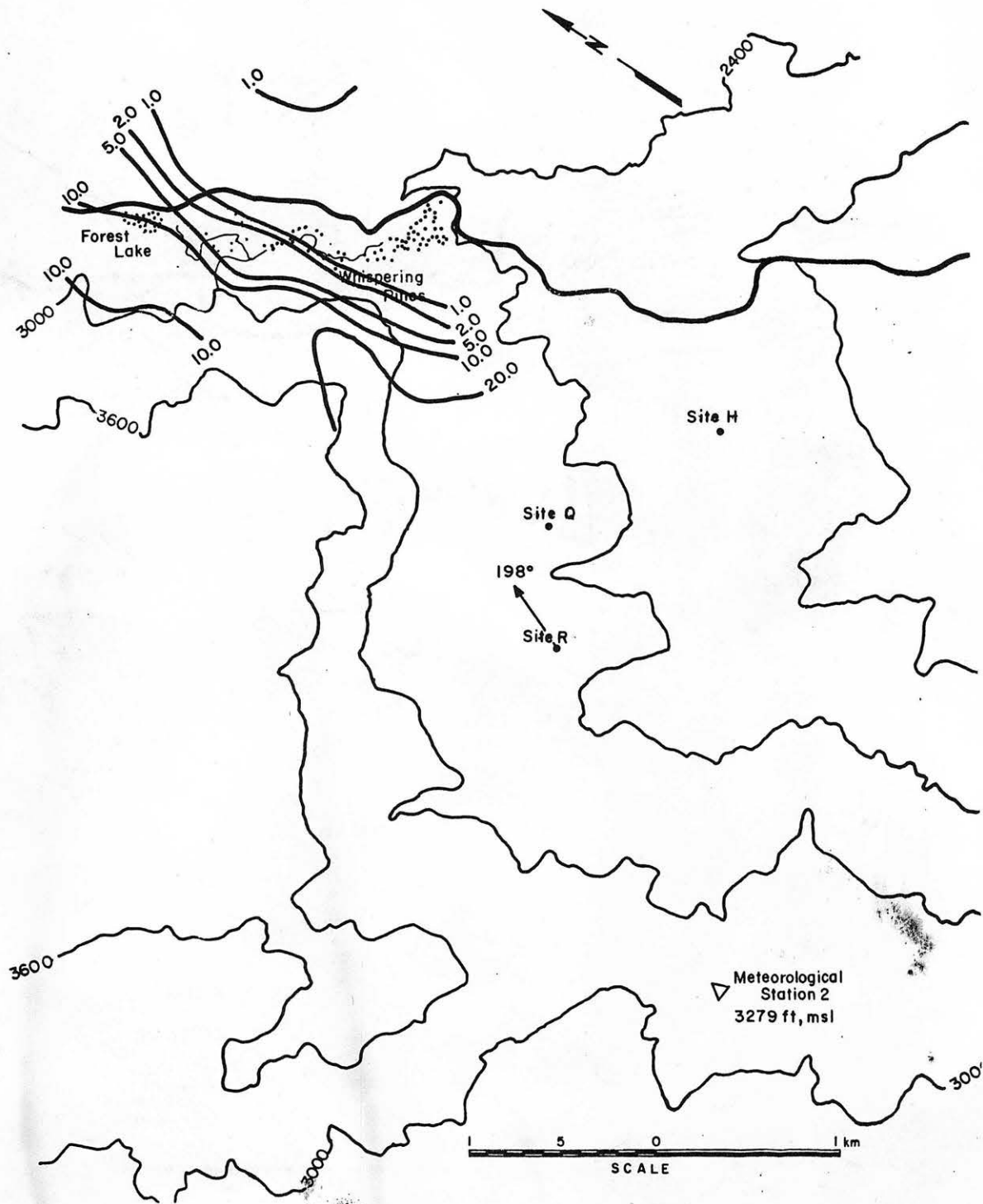


Figure 5.1-1c. Isopleths ($\times 10^5$) of nondimensional concentration coefficient K for Unit 19, Site R, and a wind speed of 8.1 m/s for the 198° wind direction.

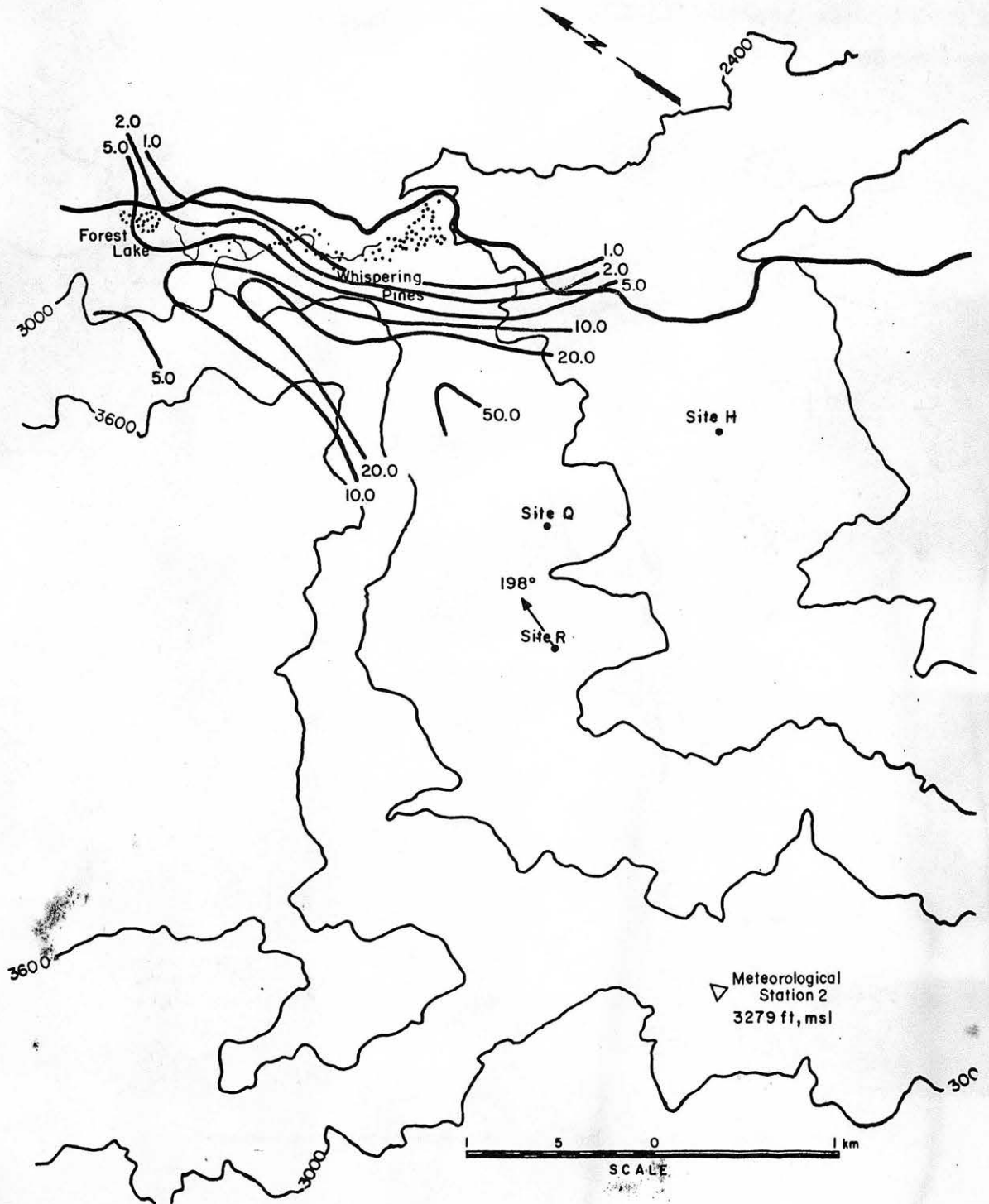


Figure 5.1-1d. Isopleths ($\times 10^5$) of nondimensional concentration coefficient K for Unit 19, Site R and a wind speed of 11.1 m/s for the 198° wind direction.

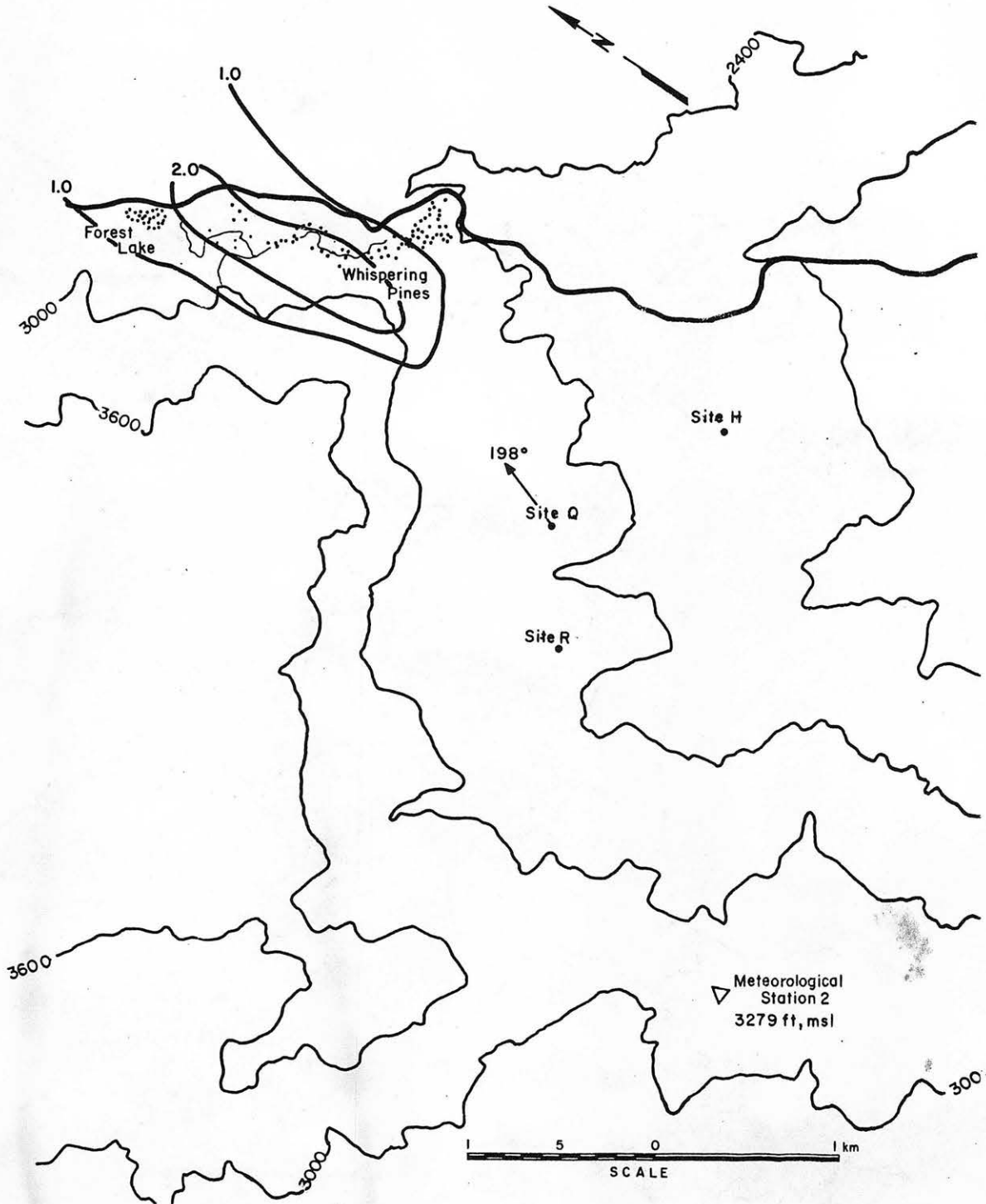


Figure 5.1-2a. Isopleths ($\times 10^5$) of nondimensional concentration coefficient K for Unit 19, Site Q and a wind speed of 3.0 m/s for the 198° wind direction.

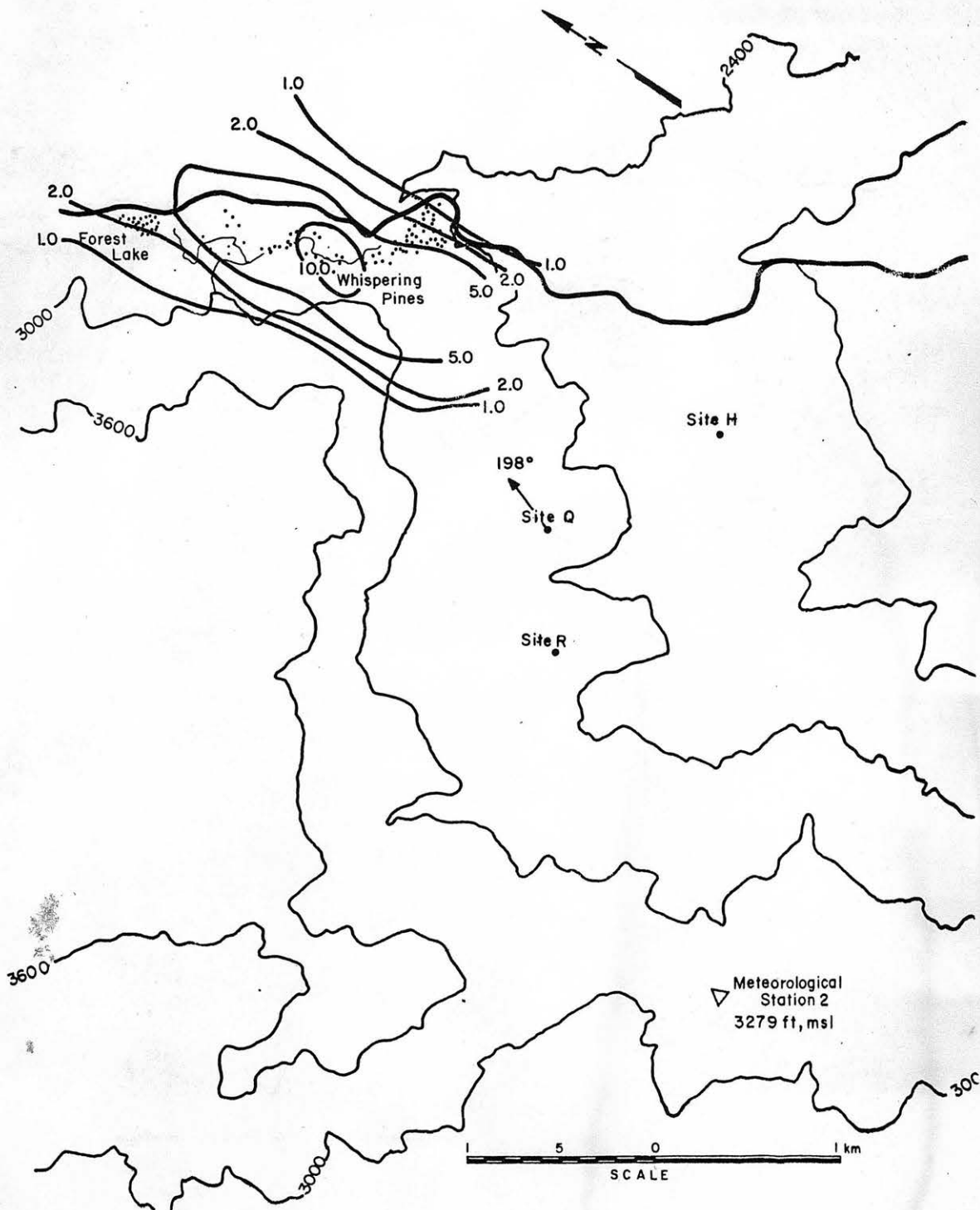


Figure 5.1-2b. Isopleths ($\times 10^5$) of nondimensional concentration coefficient K for Unit 19, Site Q and a wind speed of 4.2 m/s for the 198° wind direction.

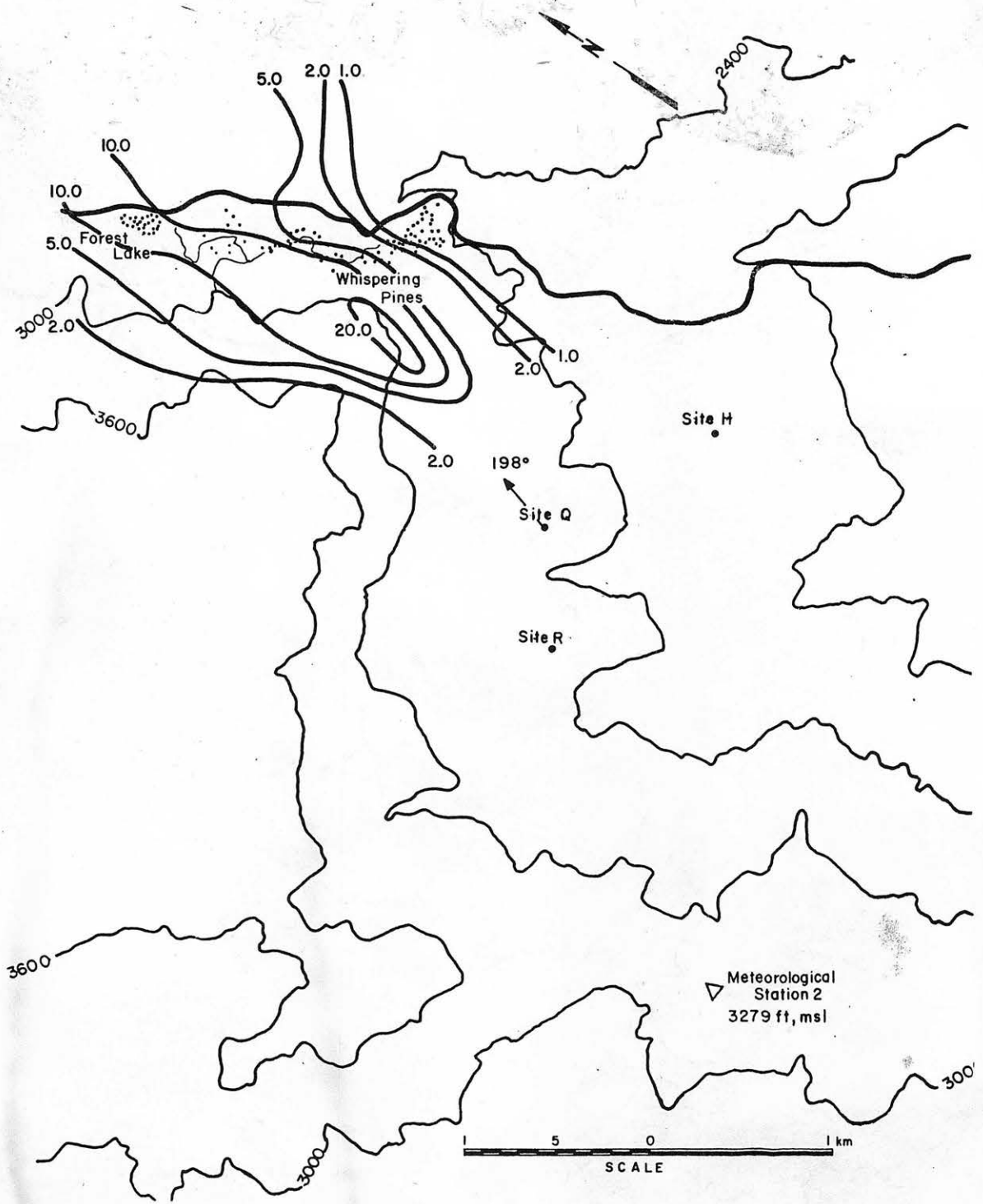


Figure 5.1-2c. Isopleths ($\times 10^5$) of nondimensional concentration coefficient K for Unit 19, Site Q and a wind speed of 8.1 m/s for the 198° wind direction.

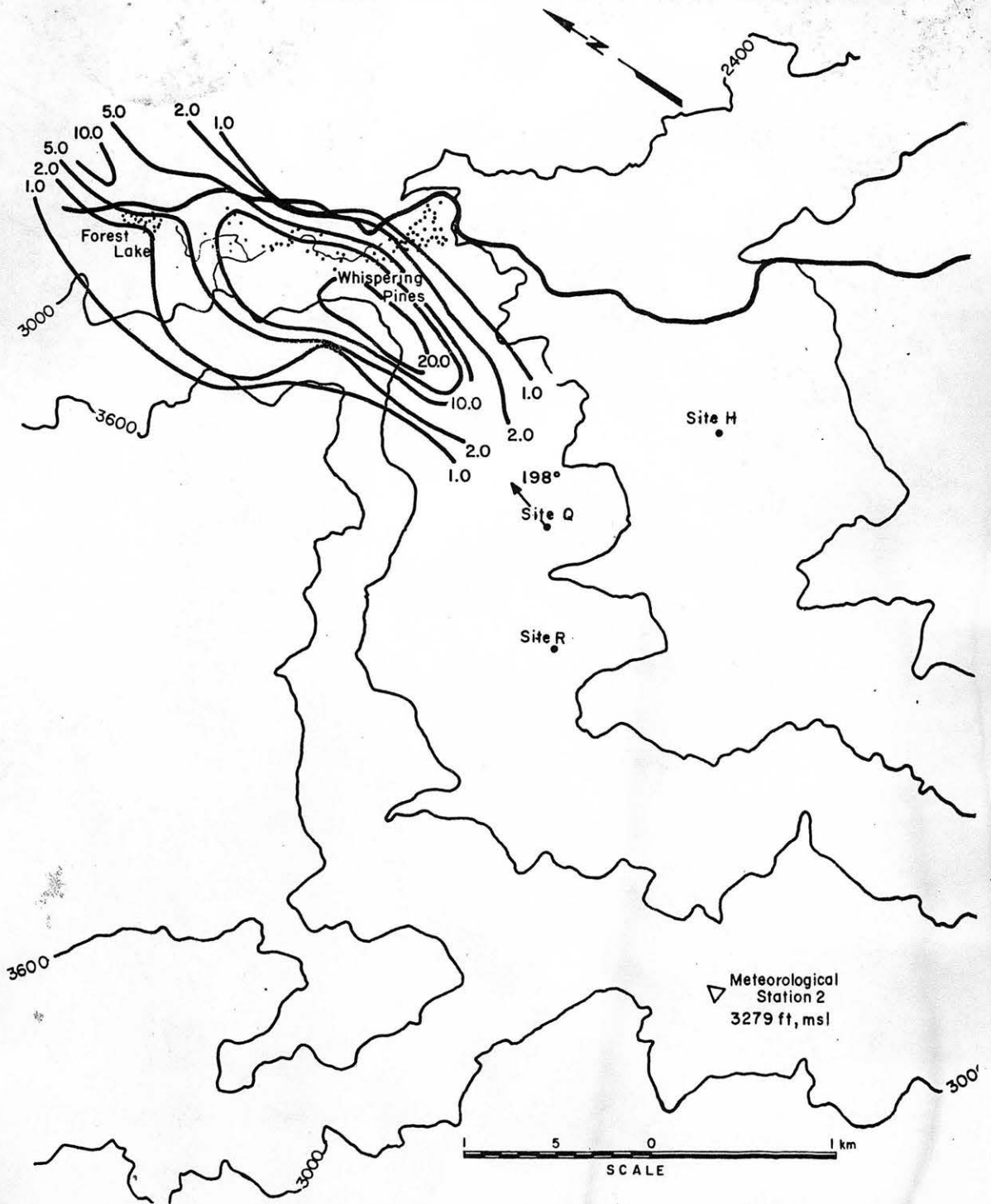


Figure 5.1-2d. Isopleths ($\times 10^5$) of nondimensional concentration coefficient K for Unit 19, Site Q and a wind speed of 11.1 m/s for the 198° wind direction.

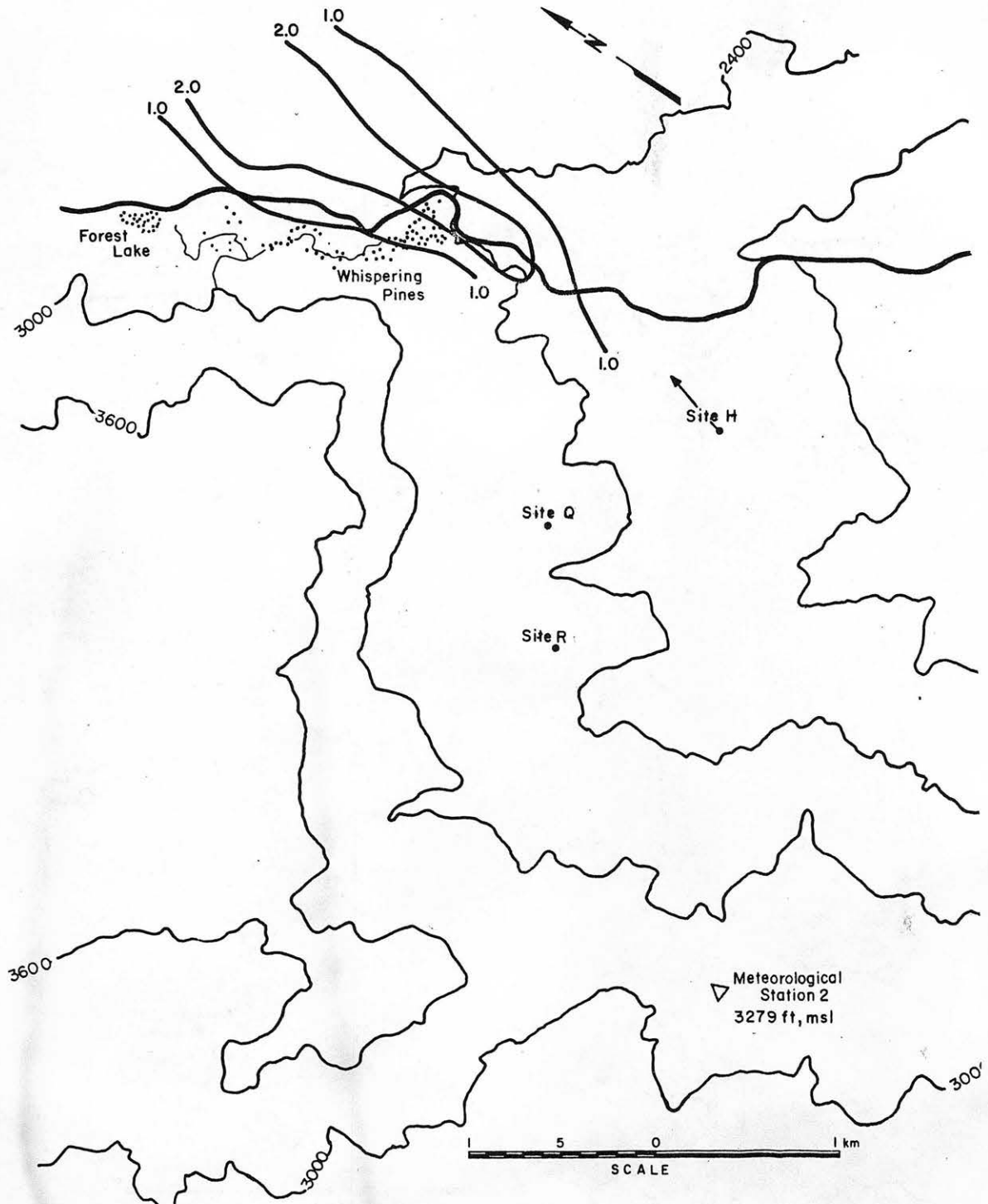


Figure 5.1-3a. Isopleths ($\times 10^5$) of nondimensional concentration coefficient K for Unit 19, Site H and a wind speed of 3.0 m/s for the 198° wind direction.

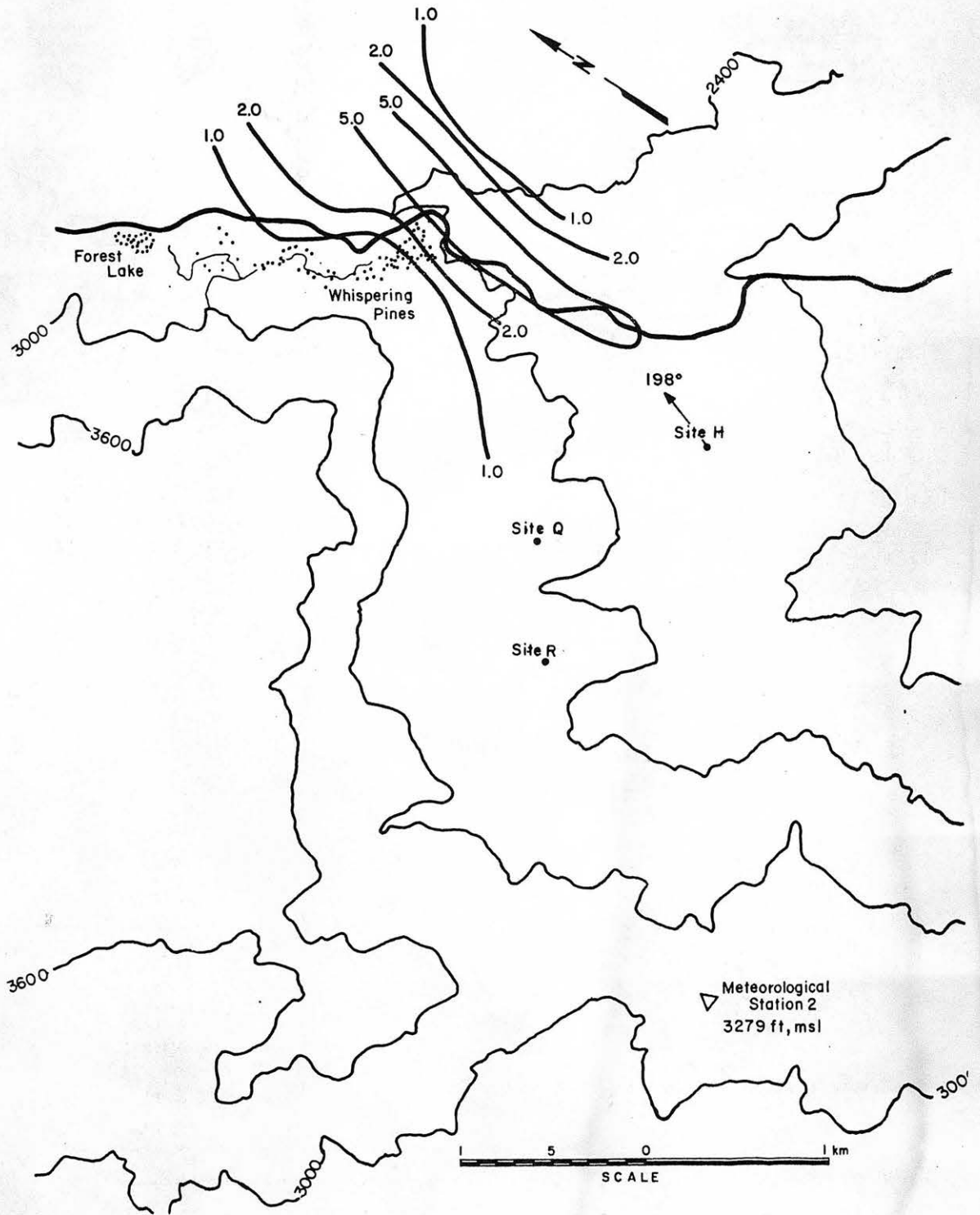


Figure 5.1-3b. Isopleths ($\times 10^5$) of nondimensional concentration coefficient K for Unit 19, Site H and a wind speed of 4.2 m/s for the 198° wind direction.

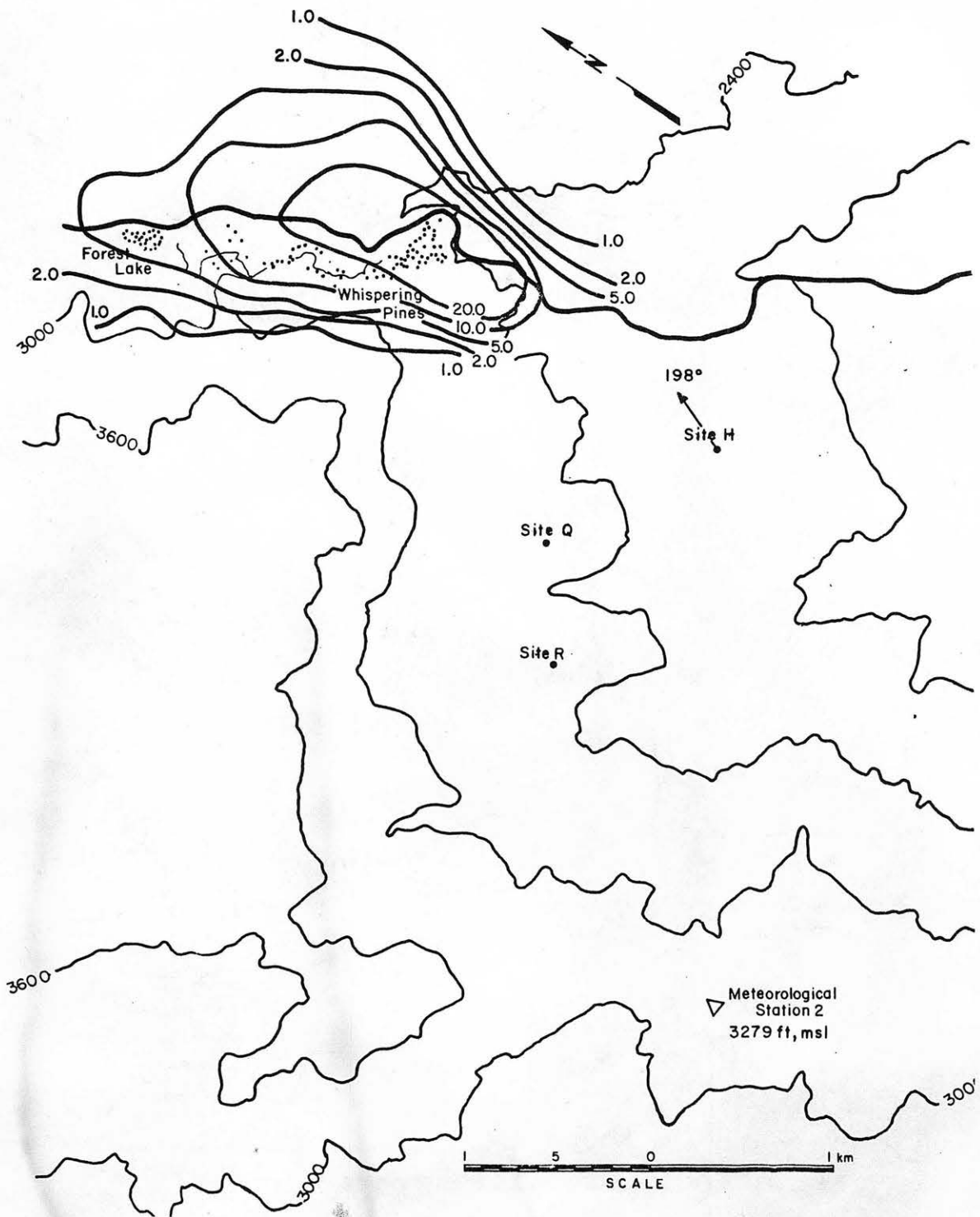


Figure 5.1-3c. Isopleths ($\times 10^5$) of nondimensional concentration coefficient K for Unit 19, Site H and a wind speed of 8.1 m/s for the 198° wind direction.

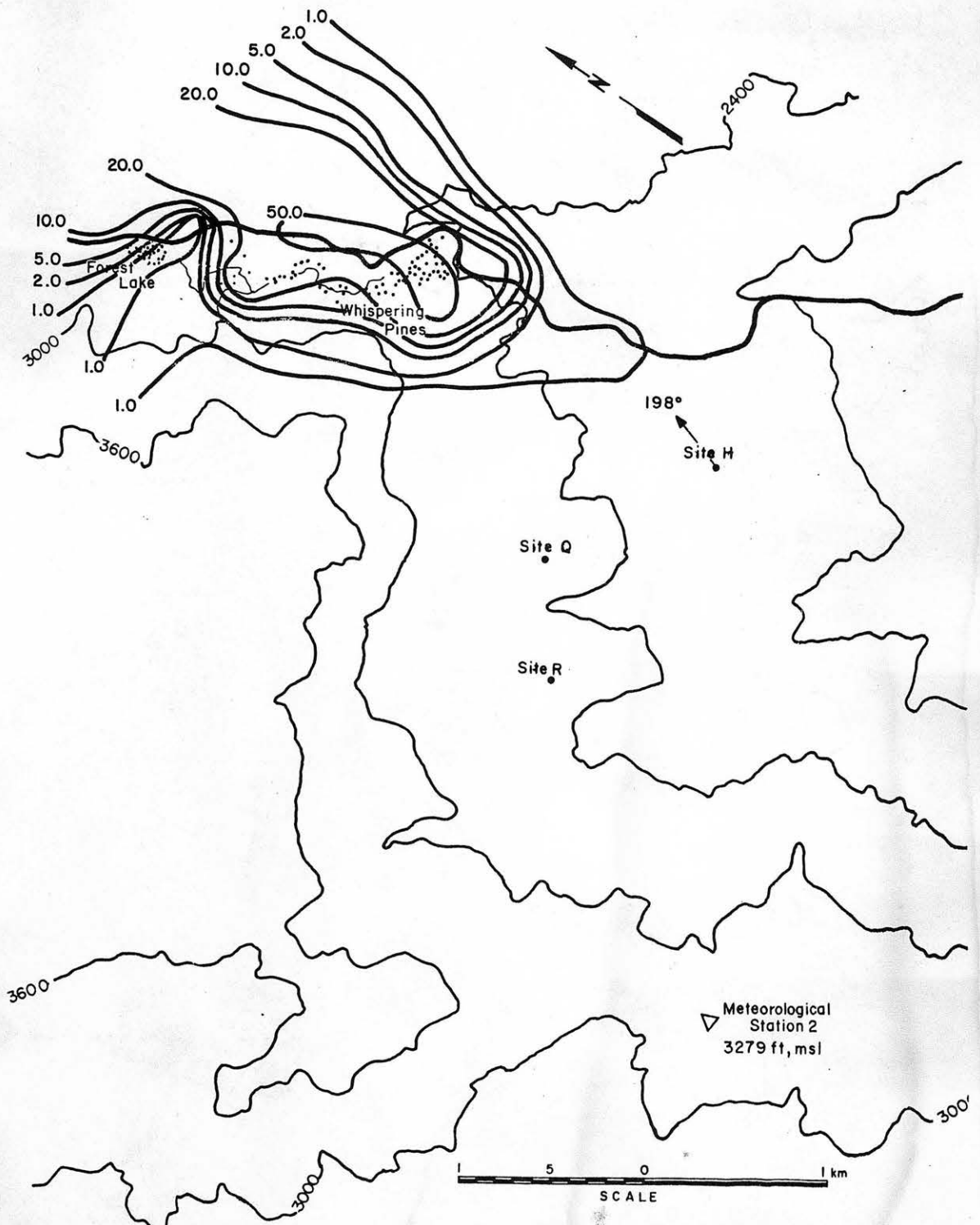


Figure 5.1-3d. Isopleths ($\times 10^5$) of nondimensional concentration coefficient K for Unit 19, Site H and a wind speed of 11.1 m/s for the 198° wind direction.

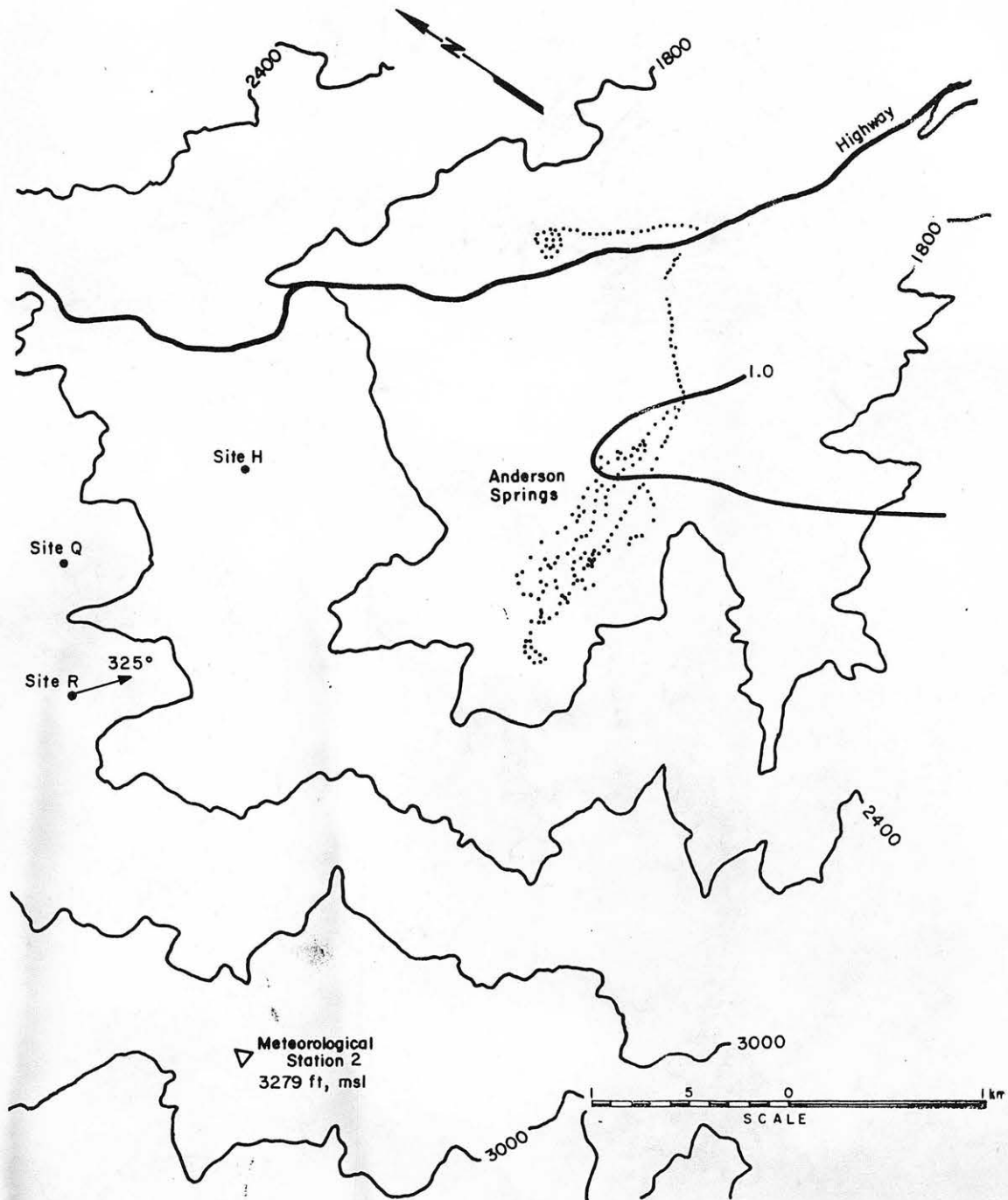


Figure 5.1-4a. Isopleths ($\times 10^5$) of nondimensional concentration coefficient K for Unit 19, Site R and a wind speed of 3.0 m/s for the 325° wind direction.

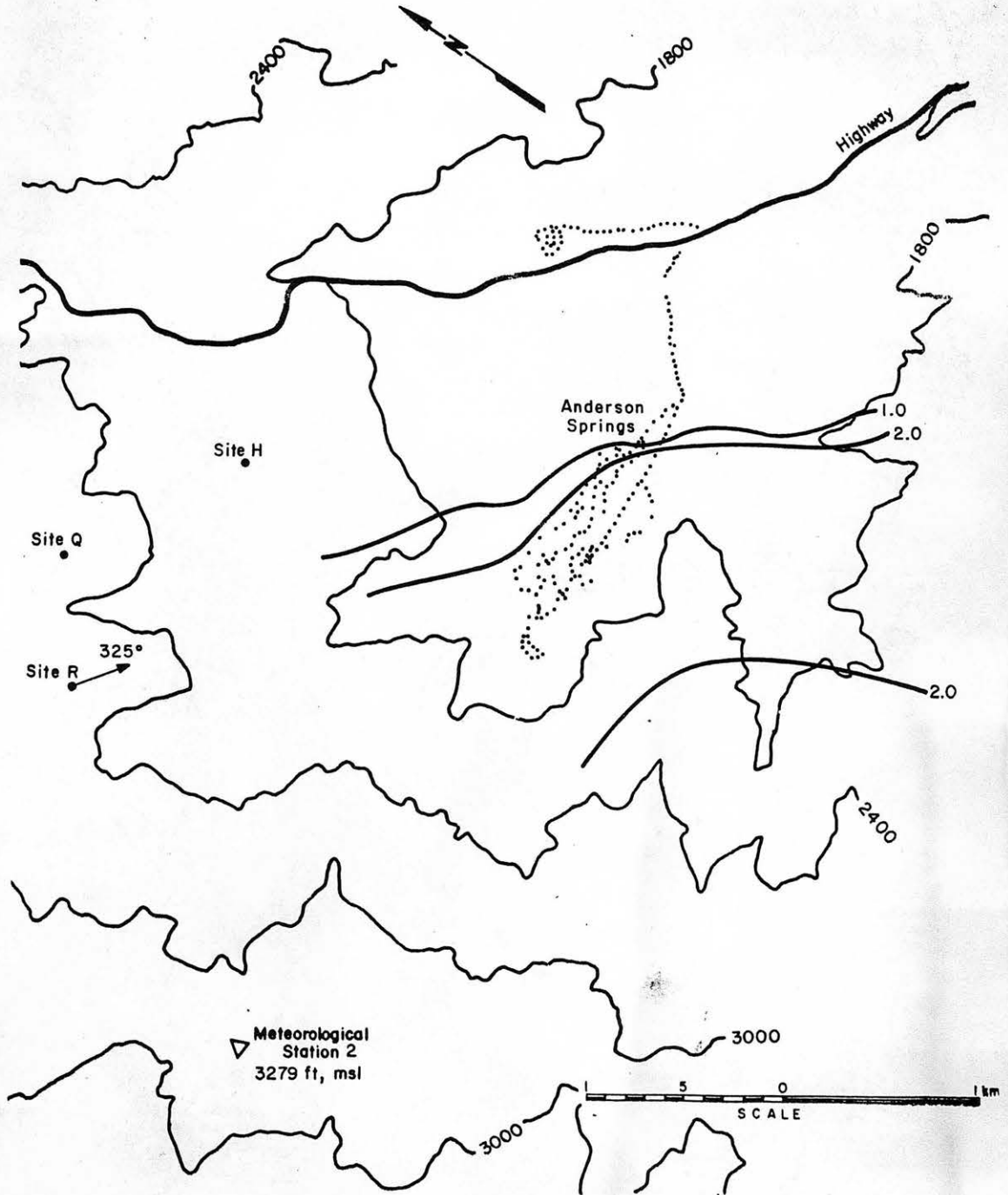


Figure 5.1-4b. Isopleths ($\times 10^5$) of nondimensional concentration coefficient K for Unit 19; Site R and a wind speed of 4.2 m/s for the 325° wind direction.

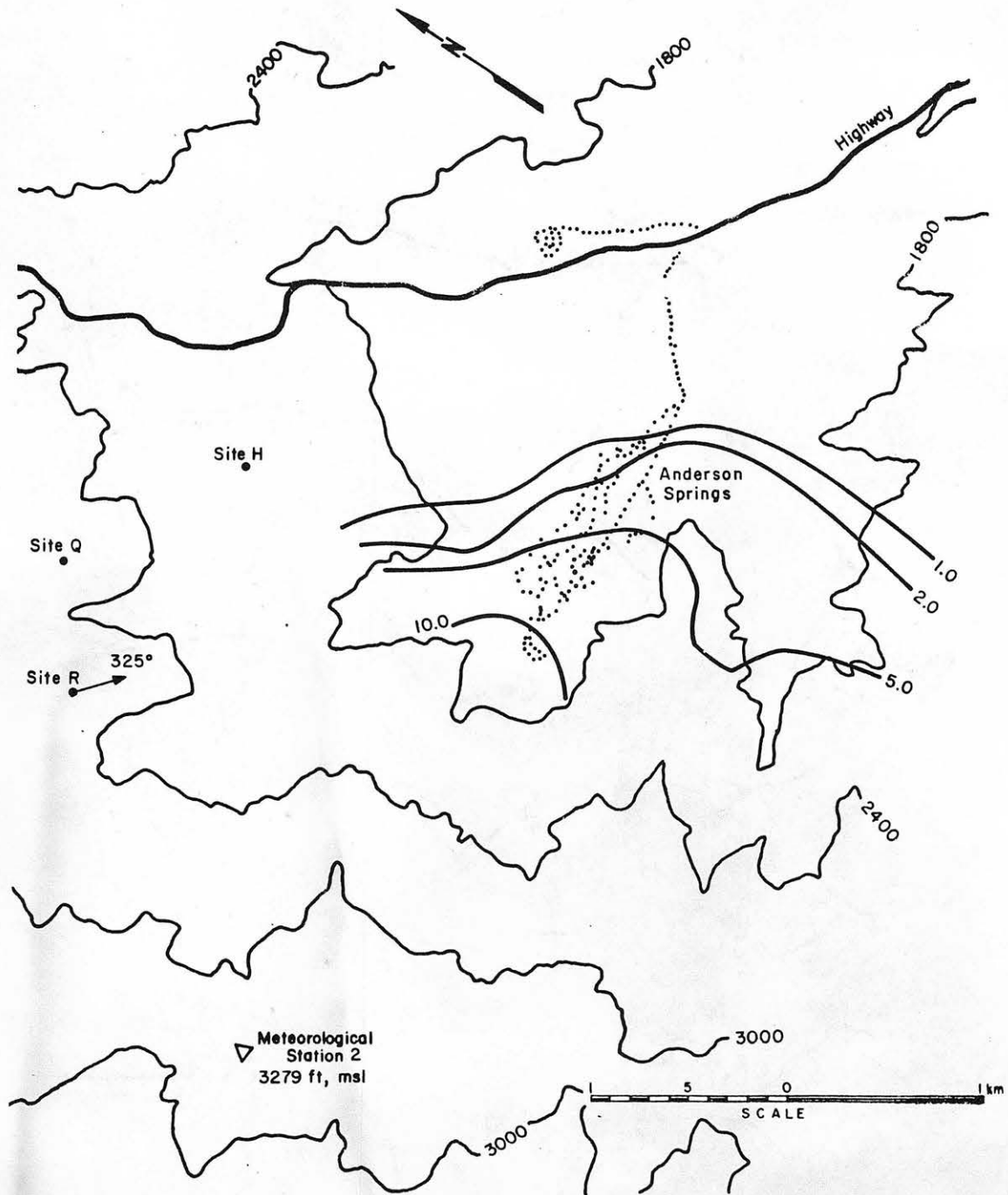


Figure 5.1-4c. Isopleths ($\times 10^5$) of nondimensional concentration coefficient K for Unit 19, Site R and a wind speed of 8.1 m/s for the 325° wind direction.

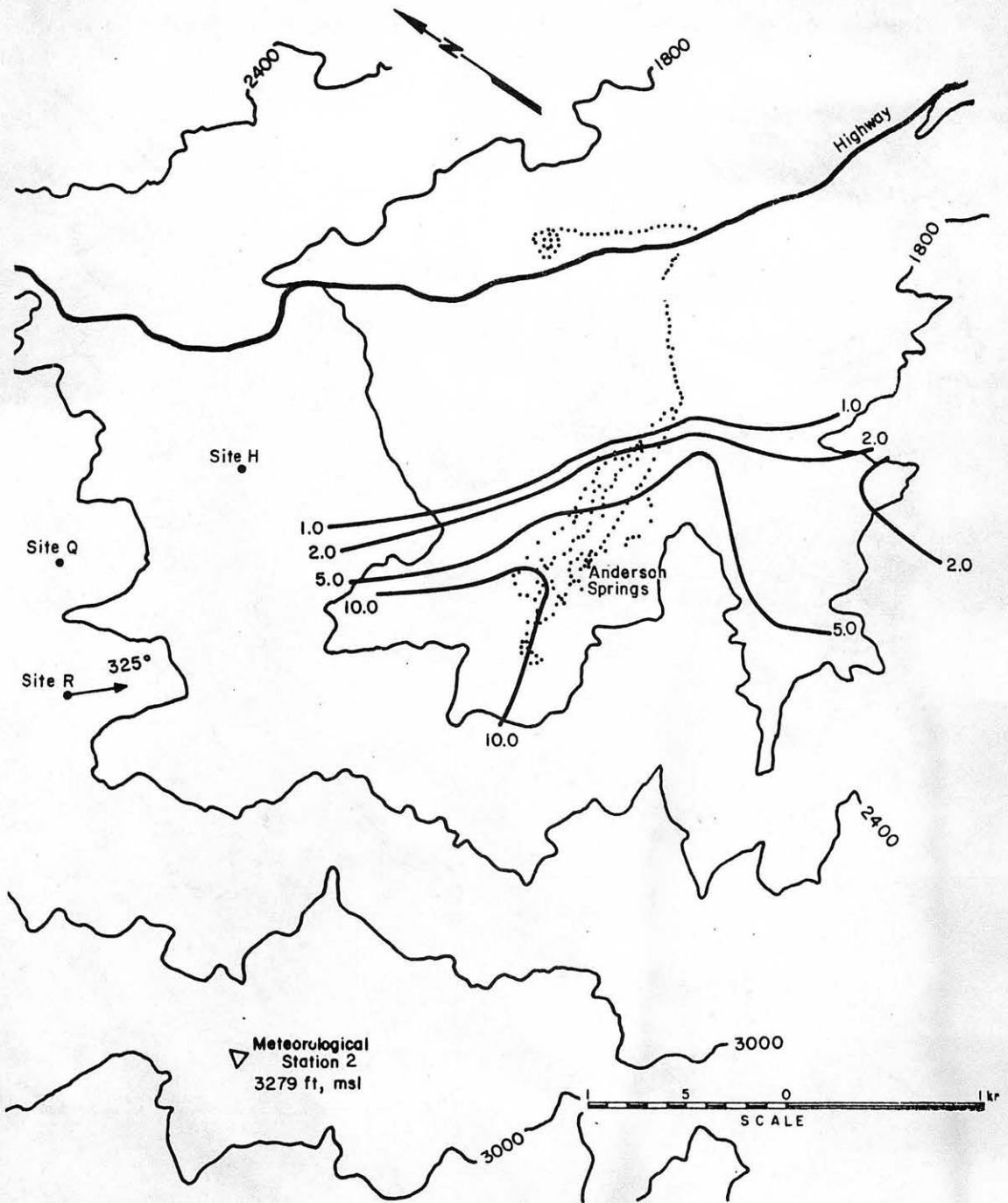


Figure 5.1-4d. Isopleths ($\times 10^5$) of nondimensional concentration coefficient K for Unit 19, Site R and a wind speed of 11.1 m/s for the 325° wind direction.

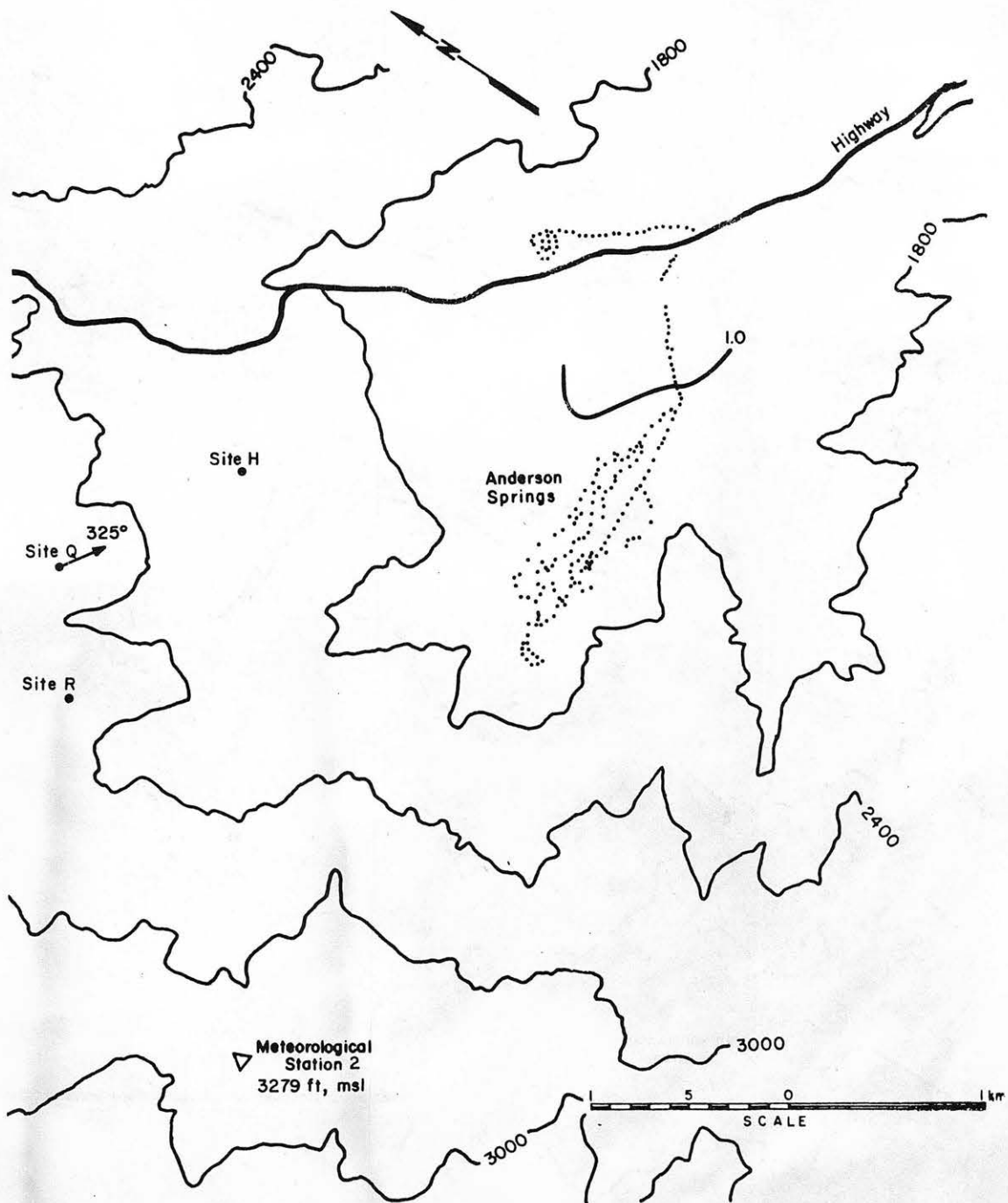


Figure 5.1-5a. Isopleths ($\times 10^5$) of nondimensional concentration coefficient K for Unit 19, Site Q and a wind speed of 3.0 m/s for the 325° wind direction.

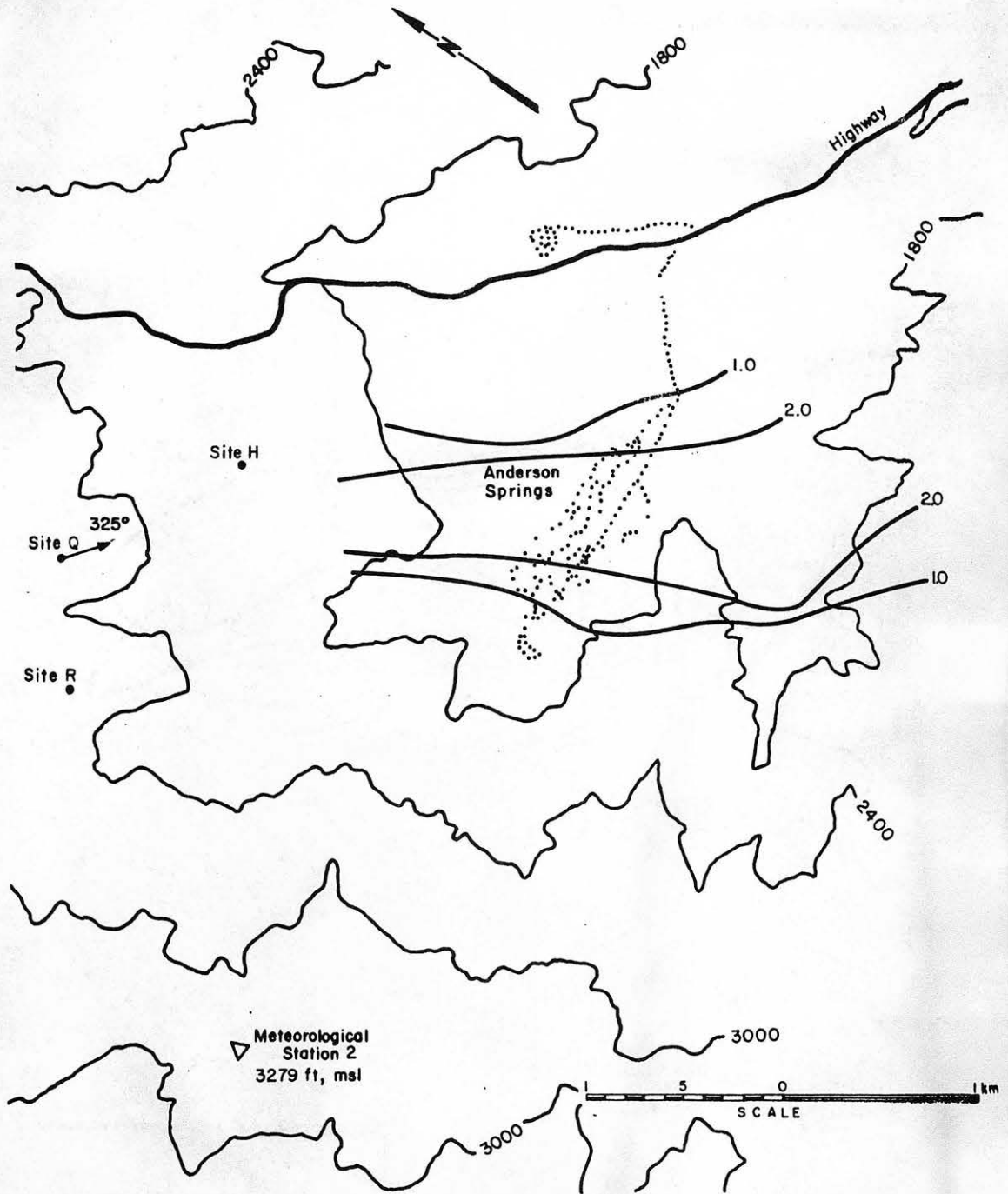


Figure 5.1-5b. Isopleths ($\times 10^5$) of nondimensional concentration coefficient K for Unit 19, Site Q and a wind speed of 4.2 m/s for the 325° wind direction.

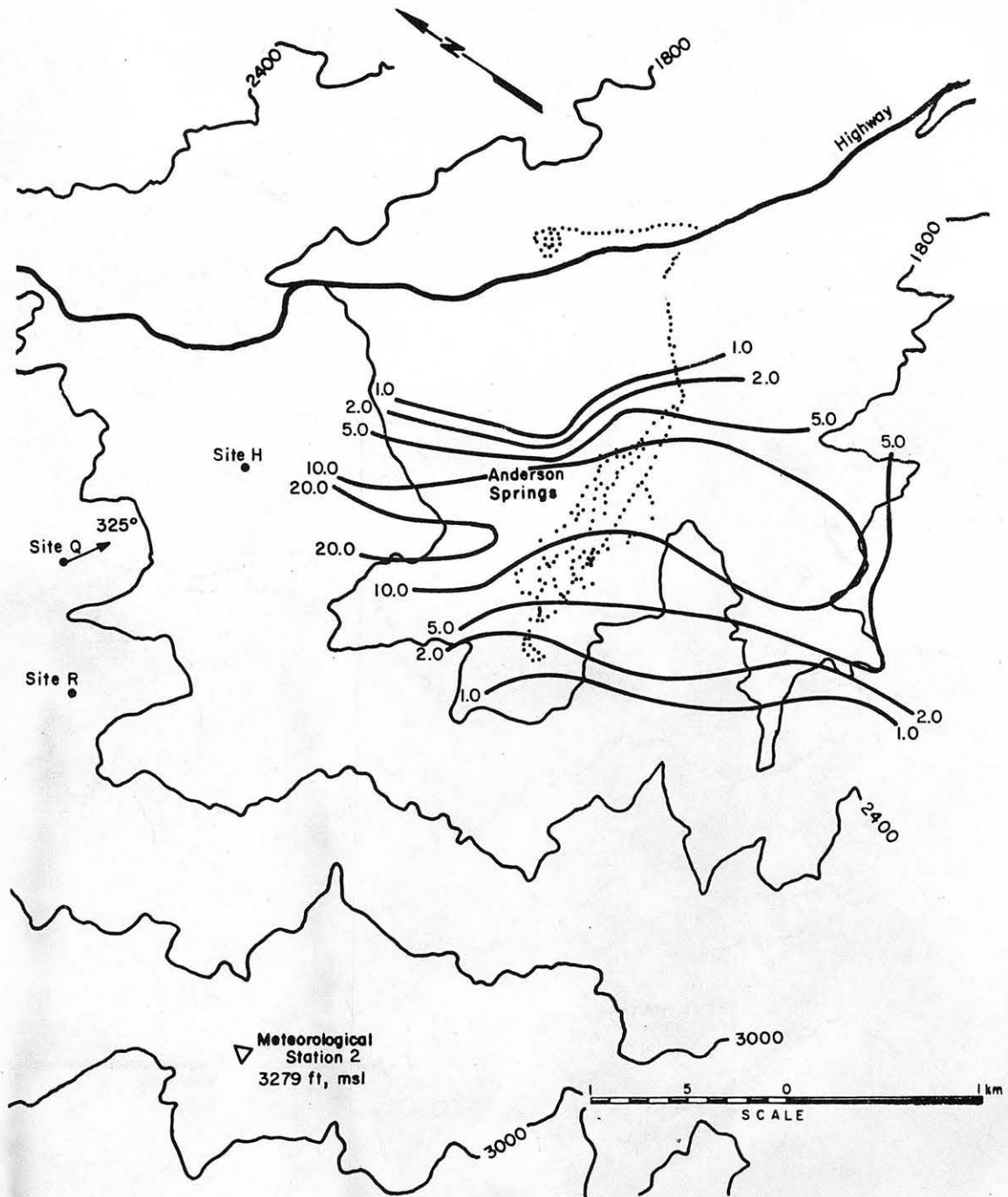


Figure 5.1-5c. Isopleths ($\times 10^5$) of nondimensional concentration coefficient K for Unit 19, Site Q and a wind speed of 8.1 m/s for the 325° wind direction.

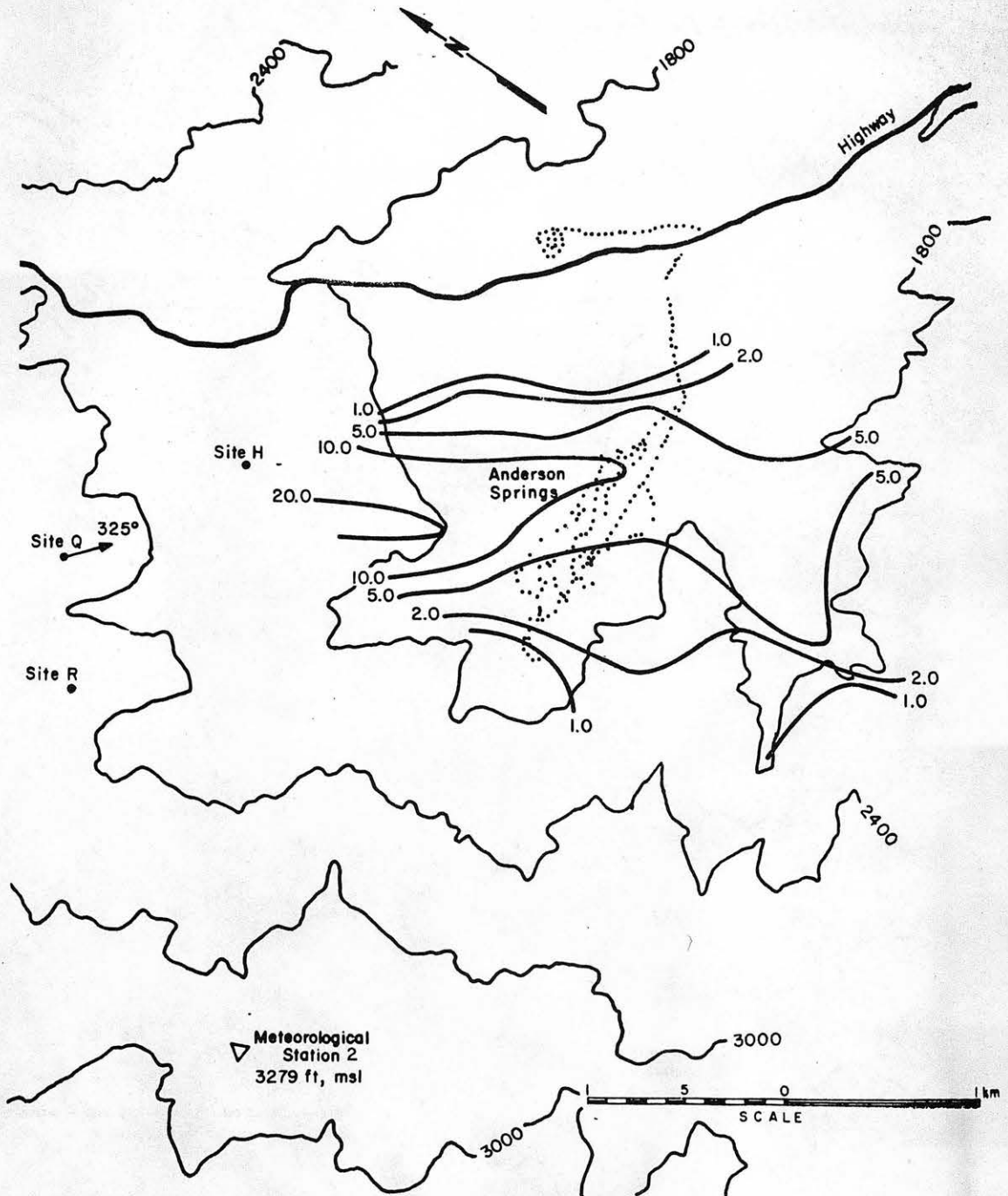


Figure 5.1-5d. Isopleths ($\times 10^5$) of nondimensional concentration coefficient K for Unit 19, Site Q and a wind speed of 11.1 m/s for the 325° wind direction.

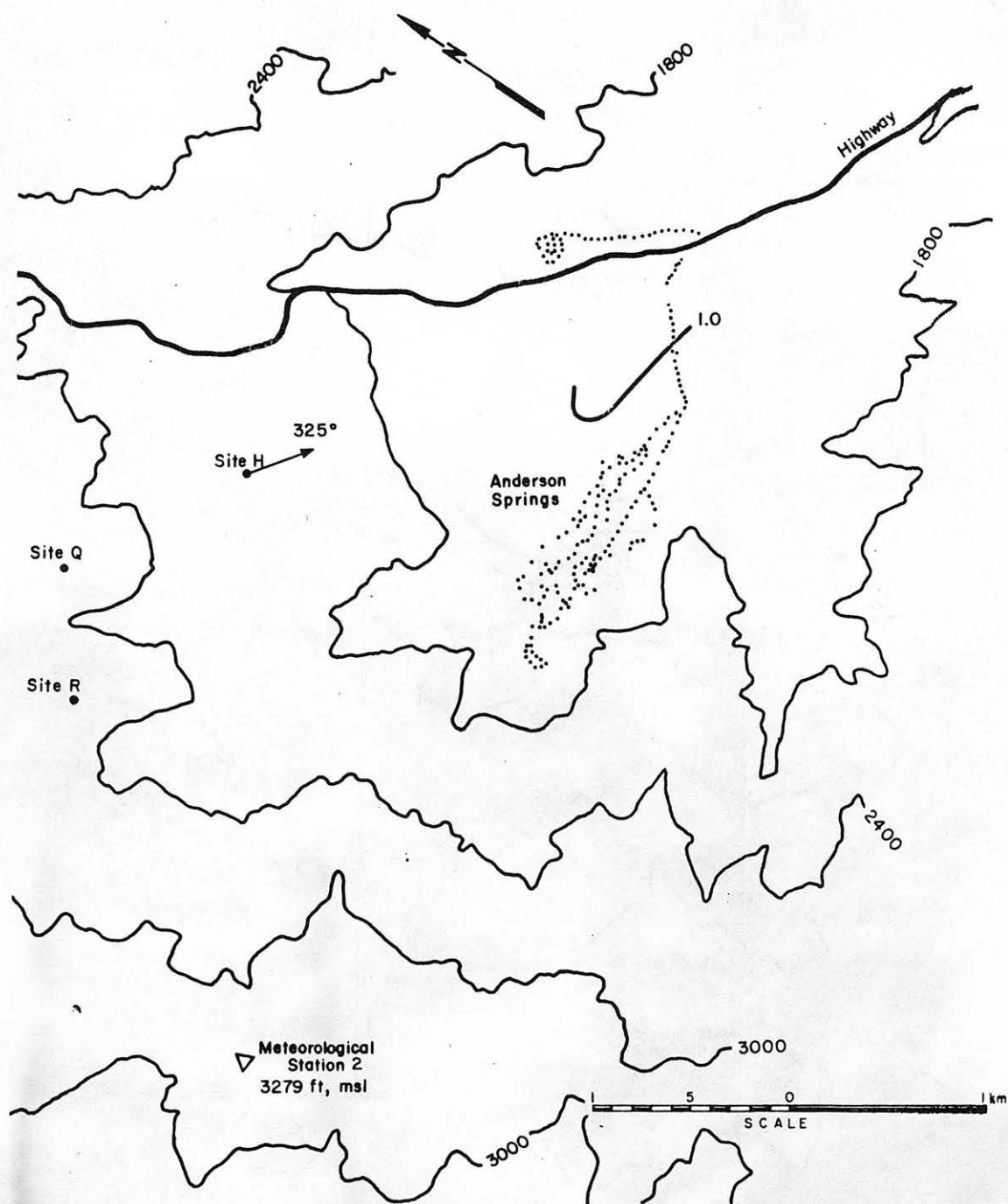


Figure 5.1-6a. Isopleths ($\times 10^5$) of nondimensional concentration coefficient K for Unit 19, Site H and a wind speed of 3.0 m/s for the 325° wind direction.

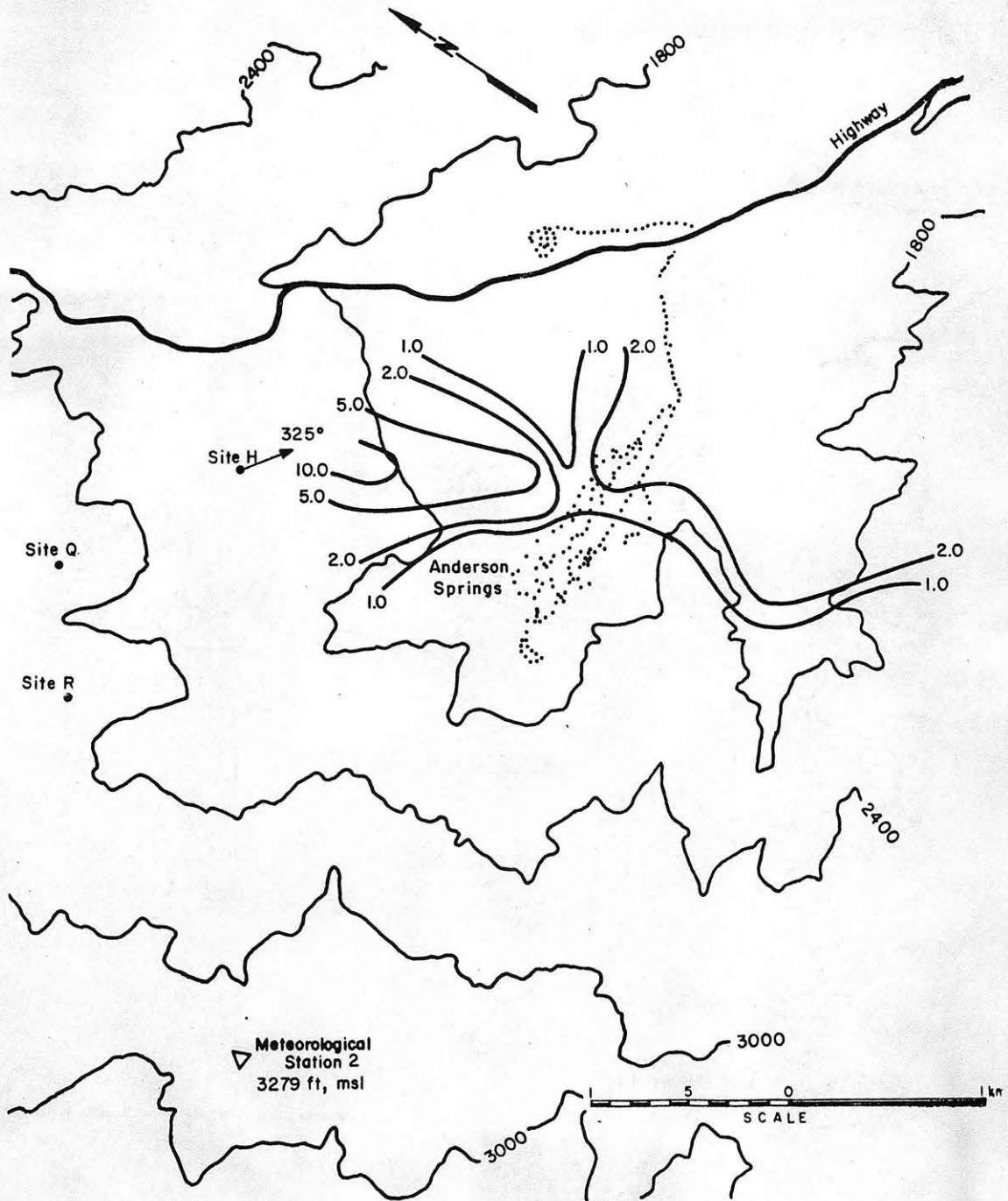


Figure 5.1-6b. Isopleths ($\times 10^5$) of nondimensional concentration coefficient K for Unit 19, Site H and a wind speed of 4.2 m/s for the 325° wind direction.

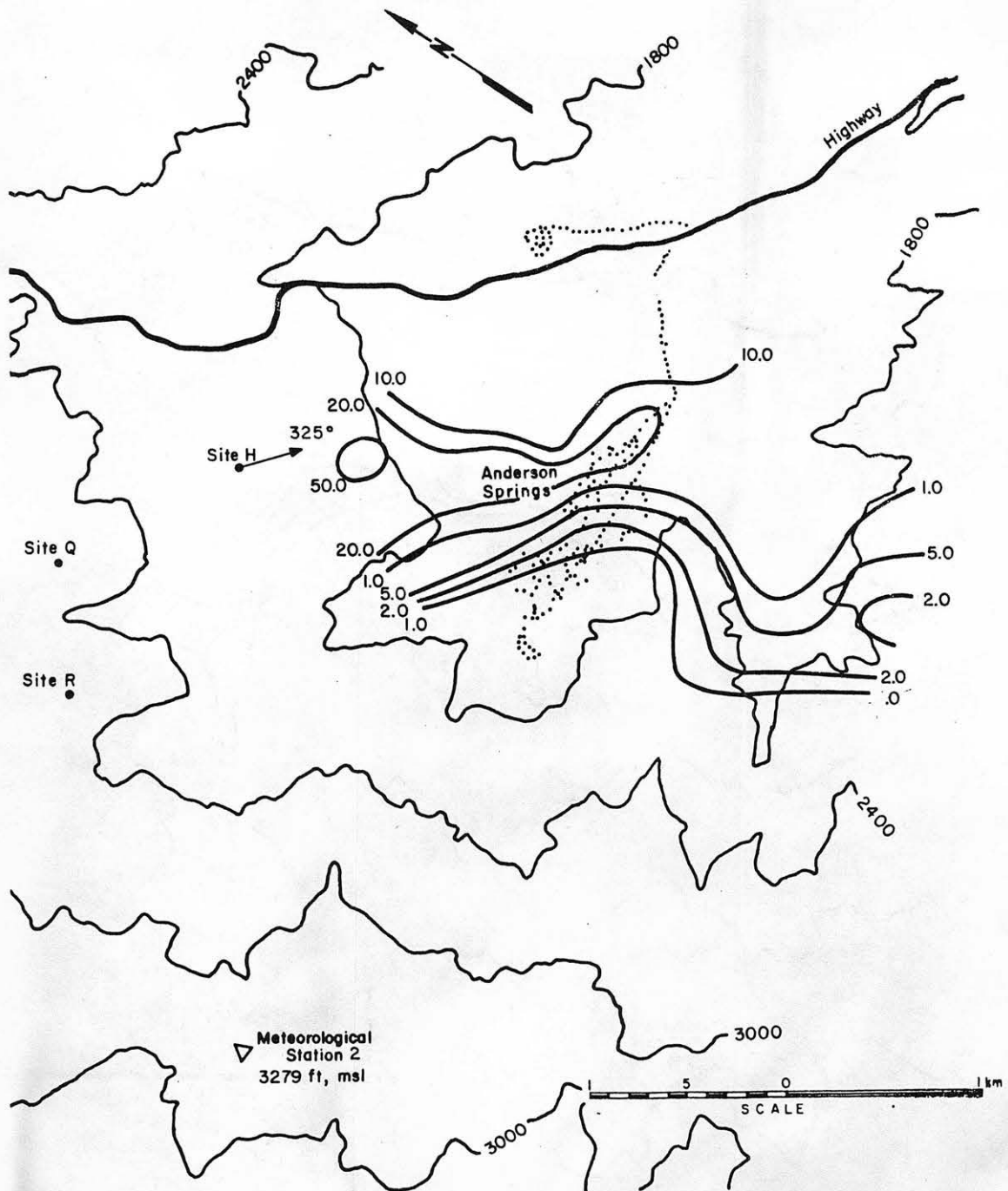


Figure 5.1-6c. Isopleths ($\times 10^5$) of nondimensional concentration coefficient K for Unit 19, Site H and a wind speed of 8.1 m/s for the 325° wind direction.

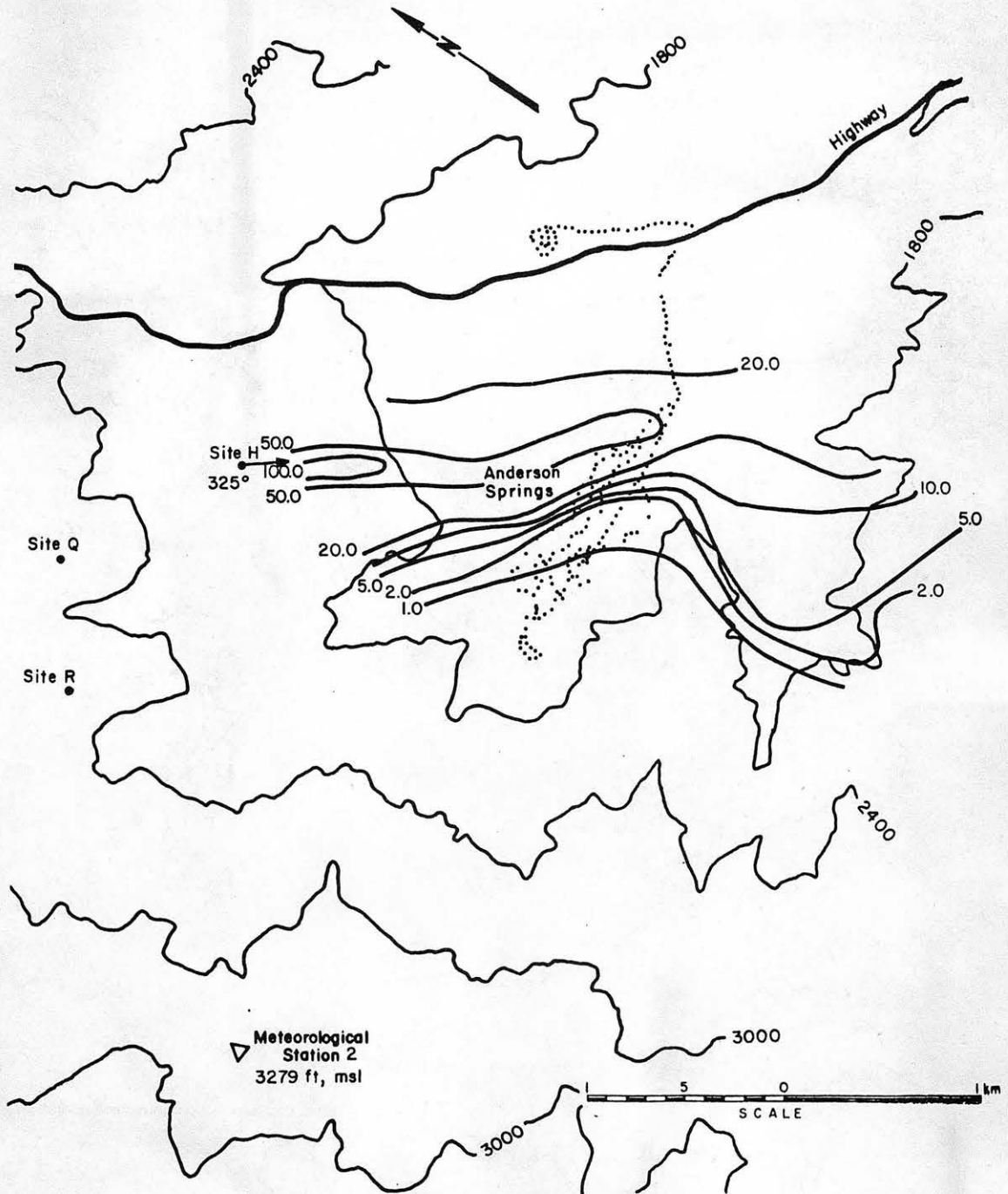


Figure 5.1-6d. Isopleths ($\times 10^5$) of nondimensional concentration coefficient K for Unit 19, Site H and a wind speed of 11.1 m/s for the 325° wind direction.

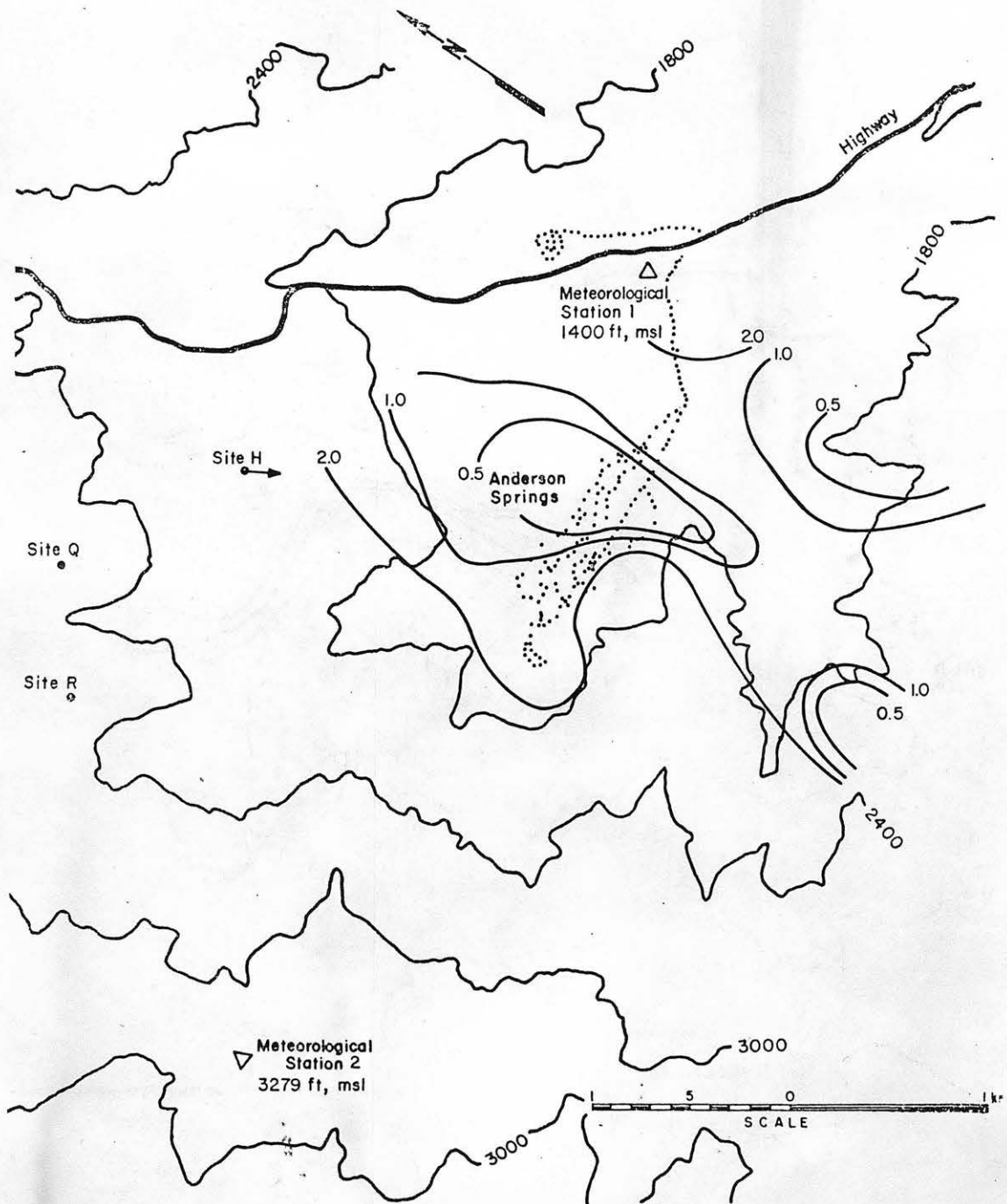


Figure 5.2-1a. Isopleths ($\times 10^6$) of nondimensional concentration coefficient K for Unit 19, Site H--nighttime drainage flow.

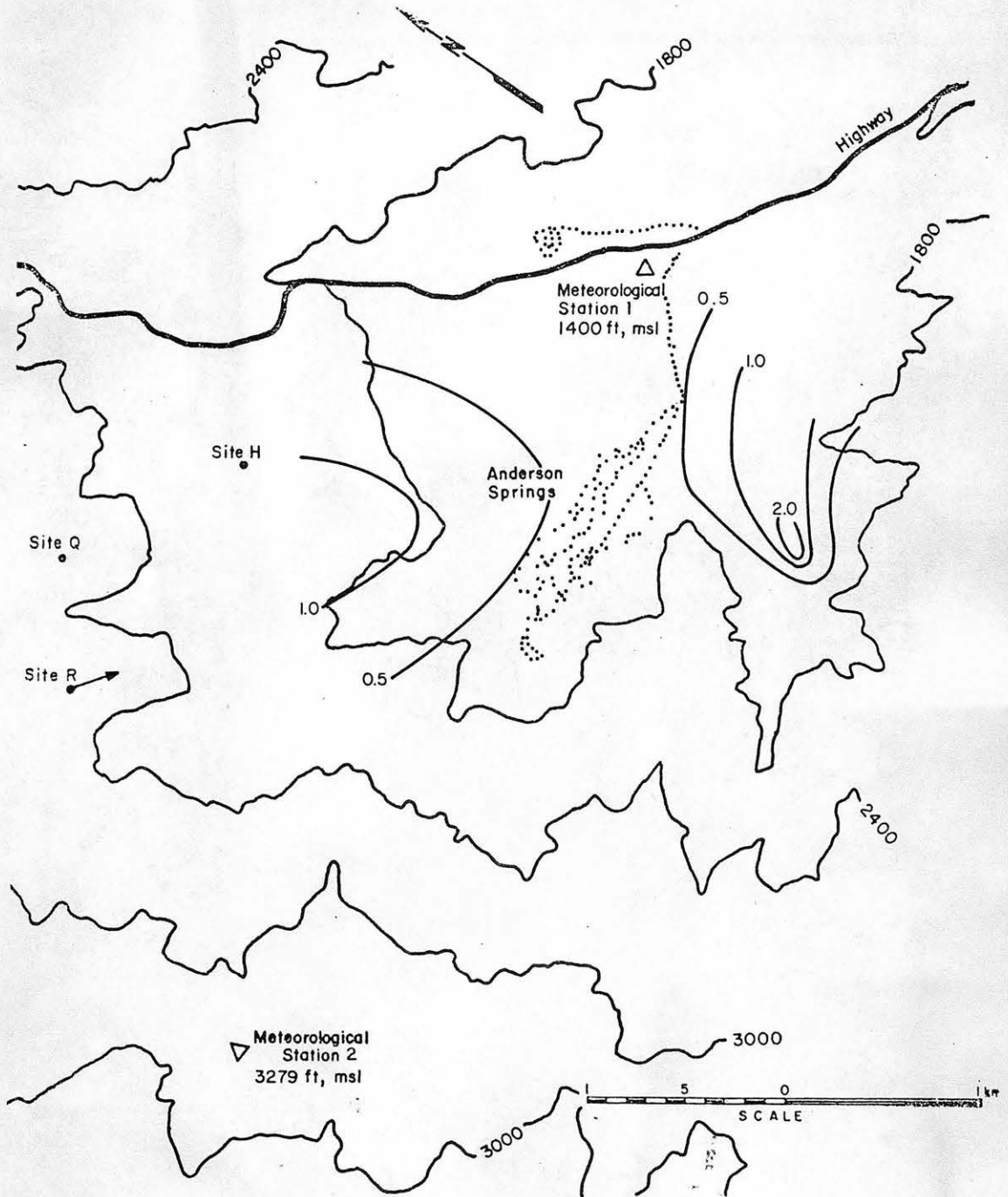


Figure 5.2-lb. Isopleths ($\times 10^6$) of nondimensional concentration coefficient K for Unit 19, Site R--nighttime drainage flow.

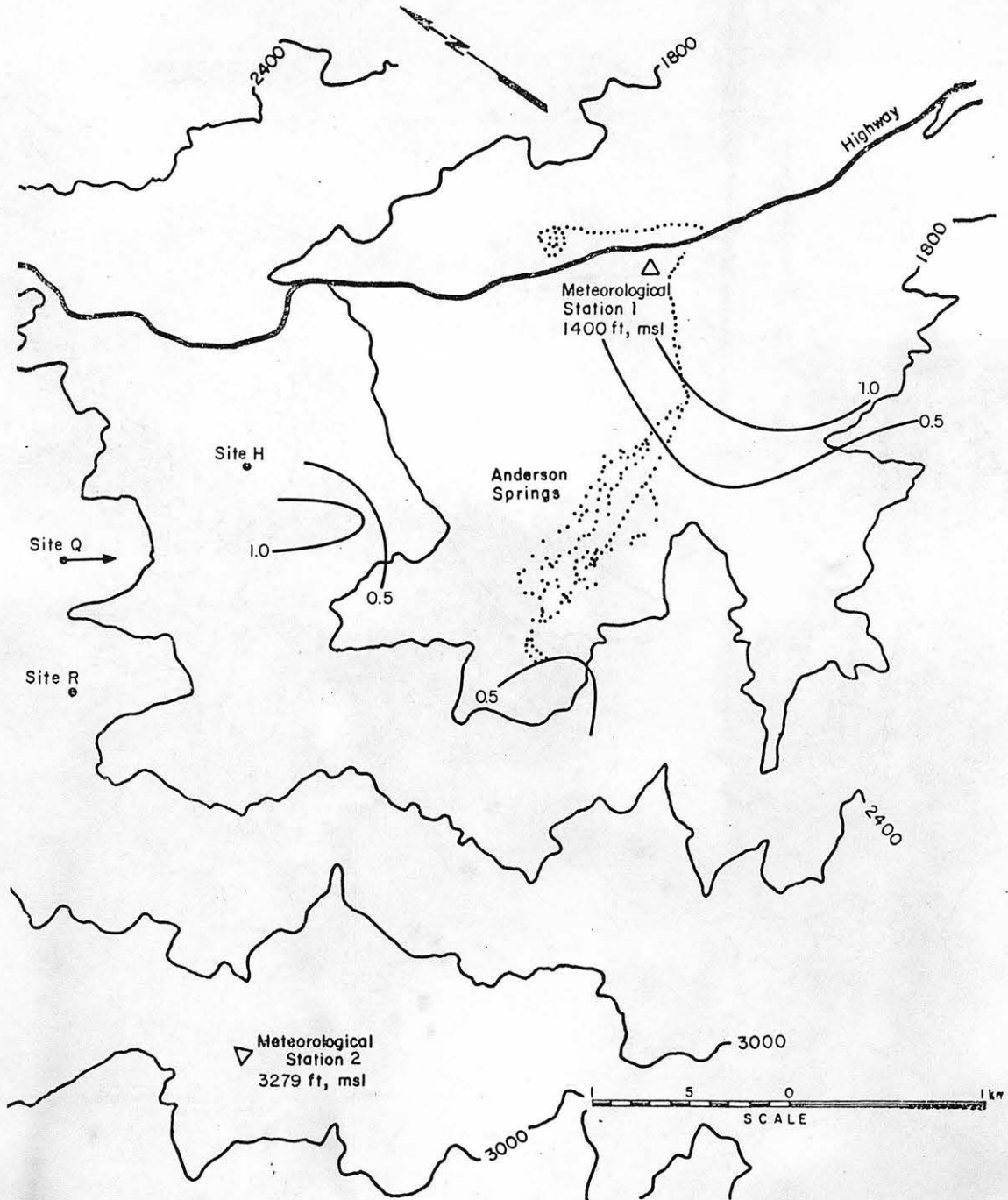


Figure 5.2-1c. Isopleths ($\times 10^6$) of nondimensional concentration coefficient K for Unit 19; Site Q--nighttime drainage flow.

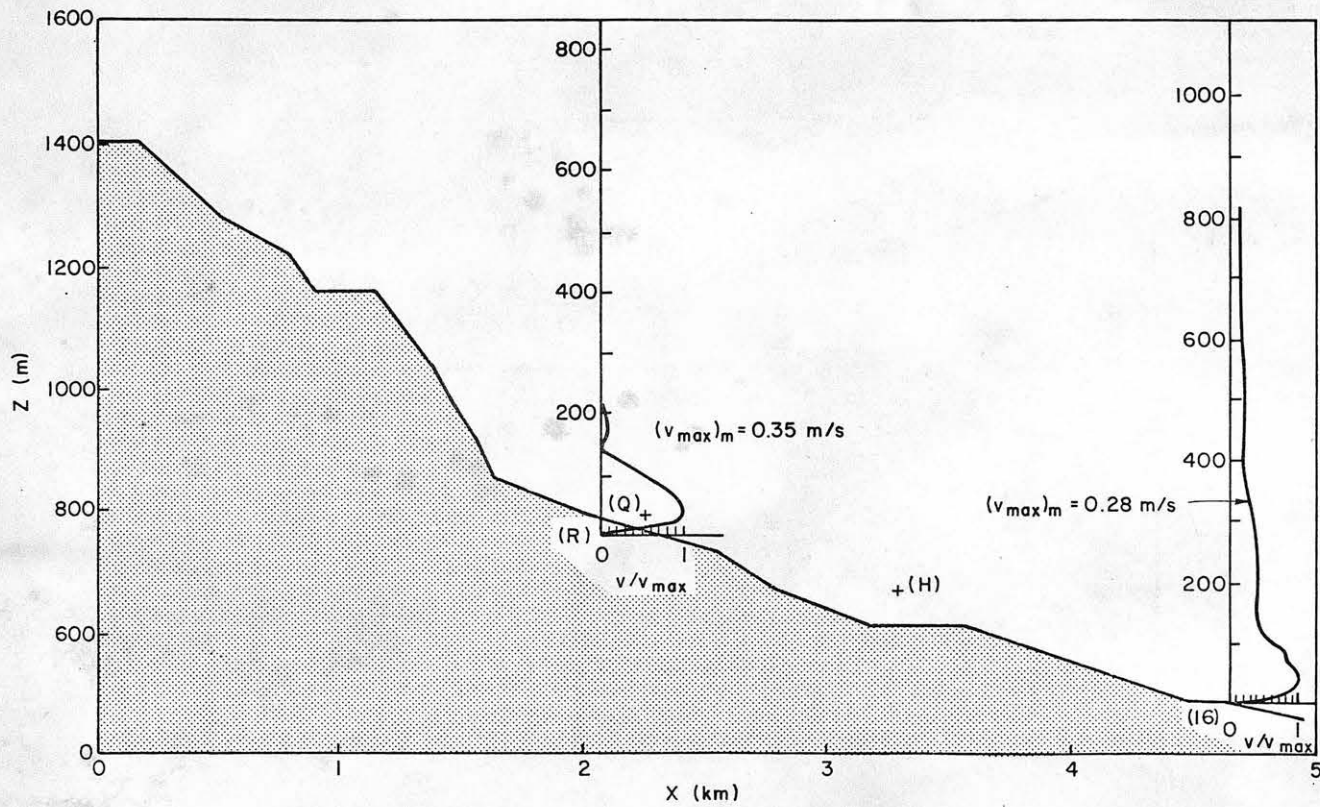


Figure 6.1-1. Velocity field plotted on a terrain cross-section for the drainage flow test.

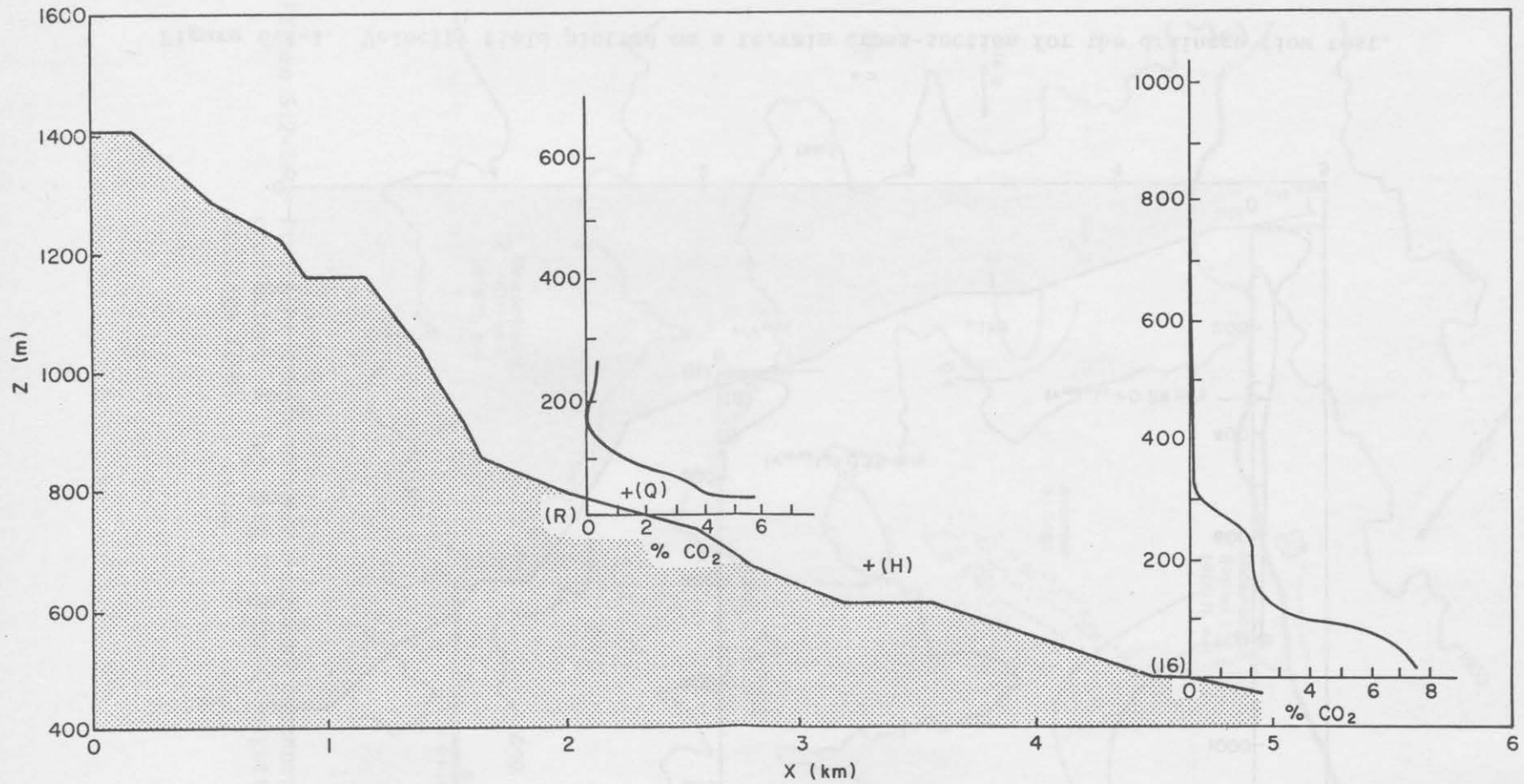


Figure 6.1-2. CO₂ distributions plotted on a terrain cross section for the drainage flow test.

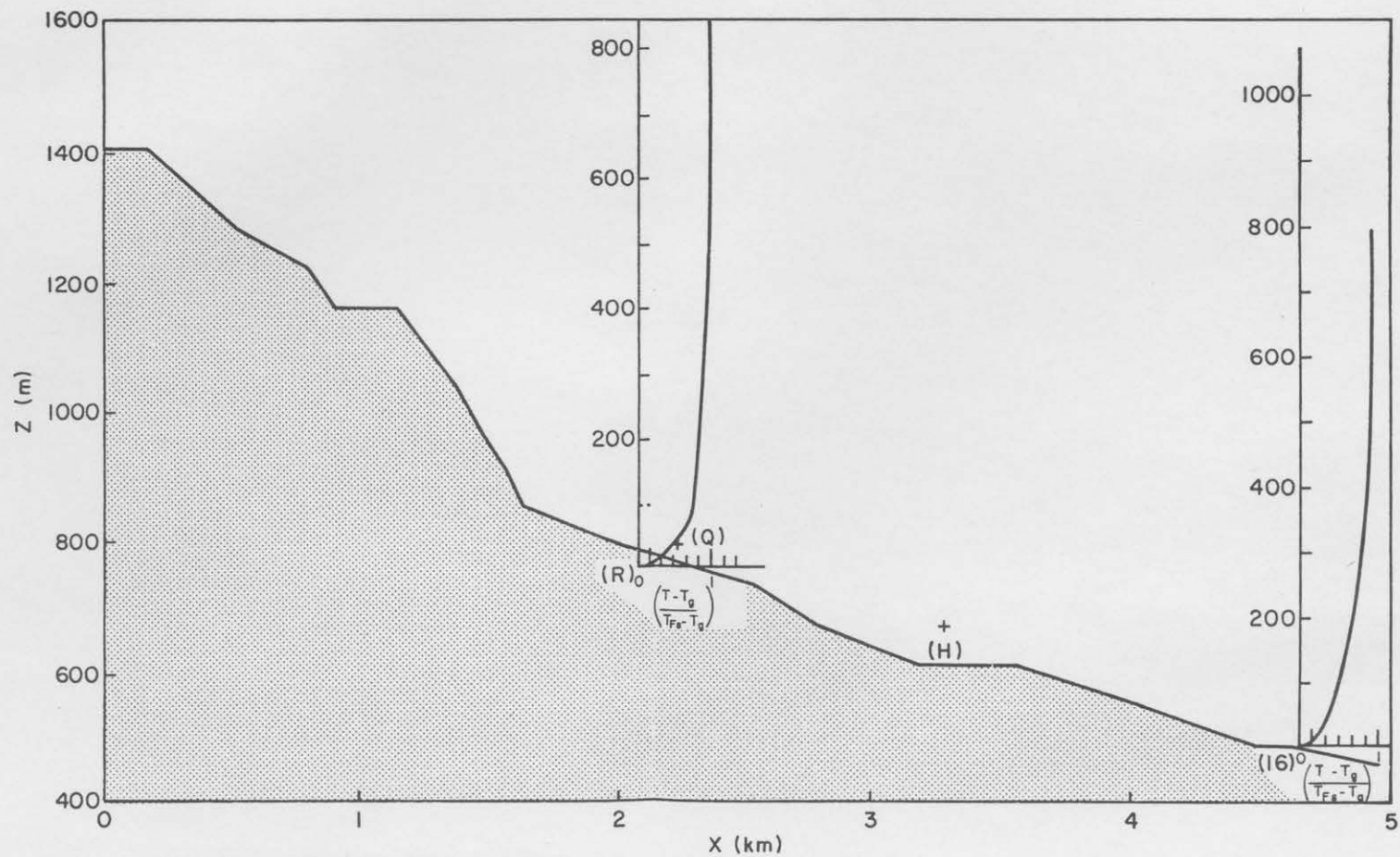


Figure 6.1-3. Temperature profile plotted on a terrain cross-section for the drainage flow tests.